MULTISCALE MODELING OF TEXTILE COMPOSITE STRUCTURES USING MECHANICS OF STRUCTURE GENOME AND MACHINE LEARNING

A Dissertation

Submitted to the Faculty

of

Purdue University

by

Xin Liu

In Partial Fulfillment of the

Requirements for the Degree

of

Doctor of Philosophy

May 2020

Purdue University

West Lafayette, Indiana

THE PURDUE UNIVERSITY GRADUATE SCHOOL
STATEMENT OF DISSERTATION APPROVAL

Dr. Wenbin Yu, Chair

     School of Aeronautics and Astronautics

Dr. R. Byron Pipes

     School of Aeronautics and Astronautics

Dr. Thomas Siegmund

     School of Mechanical Engineering

Dr. Johnathan Goodsell

     School of Aeronautics and Astronautics

Approved by:

     Dr. Gregory Blaisdell

          Head of the Departmental Graduate Program

ACKNOWLEDGMENTS

First of all, I would like to express my deepest gratitude to my PhD advisor Professor Wenbin Yu. The work presented in this dissertation would not be possible without the guidance and support of Prof. Yu. Ever since I joined his group 5 years ago, I have been constantly impressed by his encouragement for my research, wisdom for new ideas, and enthusiasm for working. I always appreciate his willingness to spend as much time as I was required discussing a problem. I have been amazingly fortunate to have such an advisor and mentor who is always kind, supportive, and helpful to my research, work and life.

I would also like to thank members of my defense committee: Prof. R. Byron Pipes, Prof. Thomas Siegmund, and Prof. Johnathan Goodsell, who provided a lot of constructive suggestions to improve my work and take their valuable time to attend my defense. I would also like to thank Prof. Pipes and Prof. Goodsell for writing job recommendation letters for me.

I would like to thank Spirit AeroSystems and Composites Manufacturing and Simulation Center (CMSC) for their financial support. My special gratitude goes to Dr. Federico Gasco in Spirit AeroSystems for giving me tremendous help in understanding the industry needs and a different perspective in conducting research. I learned a lot from our bi-weekly discussion in the two-year project with Spirit AeroSystems.

I also want to thank my lab mates in the Multiscale Structural Mechanics Lab: Dr. Liang Zhang, Dr. Fang Jiang, Dr. Bo Peng, Dr. Hamsasew M. Sertse, Dr. Ning Liu, Dr. Zhengyuan Gao, Dr. Ernesto Camarena, Yufei Long, Su Tian, Orzuri Rique Garaizar, Ankit Deo, Banghua Zhao, Fei Tao, Haodong Du and Khizar Rouf. Thanks for giving me a lot of support in the past five years.

Last but not least, I would like to thank my family for their endless love and support. I want to thank my parents, Guojing Liu and Xun Li. They take all the

work that I should do for our family so that I can concentrate on my study. I want to thank my wife, Man Li. She always stands by me no matter what decisions I make. I also want to thank my daughter, Jenny Liu, who brings the most joy in my life.

TABLE OF CONTENTS

Page

LIST OF TABLES

LIST OF FIGURES

ABSTRACT

Liu, Xin Ph.D., Purdue University, May 2020. Multiscale Modeling of Textile Composite Structures Using Mechanics of Structure Genome and Machine Learning. Major Professor: Wenbin Yu.

Textile composites have been widely used due to the excellent mechanical performance and lower manufacturing costs, but the accurate prediction of the mechanical behaviors of textile composites is still very challenging due to the complexity of the microstructures and boundary conditions. Moreover, there is an unprecedented amount of design options of different textile composites. Therefore, a highly efficient yet accurate approach, which can predict the macroscopic structural performance considering different geometries and materials at subscales, is urgently needed for the structural design using textile composites.

Mechanics of structure genome (MSG) is used to perform multiscale modeling to predict various performances of textile composite materials and structures. A two-step approach is proposed based on the MSG solid model to compute the elastic properties of different two-dimensional (2D) and three-dimensional (3D) woven composites. The first step computes the effective properties of yarns at the microscale based on the fiber and matric properties. The effective properties of yarns and matrix are then used at the mesoscale to compute the properties of woven composites in the second step. The MSG plate and beam models are applied to thin and slender textile composites, which predict both the structural responses and local stress field. In addition, the MSG theory is extended to consider the pointwise temperature loads by modifying the variational statement of the Helmholtz free energy. Instead of using coefficients of thermal expansions (CTEs), the plate and beam thermal stress resultants derived from the MSG plate and beam models are used to capture the thermal-induced behaviors in thin and slender textile composite structures. More-

over, the MSG theory is developed to consider the viscoelastic behaviors of textile composites based on the quasi-elastic approach. Furthermore, a meso-micro scale coupled model is proposed to study the initial failure of textile composites based on the MSG models which avoids assuming a specific failure criterion for yarns. The MSG plate model uses plate stress resultants to describe the initial failure strength that can capture the stress gradient along the thickness in the thin-ply textile composites. The above developments of MSG theory are validated using high-fidelity 3D finite element analysis (FEA) or experimental data. The results show that MSG achieves the same accuracy of 3D FEA with a significantly improved efficiency.

Taking advantage of the advanced machine learning model, a new yarn failure criterion is constructed based on a deep neural network (DNN) model. A series of microscale failure analysis based on the MSG solid model is performed to provide the training data for the DNN model. The DNN-based failure criterion as well as other traditional failure criteria are used in the mesoscale initial failure analysis of a plain woven composite. The results show that the DNN yarn failure criterion gives a better accuracy than the traditional failure criteria. In addition, the trained model can be used to perform other computational expensive simulations such as predicting the failure envelopes and the progressive failure analysis.

Multiple software packages (i.e., texgen4sc and MSC.Patran/Nastran-SwiftComp GUI) are developed to incorporate the above developments of the MSG models. These software tools can be freely access and download through cdmHUB.org, which provide practical tools to facilitate the design and analysis of textile composite materials and structures.

1. INTRODUCTION

1.1 Motivation

Textile composites have been widely used due to the excellent mechanical behaviors and lower manufacturing costs, but the accurate prediction of the mechanical behaviors of textile composites is very challenging due to the complexity of the mesostructures (Figure 1.1) and boundary conditions (BCs). Moreover, textile composites provide an unprecedented amount of material alternatives and design options. In order to exploit this design space, rapid yet accurate analysis tools that can predict the macro-structural behaviors by considering the micro/mesoscale features are very important in the product development (PD) phase.
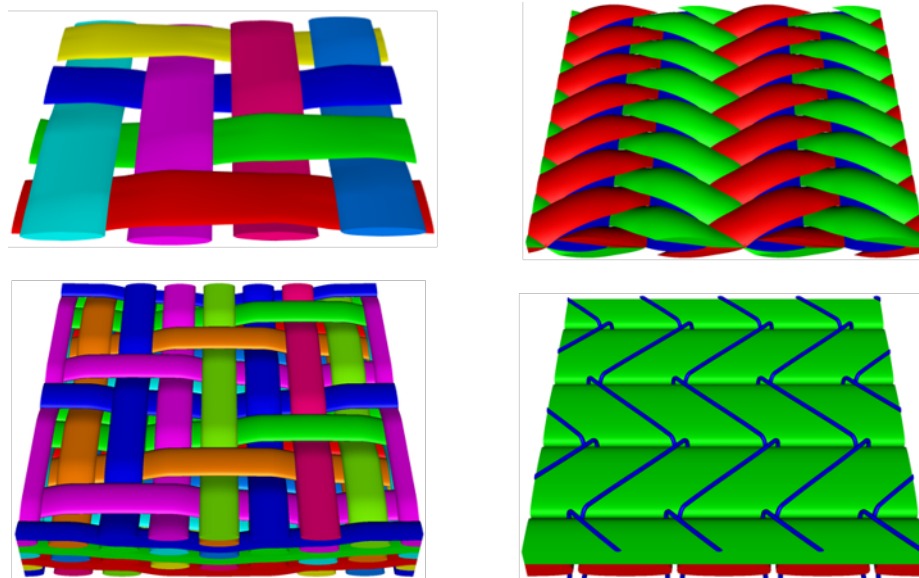
Figure 1.1. Different mesostructures of textile composites

Textile composite structures are multiscale in nature [1]. At the macroscale, structures are made of different textile composites, which are usually created by repeating

a fixed weave pattern. The fixed weave pattern is defined as the mesoscale model that is made of yarns and matrix. Yarns are made of fibers and matrix at the microscale. Therefore, a multiscale modeling approach is needed to take into account different features at various scales such as the properties of constituents at the microscale, the weave patterns at the mesoscale, and the structural geometries at the macroscale. Moreover, the geometries of macroscale structural components usually gives different BCs to the mesoscale model. For example, the thin-ply textile or 3D woven textile composites does not follow the commonly used periodic boundary conditions (PBCs) in the thickness direction. The slender textile composite structures have no periodicity in the transverse directions. However, the commonly used approach is to get the homogenized properties using representative volume element (RVE) analysis with in-plane PBCs for plate structures or x_1-direction PBCs for beam structures. The shell or beam elements can be subsequently defined using the homogenized properties. Such simplification smears the heterogeneity along the thickness or the transverse directions of the thin and slender structures, which could cause a significant loss of accuracy. Therefore, a novel multiscale modeling approach that can consider various features at different scales and connect micro/mesoscale structures to structural properties (e.g., effective properties, plate stiffness matrix, and beam stiffness matrix) is urgently needed.

Due to the inherent viscoelastic behavior of polymers [2], the long-term behaviors of textile composites should also be considered in the design and analysis. The yarns, which are made of fiber and matrix, have non-isotropic viscoelastic behavior. This behavior increases the complexity of modeling the long-term behavior of textile composites in the commercial finite element software, because the non-isotropic viscoelastic properties have to be assigned through a user-defined material subroutine (UMAT). Another challenge is from the complex BCs to be applied to the mesoscale model for the thin and slender structures such as high strain deployable thin-ply structures [3]. The mesoscale model should generate the time-dependent plate or beam stiffness matrix for the structural modeling.

In addition, the thermoelastic of textile composites has generated considerable recent research interest. Textile composites are increasingly used in the space structures [4], engine systems [5], electronic devices [6], etc., which could subject to severe temperature loads. Due to the anisotropic behavior of composites, the imposed temperature variations induce thermal stresses which cause the microcracks inside the materials and subsequently affect the macroscale performance of the structures. The current approaches are mainly developed for laminated structures, which compute the effective coefficients of thermal expansion (CTEs) of each lamina with PBCs and then apply classical lamination plate theory (CLPT) to perform thermoelastic analysis. As mentioned in the previous, textile composites used in the thin and slender structures usually do not follow PBCs and its structural properties are better to be described using plate or beam stiffness matrix. Moreover, the complex mesoscale structures of textile composites introduce non-uniform temperature changes inside the composites instead of uniform temperature changes in the most RVE analyses. Therefore, a new approach that can capture complex temperature variations inside textile composites and homogenize the thermoelastic behavior into shell and beam elements should be developed.

Textile composites also have a better performance in damage tolerance and cracking resistance. As a result, a considerable amount of literature has been published on the failure and damage modeling of textile composites. In general, the initial failure analysis is the first step in the modeling of failure behavior of textile composites. In the multiscale modeling framework, the effective strength constants of yarns are first computed based on the failure criteria of fiber and matrix at the microscale. At the mesoscale, failure criteria such as Tsai-Wu and Hashin are then assumed for yarns using the effective strength constants, and the failure initiates once the criterion is met. Subsequently, a damage evolution law and a stiffness degradation algorithm are applied to predict the nonlinear behavior of the composite material during failure progression. Therefore, choosing an appropriate failure criterion is crucial in determining the overall failure behavior. However, experimental evidence shows that the current

failure criteria are still not mature enough to give an accurate prediction of failure initiation [7]. In addition, most of the existing failure criteria are developed for the UD fiber reinforced lamina. There is limited evidence that these failure criteria can be safely applied to yarns which are often in more complex stress states due to the yarn crimp in fabrics. In addition to using failure criterion of yarns at a single scale, a coupled multiscale analysis such as FE^2 [8,9] is believed to be more accurate as it considers the failure in the microstructures at each integration point at mesoscale. However, such coupled multiscale analysis is often computationally expensive that is not practical for the design and analysis at the product design phase.

1.2   Previous Work

Copyright permissions have been obtained to reuse the published materials from [10–15] in this section.

1.2.1   Homogenization Analysis of Textile Composites

Many models have been proposed to predict the effective elastic behavior of textile composites. These models can be roughly divided into two categories: analytical models and numerical models. Hallal et al. [16] reviewed the widely accepted analytical models for the modeling of textile composites. Ishikawa and Chou [17, 18] proposed analytical models to predict the homogenized response of woven fabric composites (WFCs), which were based on the CLPT combined with iso-strain or iso-stress assumptions. Many researchers also proposed analytical models using the similar assumptions or mixed iso-strain/iso-stress assumptions [19]. Gommers et al. [20] proposed an improved analytical model based on the inclusion method that removes the iso-stress/strain assumptions, which has been implemented in the commercialized software WiseTex [21]. Although analytical models provide good estimation of the in-plane properties, they are not good at predicting the shear and out-of-plane properties of textile composites. Moreover, the analytical approaches often fail in

predicting the local stress/strain fields while the local fields are crucial in the failure analysis. In addition to that, due to the various assumptions made in the contemporary analytical models, it is hard to find a unified analytical model that can be applied to textile composites with all possible mesostructures.

In addition to analytical models, the finite element method (FEM) based numerical models have been widely used to study the two-dimensional (2D) and three-dimensional (3D) textile composites [22–24]. Compared with analytical models, numerical models usually provide better predictions for both effective properties and local stress and strain fields which can be used in the failure analysis [25]. However, the numerical analysis of complex textile composites requires significant resources and time to model the complexities and to run the 3D finite element analysis (FEA). In addition to that, FEM also requires to create representative volume elements (RVE) with appropriate BCs which are not always straightforward. Another popular numerical approach for modeling textile composites is asymptotic homogenization (AH) [26]. Angioni et al. [27] compared AH with several analytical methods and the results show that AH provides a good estimation of the mechanical properties for all the cases especially for the in-plane properties, while the out-of-plane properties are estimated less accurately. Recently, Nasution et al. [28] used AH to relieve the periodicity in the thickness direction of 3D orthogonal interlock composites and calculated the in-plane properties. As textile composites are often used in some thin structures, the unit cell of textile composites usually only repeats a few times in the thickness direction and the finite thickness effect should be taken into account.

1.2.2 Multiscale Structural Analysis

Many engineering structures are composed of thin or slender structural components which might be made of textile composites such as I-beams, skin panels, wing-cover panels, stitched stiffeners etc. Engineers usually use shell or beam elements to analyze this kind of textile composite structures. However, there are not many models

available to predict the beam and plate stiffness matrices for textile composites that can be used directly for the macroscopic structural analysis.

For beam-like textile structures, Sankar and Marrey [29] proposed a FEA based model to predict the beam stiffness matrix. In this analysis, they implemented PBCs on the lateral faces of unit cell, while top and bottom surfaces were assumed traction free. They applied three independent deformations (pure extension, pure bending, and pure shear) to predict the beam stiffness coefficients. The predicted results for plain weave textile were compared with the estimated results from mosaic model, and a good agreement was found. For plate-like textile structures, most of the predictions are based on the CLPT [17, 18, 30]. In these predictions, 2D woven composites were modeled in series and parallel based on the loading direction, and A, B, D matrices were predicted. Chaphalkar and Kelkar [31] developed another analytical model based on the CLPT to determine the A, B, D of twill composites. The predicted results compared well with the experimental ones. Marrey and Sankar [32] developed a direct FEA based micromechanical model with the main focus to predict A, B, D matrices. That model was applied to plain woven composites and satin woven composites, and the predicted results were compared with those predicted by mosaic model and CLPT. Many other researchers have attempted to predict 3D elastic properties of 2D and 3D textiles which are based on different assumptions such as iso-strain, iso-stress, mixed iso-strain and iso-stress. Besides the loss of accuracy due to the associated assumptions in the derivations of 3D elastic properties, Marrey and Sankar [32] have pointed out that textile plate stiffness matrices, especially B and D matrices, cannot be predicted using the homogenized elastic constants and plate thickness in conjunction with CLPT; therefore, plate stiffness properties should be predicted directly in terms of the textile mesostructures.

Based on the literature review, there are several issues with the available models for predicting the beam and plate stiffness matrices. First, various assumptions such as iso-strain/stress and the yarn path are made, which not only might affect the accuracy but also hinder the applications of these methods to the textile composites with

different weave patterns. Second, the BCs applied to the RVE of textile composites in the thin and slender structures are not straightforward due to the violation of periodicity in the thickness or transverse directions. Third, very few plate and beam models can accurately predict the local stress and strain fields which are important for the failure analysis of textile structures.

1.2.3 Viscoelastic Behavior of Textile Composites

For unidirectional fiber reinforced composites, analytical approaches have been proposed using correspondence principle [2,33], but more general results have been obtained from numerical models [34–36]. However, there are not many models available for predicting the viscoelastic properties of textile composites. The main difference is that both yarns and matrix in textile composites exhibit viscoelastic behaviors while only matrix is considered to be viscoelastic in unidirectional fiber reinforced composites. Models using CLPT along with micromechanical approaches have been proposed to study the viscoelastic properties of plain woven composites [37,38]. The main limitation is the assumptions made to describe the geometry of textile composites, which makes the models hard to apply for the textile composites with different weave patterns. 3D RVE analysis using FEA has provided a more robust approach in studying the viscoelastic problems in textile composites [39,40]. The RVE analysis using FEA is easy to apply for the textile composites with different weave pattern without any ad hoc assumptions. The main disadvantages of using RVE analysis are still the computational costs and applying right BCs. For example, the viscoelastic behavior is very critical in the application of thin-ply deployable textile composite structures. To capture the thin yarn cross section, a very dense mesh is usually needed. Moreover, the structural modeling often uses shell element to model the thin-ply structures. In addition, anisotropic viscoelastic materials are not available in most FEA software, and additional efforts are needed to define the properties through user-defined functions, such as Abaqus user-defined material subroutine (UMAT) [41]. Therefore, an

efficient and effective approach to predicting time-dependent plate stiffness matrix due to the viscoelastic behavior of composites is required.

1.2.4 Thermoelastic Behavior of Textile Composites

In recent years, some advanced homogenization approaches [42–44] are proposed to compute the effective thermoelastic properties of textile composites. The effective thermoelastic properties, including elastic properties and CTEs, can be used as inputs for solid elements in the structural analysis. For laminated structures, effective thermoelastic properties can also be used to define lamina properties and then carry out laminated structural analysis [45]. However, for complex composite structures such as 3D woven structures, the lamination theory may not be applicable since yarns are interlaced in the thickness direction. On the other hand, shell and beam elements are widely used in structural designs due to the simplicity and computation efficiency. Using homogenized elastic properties along with shell and beam elements could cause significant loss of accuracy. Therefore, instead of using homogenized CTEs to capture the thermal stresses for beam and plate structures, an alternative constitutive parameter should be used so that thermoelastic behaviors of composite structures can be captured using shell and beam elements.

Another challenge for accurately predicting the thermoelastic behaviors of composite structures is the complexity of temperature loads. Although thermal stresses can be predicted under linear and non-linear temperature loads for traditional laminated structures [46], the real temperature distribution in composites could be pointwise different. For example, advanced composites manufacturing methods like 3D printing can produce a very complex temperature field during the manufacturing [47]. For plate and beam structures, the temperature load could be distributed along the thickness or over the cross-section. If a pointwisely distributed temperature load is applied to a complex composite structure such as a woven composite structure, 3D thermal stresses in yarns and matrix are difficult to accurately predict. Currently,

the commonly used approach for solving 3D thermoelastic problems in complex composite structures is direct numerical simulation (DNS) using 3D FEA. However, this approach is very computation expensive since a dense mesh is always required for describing the complex mesostructures and stress variations in the composite structures. Therefore, there is a need for a unified approach to compute thermoelastic constitutive information for beam, plate and solid elements. In addition, the model should be able to capture pointwise temperature distribution of general composite structures, and to accurately and efficiently recover the 3D stress field.

1.2.5   Initial Failure Analysis of Textile Composites

Currently, mesoscale RVE models containing yarns and matrix are frequently used in predicting the failure initiation of textile composites [48]. In these mesoscale models, yarns are often treated as homogeneous material where failure criteria such as Tsai-Wu [49] and Hashin [50] criteria are applied to predict the failure initiation. However, failure should occur at the fiber and matrix level inside a yarn instead of at the yarn level. Therefore, in order to pass failure information at the microscale to the mesoscale, some multiscale models are proposed which provided the effective properties and strength constants of yarns based on a microscale analysis with the fiber and matrix [51,52]. Nevertheless, the failure criteria are still applied at the yarn level. However, the traditional failure criteria applied to yarns assume that yarns are characterized locally as UD composites, but this assumption is still questionable due to the differences between unidirectional plies and yarns [53]. Therefore, it is more reasonable if the failure initiation of textile composites can be predicted using failure criteria at fiber and matrix level. Wang et al [53] proposed a meso-micro "partially coupled" approach to predict the progressive failure of 2D woven composites. Instead of recovering the stress field over the whole microstructure, only the microscale stress field at several key points was recovered. As these key points were first identified for the analysis of UD laminates [54], it is not clear if these points can represent the

critical locations for yarns. Therefore, a full meso-micro coupled approach should be used in order to capture all the possible failure behaviors at the entire microscale level.

Another issue for predicting the failure initiation of textile composites is the consideration of the non-uniform stress field in slender and thin textile composite structures. Karkkainen and Sankar [55, 56] proposed a direct micromechanics method (DMM) which uses plate stress resultants (i.e. plate forces and moments) as macrostress to represent the initial failure strength. Then, the failure initiation is determined based on the 3D stress field recovered at the mesoscale level. This approach captures the non-uniform stress state using plate stress resultants and has been implemented into Abaqus micromechanics plugin [57] at Dassault Systèmes. Moreover, such approach offers a benefit for the structural design. As thin structures are often modeled using shell elements in FEA at macroscopic structural level, it is more straightforward for the structural design if the initial failure strength constants are expressed in terms of structural loads such as plate stress resultants. However, the DMM also requires a high computational cost as a result of 3D FEA. In addition, the non-uniform stress issue also exists in slender textile composite structures which are often modeled using beam elements in the structural level design which was not solved using the DMM. Therefore, it is better to have an approach which can capture all the non-uniform stress state in slender and thin structures while offers a better computational efficiency.

1.2.6 Artificial Neural Networks

As mentioned in the previous sections, the "fully coupled" approach is very computationally expensive as a dense mesh is often required to capture the yarn geometries and a microscale analysis needs to perform for each material point inside the yarns. To solve the efficiency challenge, a rapid yet accurate surrogate model is developed based on the artificial neural network (ANN) model. In recent years, ANN approach

has been used in modeling mechanical behavior of composite structures [58–60]. An ANN model usually contains three kinds of layers: input layer, hidden layer(s) and output layer. Models with more than three hidden layers are referred to deep neural network (DNN) models [61].

The relations between machine learning, neural network and deep learning are given in Figure 1.2. Compared with other machine learning approaches, deep learning approach has three main advantages. First, deep learning model is good at solving complex problems. Second, the model shows better performance when the training database is growing (see Figure 1.3). Third, deep learning model has relative less requirements for the pre-processing of the training data compared with other machine learning approaches which require careful engineering and considerable domain expertise to transform the raw data into a suitable internal representation or feature vector [61]. Although the ANN approach has been used in solving structural engineering problems decades ago, deep learning approach has led to remarkable achievements in recent years due to three technical forces driving advances in deep learning: Hardware, Datasets and Algorithmic advances [62].
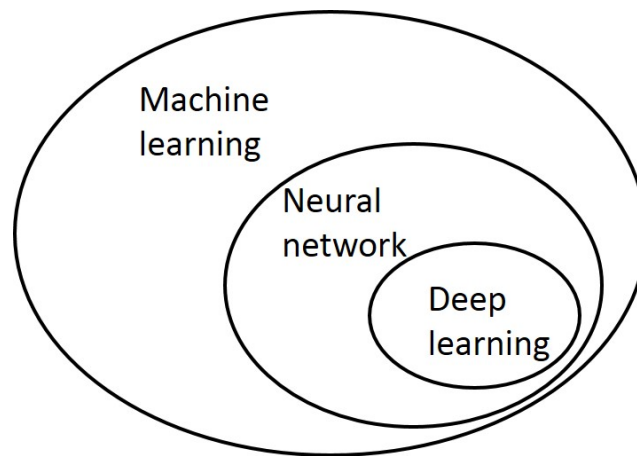
Figure 1.2. Relations between machine learning, neural network and deep learning

In most applications, ANN serves as an advanced curve-fitting method to construct a surrogate model that can improve the computational efficiency in some expensive
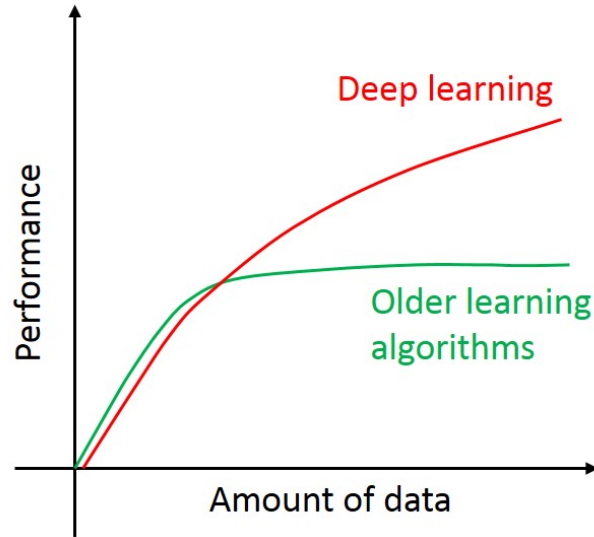
Figure 1.3. Comparison between deep learning and other machine learning approaches with increasing data

simulations. On the other hand, ANN can also be used as an universal approximation theorem tool [63] to approximate any functions when its explicit mathematical formulation is unknown or does not exist. The current failure criteria used in composites are mainly based on postulated polynomial functions of stress or strain fields with coefficients to be determined from experiments or sub-scale numerical models. Taking advantage of ANN, a failure criterion can be directly constructed using appropriate inputs and outputs, thereby avoiding the possible inaccuracies associated with postulated polynomial expressions.

1.3 Present Work and Outline

As reviewed in the above section, the traditional multiscale modeling approaches are mostly developed for laminated structures made of UD composites using CLPT, which may not work for the textile composites due to the interlaced yarns and aperiodic boundary conditions (aPBCs) in the thin and slender structures. In addition, the advanced approaches such as 3D RVE analysis using FEA are too expensive as a

dense mesh is often needed to capture the yarn path and cross-section shapes. For the modeling of thermoelastic and viscoelastic behaviors, in addition to the accuracy and efficiency issues, the current approaches also have limitations in capturing complex temperature loads or defining non-isotropic viscoelastic properties in commercial FEA software. Furthermore, most approaches in failure initiation analysis cannot capture the stress gradient along the thickness direction of thin structures or the transverse directions of slender structures. Also, the yarn failure criteria used in the initial failure analysis are questionable, while the scale coupled approach, although avoids using yarn failure criteria, is very computationally expensive.

To solve the above issues in the current multiscale modeling approaches of textile composites, this dissertation develops a novel multiscale modeling approach based on a powerful theory called mechanics of structure genome (MSG) [64] and advanced machine learning models. The multiscale models (Figure 1.4) in this dissertation starts from the microscale which contains the fiber and matrix. The effective properties of yarns are computed from the microscale analysis and then assigned to mesoscale model with different weave patterns. Finally, the effective structural properties such as 3D effective material properties, plate stiffness matrix or beam stiffness matrix can be computed based on effective properties of yarns and matrix with different BCs.

Figure 1.4. MSG-based multiscale models for textile composites

In Chapter 2, a MSG-based two-step homogenization approach is proposed to perform multiscale modeling of textile composites based on the properties of constituents at the microscale and different weave patterns at the mesoscale. MSG is enabled to capture pointwise anisotropy due to woven mesostructures. The finite thickness effects and inter-ply shift effects of textile composites are also accurately predicted by enabling MSG to treat aperiodic conditions in the thickness direction. This approach is extended to the structural analysis of thin and slender textile composite structures. Both the structural level response and local stress fields are predicted, which are compared with those predicted by DNS to compare accuracy and computational efficiency. The developed multiscale modeling approach is integrated into commercial FEM software MSC.Patran/Nastran as a multiscale modeling module. The constitutive information obtained from the MSG models can be directly converted to the information needed for defining the normal structural elements in MSC.Nastran. Examples are given to demonstrate the application of this multiscale modeling module in analyzing textile composite structures.

In Chapter 3, the MSG theory is extended to provide a novel two-step homogenization approach to predicting the viscoelastic behaviors of textile composites. The first homogenization step (micro-homogenization) deals with determining the viscoelastic properties of yarns from fibers (assumed to be linear elastic) and matrix (assumed to be linear viscoelastic) using the MSG solid model. In the second homogenization step (macro-homogenization), the viscoelastic behaviors of textile composites are computed from the homogenized yarns and matrix properties using the MSG plate model. RVE homogenization using FEA at microscale is conducted to verify the accuracy of MSG micro-homogenization. The viscoelastic behaviors of textile composites at macroscale using the MSG plate model are compared with experimental data.

In Chapter 4, MSG is extended to provide a unified approach to predicting the thermoelastic behaviors of composite structures. The variational statement of the MSG models has been modified to capture pointwise temperature distribution in composite structures. The effective CTEs are predicted using the MSG solid model

whose accuracy is validated using the 3D FEA. Thermal induced stress resultants are derived based on the extended MSG plate and beam models, which are used to describe the thermoelastic behaviors of thin or slender structures. The woven composite structures subjected to distributed temperature loads are analyzed using the proposed method. The results, including both the structural responses and local 3D stress fields, are predicted and compared with the ones from DNS using 3D FEA.

In Chapter 5, MSG-based multiscale modeling is extended for initial failure analysis of textile composite structures. A meso-micro scale coupled approach is proposed to predict initial failure strength constants of solid- and plate-like textile composite structures. The strength constants of the mesoscale model are predicted by directly connecting the stress field of each material point in the yarns to a microscale failure analysis. The failure criteria are used for fiber and matrix at the microscale so that no failure criterion is required for yarns at the mesoscale. Moreover, the strength constants predicted based on the MSG plate model are expressed in terms of plate stress resultants (i.e. plate forces and moments), which can capture the stress gradient in thin composite structures. The accuracy and efficiency of the proposed approach is validated using the corresponding 3D RVE analysis.

In Chapter 6, a new failure criterion for yarn is developed based on a micromechanical model using the MSG solid model and a deep learning neural network model. The proposed failure criterion can be applied to yarns in mesoscale textile composites modeling while capturing the failure initiation at the fiber and matrix level. A plain weave fiber reinforced composite material example is used to compute the initial failure strength constants of a woven lamina based on the proposed yarn failure criterion. The failure envelope analysis of the example is also carried out using the MSG solid model to further demonstrate the accuracy and efficiency of the new yarn failure criterion under combined loading conditions.

Finally, Chapter 7 summarizes this dissertation.

2. MULTISCALE ELASTIC ANALYSIS OF TEXTILE COMPOSITES

2.1 Mechanics of Structure Genome (MSG)

Mechanics of structural genome (MSG) is the key concept in our modeling approach in this dissertation, so the definition of MSG is introduced first. MSG was developed by Prof. Wenbin Yu in 2016 [64]. Starting from the original model which could be formulated using the 3D continuum mechanics, the structure gene (SG) is first identified, which is defined as the smallest mathematical block of the structure. The original problem is decoupled into a constitutive modeling over the SG and a corresponding macroscopic structural analysis. The constitutive modeling based on MSG models will not only compute the effective constitutive information for the macroscopic structural analysis but also performs dehomogenization to compute the local stress/strain/displacement fields. The effective constitutive information can be used to carry out structural analysis using conventional finite element software packages. Copyright permissions have been obtained to reuse the published materials from $[10, 11, 13, 14]$ in this chapter.

2.1.1 Kinematics of the MSG Models

Based on the MSG theory, the original 3D linear elasticity model is formulated in terms of 3D displacements (u_i), strains (ε_{ij}), stresses (σ_{ij}), and 3D Hooke's law. Then, macro-coordinates x_i and micro-coordinates y_i are introduced. The macro-coordinates x_i are used to describe the original structure, and micro-coordinates $y_i = x_i/\varepsilon$ are used to describe the SG. The ε is a small parameter because the microscopic size of the SG is much smaller than the macroscopic size of the structure. In multiscale

modeling, a field function of the original heterogeneous structure can be commonly expressed in terms of the macro-coordinates x_k which remain in the macroscopic structural model and the micro-coordinates y_j. The partial derivative of a function $f(x_k, y_j)$ can be expressed as:

$$\frac{\partial f(x_k, y_j)}{\partial x_i} = \frac{\partial f(x_k, y_j)}{\partial x_i}\Big|_{y_j=\text{const}} + \frac{1}{\varepsilon}\frac{\partial f(x_k, y_j)}{\partial y_i}\Big|_{x_k=\text{const}} \equiv f_{,i} + \frac{1}{\varepsilon}f_{|i} \qquad (2.1)$$

The 3D displacements of the MSG solid, plate and beam models are defined as the following [64]:

MSG solid model:

$$u_i(x_1, x_2, x_3, y_1, y_2, y_3) = \bar{u}_i(x_1, x_2, x_3) + \varepsilon\chi_i(x_1, x_2, x_3, y_1, y_2, y_3) \qquad (2.2)$$

MSG plate model:

$$u_1(x_1, x_2, y_1, y_2, y_3) = \bar{u}_1(x_1, x_2) - \varepsilon y_3\bar{u}_{3,1}(x_1, x_2) + \varepsilon\chi_1(x_1, x_2, y_1, y_2, y_3)$$
$$u_2(x_1, x_2, y_1, y_2, y_3) = \bar{u}_2(x_1, x_2) - \varepsilon y_3\bar{u}_{3,2}(x_1, x_2) + \varepsilon\chi_2(x_1, x_2, y_1, y_2, y_3) \qquad (2.3)$$
$$u_3(x_1, x_2, y_1, y_2, y_3) = \bar{u}_3(x_1, x_2) + \varepsilon\chi_3(x_1, x_2, y_1, y_2, y_3)$$

MSG beam model:

$$u_1(x_1, y_1, y_2, y_3) = \bar{u}_1(x_1) - \varepsilon y_2\bar{u}_{2,1}(x_1) - \varepsilon y_3\bar{u}_{3,1}(x_1) + \varepsilon\chi_1(x_1, y_1, y_2, y_3)$$
$$u_2(x_1, y_1, y_2, y_3) = \bar{u}_2(x_1) - \varepsilon y_3\Phi_1(x_1) + \varepsilon\chi_2(x_1, y_1, y_2, y_3) \qquad (2.4)$$
$$u_3(x_1, y_1, y_2, y_3) = \bar{u}_3(x_1) + \varepsilon y_2\Phi_1(x_1) + \varepsilon\chi_3(x_1, y_1, y_2, y_3)$$

where $\bar{u}_i$ and u_i are the displacements of the homogenized structure and the original heterogeneous structure respectively. Φ_1 is the beam sectional rotation. χ_1, χ_2, and χ_3 are the unknown fluctuating functions.

Next, we define the beam and plate strain measures. Beam strain measures:

$$\epsilon_1 = \bar{u}_{1,1}; \ \kappa_1 = \Phi_{1,1}; \ \kappa_2 = -\bar{u}_{3,11}; \ \kappa_3 = \bar{u}_{2,11} \qquad (2.5)$$

where ϵ_1 is the extensional strain, κ_1 is the twist rate, κ_2 and κ_3 are the beam bending curvatures about the x_2 and x_3 axes respectively.

Plate strain measures:

$$\epsilon_{\alpha\beta}(x_1, x_2) = \frac{1}{2}(\overline{u}_{\alpha,\beta} + \overline{u}_{\beta,\alpha}); \ \kappa_{\alpha\beta}(x_1, x_2) = -\overline{u}_{3,\alpha\beta} \tag{2.6}$$

where $\epsilon_{\alpha\beta}$ denote the in-plane strains, $\kappa_{\alpha\beta}$ denote the curvature strains.

The infinitesimal strain field can be defined as:

$$\varepsilon_{ij} = \frac{1}{2}(\frac{\partial u_i}{\partial x_j} + \frac{\partial u_j}{\partial x_i}) \tag{2.7}$$

Some constraints are needed for the fluctuating functions to satisfy several basic relations between original model and homogenized model, such as:

$$\overline{u}_i = \langle u_i \rangle; \qquad \overline{\varepsilon}_{ij} = \langle \varepsilon_{ij} \rangle \tag{2.8}$$

where the angle bracket "$\langle \cdot \rangle$" denotes the integration over the SG. Based on Eq. (2.7), the constraints for the fluctuating functions are:

$$\langle \chi_i \rangle = 0 \tag{2.9}$$

$$\langle \chi_{i|j} \rangle = 0 \tag{2.10}$$

For the MSG solid model, the Eqs. (2.9) and (2.10) must be satisfied. For the MSG plate and beam models, the Eq. (2.9) must be satisfied. For MSG beam model, additional constrains need to be applied as [65]:

$$\langle \chi_{3|2} - \chi_{2|3} \rangle = 0 \tag{2.11}$$

Eq. (2.9) indicates that the averaged displacements of the original structure and homogenized structure are the same based on the first equation in Eq. (2.8). Eq. (2.10) means that the averaged strains of the original structure and homogenized structure are the same based on the second equation in Eq. (2.8). Eq. (2.11) defines the twist angle of the macroscopic beam model in terms of the original position vector as pointed out in [65]. Note that we can also add additional constraints as needed. If the SG has periodicity along y_i direction, the equality of χ_i can be introduced on the corresponding periodic boundary in y_i direction as:

$$\chi_i^+ = \chi_i^- \tag{2.12}$$

The asymptotically smaller terms can be dropped based on variational asymptotic method (VAM) [66]. Then, the 3D strain field of MSG solid, plate and beam models can be written in a unified expression:

$$\Gamma = \Gamma_\epsilon \bar{\epsilon} + \Gamma_h \chi \tag{2.13}$$

where $\Gamma = \begin{bmatrix} \Gamma_{11} & \Gamma_{22} & \Gamma_{33} & 2\Gamma_{23} & 2\Gamma_{13} & 2\Gamma_{12} \end{bmatrix}^T$ is the strain field of the original structure, $\chi = \begin{bmatrix} \chi_1 & \chi_2 & \chi_3 \end{bmatrix}^T$ is the fluctuating function, and $\bar{\epsilon}$ is the generalized strain measures for the macroscopic structural model. For instance, the strain measures are $\bar{\epsilon} = \begin{bmatrix} \epsilon_1 & \kappa_1 & \kappa_2 & \kappa_3 \end{bmatrix}^T$ if the macroscopic structural model is a beam model. The strain measures are $\bar{\epsilon} = \begin{bmatrix} \epsilon_{11} & \epsilon_{22} & 2\epsilon_{12} & \kappa_{11} & \kappa_{22} & 2\kappa_{12} \end{bmatrix}^T$ if the macroscopic structural model is a plate/shell model. The strain measures are $\bar{\epsilon} = \begin{bmatrix} \bar{\epsilon}_{11} & \bar{\epsilon}_{22} & \bar{\epsilon}_{33} & 2\bar{\epsilon}_{23} & 2\bar{\epsilon}_{13} & 2\bar{\epsilon}_{12} \end{bmatrix}^T$ if the macroscopic structural model is a 3D Cauchy continuum model, where $\bar{\epsilon}_{ij}$ denotes the strain field of 3D homogenized body. Γ_ϵ is an operator matrix depending on the macroscopic structural model. Γ_h is an operator matrix depending on the dimensionality of the SG. The operator matrices can be derived based on the 3D displacements of MSG solid, plate and beam models given in Eqs. (2.2)-(2.4) and the infinitesimal strain field in Eq. (2.7). Note the asymptotically smaller terms have been dropped [67]. The explicit expressions for these operators can be found in Appendix A.

2.1.2 Variational Statement and Finite Element Implementation

The linear constitutive equation can be expressed as:

$$\sigma_{ij} = C_{ijkl}\varepsilon_{kl} \tag{2.14}$$

where C_{ijkl} is the elasticity tensor. Using the strain measures defined in Eq. (2.13), the strain energy density can be expressed as [68]:

$$U = \frac{1}{2\omega}\left\langle \Gamma^T C \Gamma \right\rangle \tag{2.15}$$

where ω denotes the volume of the domain spanned by y_k. MSG minimizes the energy loss of the original model and homogenized model. Since the energy of the homog-

enized model is independent of the fluctuating functions. The problem is equivalent to minimize Eq. (2.15) with respect to the fluctuating functions. The variational statement is:

$$\delta \frac{1}{2\omega} \left\langle \Gamma^T C \Gamma \right\rangle = 0 \qquad (2.16)$$

Plugging Eq. (2.13) into Eq. (2.16), the following equation can be obtained

$$\delta \frac{1}{2\omega} \left\langle (\Gamma_h \chi + \Gamma_\epsilon \bar{\epsilon})^T C (\Gamma_h \chi + \Gamma_\epsilon \bar{\epsilon}) \right\rangle = 0 \qquad (2.17)$$

In general, a numerical technique such as the finite element method is used to solve the variational statement in Eq. (2.17). Note that the usual finite element method uses the shape functions to approximate the displacements while MSG uses the shape functions to approximate the fluctuating functions. To this end, the fluctuating functions χ over SG can be expressed as:

$$\chi(x_k, y_j) = S(y_j)V(x_k) \qquad (2.18)$$

where S are the standard shape functions depending on the type of elements. V is what we need to solve for as the nodal values. Plugging Eq. (2.18) into Eq. (2.17), we obtain the following discretized version of the variational statement:

$$\delta \frac{1}{2\omega} \left(V^T E V + 2V^T D_{h\epsilon} \bar{\epsilon} + \bar{\epsilon}^T D_{\epsilon\epsilon} \bar{\epsilon} \right) = 0 \qquad (2.19)$$

where

$$E = \left\langle (\Gamma_h S)^T C(\Gamma_h S) \right\rangle, \quad D_{h\epsilon} = \left\langle (\Gamma_h S)^T C \Gamma_\epsilon \right\rangle, \quad D_{\epsilon\epsilon} = \left\langle \Gamma_\epsilon^T C \Gamma_\epsilon \right\rangle \qquad (2.20)$$

Performing the variation in Eq. (2.19) subjected to the constraints in Eqs. (2.9)-(2.11) based on different MSG models as well as other constrains (e.g. $\chi_i^+ = \chi_i^-$ if there is a periodic boundary condition in y_i direction) if needed, we can obtain the following linear system:

$$EV = -D_{h\epsilon} \bar{\epsilon} \qquad (2.21)$$

The solution V can be symbolically expressed as:

$$V = V_0 \bar{\epsilon} \qquad (2.22)$$

where $V_0 = -E^{-1}D_{h\epsilon}$.

Based on Eq. (2.22), the strain energy density can be rewritten as:

$$U = \frac{1}{2}\bar{\epsilon}^T\bar{C}\bar{\epsilon} \tag{2.23}$$

where

$$\bar{C} = \frac{1}{\omega}(V_0^T D_{h\epsilon} + D_{\epsilon\epsilon}) \tag{2.24}$$

Eq. (2.24) gives effective elastic properties of the macroscopic structural model. For the Euler-Bernoulli beam model, $\bar{C}$ could be a fully populated 4×4 stiffness matrix. For the Kirchhoff-Love plate/shell model and Cauchy continuum model, $\bar{C}$ could be a fully populated 6×6 stiffness matrix. The above constitutive information can be used to perform beam, plate or solid structural analysis. If the MSG plate model is used, the corresponding constitutive relation can be written as:

$$\begin{Bmatrix} N_{11} \\ N_{22} \\ N_{12} \\ M_{11} \\ M_{22} \\ M_{12} \end{Bmatrix} = \begin{bmatrix} A_{11} & A_{12} & A_{16} & B_{11} & B_{12} & B_{16} \\ A_{12} & A_{22} & A_{26} & B_{12} & B_{22} & B_{26} \\ A_{16} & A_{26} & A_{66} & B_{16} & B_{26} & B_{66} \\ B_{11} & B_{12} & B_{16} & D_{11} & D_{12} & D_{16} \\ B_{12} & B_{22} & B_{26} & D_{12} & D_{22} & D_{26} \\ B_{16} & B_{26} & B_{66} & D_{16} & D_{26} & D_{66} \end{bmatrix} \begin{Bmatrix} \epsilon_{11} \\ \epsilon_{22} \\ 2\epsilon_{12} \\ \kappa_{11} \\ \kappa_{22} \\ 2\kappa_{12} \end{Bmatrix} \tag{2.25}$$

where $\bar{C}$ is expressed in terms of the ABD matrix. Similarly, if the MSG beam model is used, the corresponding constitutive relation can be written as:

$$\begin{Bmatrix} F_1 \\ M_1 \\ M_2 \\ M_3 \end{Bmatrix} = \begin{bmatrix} C_{11}^b & C_{12}^b & C_{13}^b & C_{14}^b \\ C_{12}^b & C_{22}^b & C_{23}^b & C_{24}^b \\ C_{13}^b & C_{23}^b & C_{33}^b & C_{34}^b \\ C_{14}^b & C_{24}^b & C_{34}^b & C_{44}^b \end{bmatrix} \begin{Bmatrix} \epsilon_1 \\ \kappa_1 \\ \kappa_2 \\ \kappa_3 \end{Bmatrix} \tag{2.26}$$

where $\bar{C}$ is expressed in terms of a 4×4 stiffness matrix. After the structural analysis, the global structure responses $\bar{\epsilon}$ can be used to recover the local stress and strain field. The fluctuating function can be obtained as:

$$\chi = SV_0\bar{\epsilon} \tag{2.27}$$

Plug Eq. (2.27) into Eq. (2.13), the local strain field can be obtained as:

$$\Gamma = (\Gamma_h S V_0 + \Gamma_\epsilon)\bar{\epsilon} \qquad (2.28)$$

Based on the 3D constitutive relations in Eq. (2.14) for each constituent material, the local stress field can be recovered as:

$$\sigma = C\Gamma \qquad (2.29)$$

2.1.3 Material Coordinate System

For textile composites, material orientation varies along yarn path as shown in Figure 2.1. Since yarns are often modeled as orthotropic materials, the local material orientation must be captured. Due to the complexity of the microstructure in textile composites, a general purpose yet accurate description of material orientation is needed. Since MSG uses a finite element mesh to discretize the analysis domain, it can be extended to represent material orientation using element coordinates.
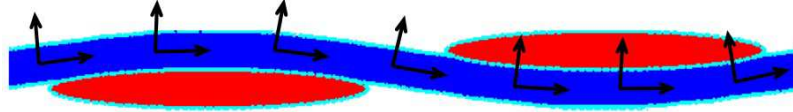
Figure 2.1. Material orientation varies along yarn path

MSG uses three points a, b, c to define the material coordinate system. Let's define x_i as the problem coordinate system and x_i' as the material coordinate system for each element. A line from point c to point a denotes the first direction and the line from point c to point b is in the x_1'-x_2' plane as shown in Figure 2.2. Speaking in the language of vectors, the material coordinate system is defined by three points with position vectors in the original coordinate system by $\boldsymbol{a}$, $\boldsymbol{b}$, $\boldsymbol{c}$. $\boldsymbol{a} - \boldsymbol{c}$ denotes a vector along the direction of $\boldsymbol{e}_1'$, $\boldsymbol{b} - \boldsymbol{c}$ is a vector in the x_1'-x_2' plane. With this information, one can compute the direction cosine matrix relating x_i to x_i' according to the following steps:

- Obtain e'_1 through normalization of $a - c$:

$$e'_1 = \frac{a - c}{|a - c|} \tag{2.30}$$

- Obtain e'_3 through normalization of the cross product of e'_1 and $b - c$:

$$e'_3 = \frac{e'_1 \times (b - c)}{|e'_1 \times (b - c)|} \tag{2.31}$$

- Obtain e'_2 through the cross product of e'_3 and e'_1:

$$e'_2 = e'_3 \times e'_1 \tag{2.32}$$
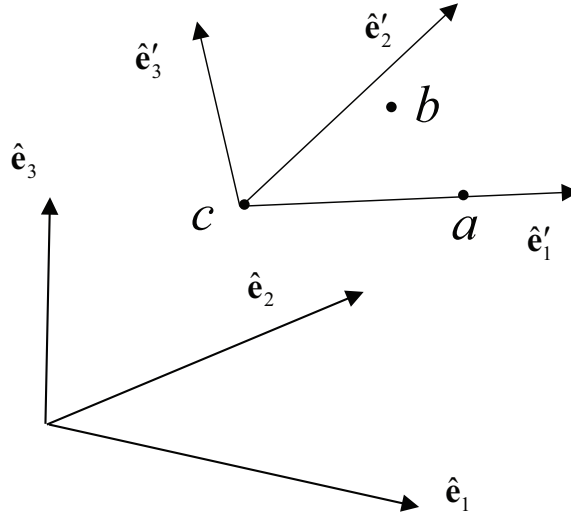
Figure 2.2. Material coordinate system defined by three points

The direction cosine matrix can be obtained by $\beta_{ij} = e_i \cdot e'_j$, then the transformation matrix R_σ is

$$R_\sigma = \begin{bmatrix} \beta_{11}^2 & \beta_{12}^2 & \beta_{13}^2 & 2\beta_{12}\beta_{13} & 2\beta_{11}\beta_{13} & 2\beta_{11}\beta_{12} \\ \beta_{21}^2 & \beta_{22}^2 & \beta_{23}^2 & 2\beta_{22}\beta_{23} & 2\beta_{21}\beta_{23} & 2\beta_{21}\beta_{22} \\ \beta_{31}^2 & \beta_{32}^2 & \beta_{33}^2 & 2\beta_{32}\beta_{33} & 2\beta_{31}\beta_{33} & 2\beta_{31}\beta_{32} \\ \beta_{21}\beta_{31} & \beta_{22}\beta_{32} & \beta_{23}\beta_{33} & \beta_{23}\beta_{32} + \beta_{22}\beta_{33} & \beta_{23}\beta_{31} + \beta_{21}\beta_{33} & \beta_{22}\beta_{31} + \beta_{21}\beta_{32} \\ \beta_{11}\beta_{31} & \beta_{12}\beta_{32} & \beta_{13}\beta_{33} & \beta_{13}\beta_{32} + \beta_{12}\beta_{33} & \beta_{13}\beta_{31} + \beta_{11}\beta_{33} & \beta_{12}\beta_{31} + \beta_{11}\beta_{32} \\ \beta_{11}\beta_{21} & \beta_{12}\beta_{22} & \beta_{13}\beta_{23} & \beta_{13}\beta_{22} + \beta_{12}\beta_{23} & \beta_{13}\beta_{21} + \beta_{11}\beta_{23} & \beta_{12}\beta_{21} + \beta_{11}\beta_{22} \end{bmatrix} \tag{2.33}$$

The material properties in the material coordinate system can be transformed to the problem coordinate system as

$$C = R_\sigma C' R_\sigma^T \tag{2.34}$$

2.1.4 Advantages of using MSG for Modeling Textile Composites

MSG offers two main advantages over the contemporary analytical approaches. First, local material orientation varies along with the yarn path, which usually needs to be prescribed using some functions in most analytical approaches. Since MSG discretizes the analysis domain using finite elements, the local material orientation is easily described using element local coordinates. Second, it is difficult to use just one analytical approach to solve all kinds of textile composites (e.g. 2D woven, non-crimp fabric and weft knit fabric). Usually, analytical models are formulated for a specific weave style and geometry, then different assumptions must be made for different textile composites. However, MSG provides a unified approach to all kinds of textile composites, because a general microstructure can be accurately described using finite element meshes.

The above two issues may also be solved by the RVE analysis using 3D FEA, but MSG also has some advantages over RVE analysis. First, applying the right boundary conditions is crucial for RVE analysis and it is not always straightforward. On the contrary, one can directly use MSG to compute effective properties without applying boundary conditions by the user. Second, RVE analysis usually requires the periodicity in three directions (i.e. x-, y- and z-directions). However, for very thin textile composites the periodicity requirement is not satisfied in the thickness direction. In this case, applying the right boundary conditions to get the complete set of 3D properties is not trivial in RVE analysis. However, MSG can easily handle aPBCs in any directions for textile composites, because the theory does not require the regular boundary conditions in terms of traction or displacements as in the RVE analysis. If the SG is indeed periodic, then MSG can also solve the problem by enforcing the

periodicity of the fluctuating functions. Moreover, MSG unifies the micromechanics and structural mechanics so that the structural properties can be directly computed from the micro/mesostructures. In addition to the effective material properties, the structural properties also include beam and plate stiffness matrix which can be used to analyze slender and thin composite structures. The SG of textile composites especially for 3D woven composites does no follow the commonly used scale separation assumptions and therefore is better captured by beam or plate stiffness matrix for a structural analysis. Third, computational efficiency is another issue for RVE analysis. RVE analysis requires solving six static problems to obtain the complete set of 3D properties because the coefficient matrix of the linear system is affected by the coupled equation constraints used to apply the PBCs. While MSG can be implemented using the finite element method so that the linear system will be factorized once. Theoretically speaking, MSG could be five to six times more efficient than RVE analysis. In reality, since MSG computes effective properties directly without computing the stress first then average the stress as those been done in RVE analysis. MSG can achieve the same accuracy as RVE analysis with much better efficiency. In addition, MSG models only require to solve the system of equations once for recovering local fields under different loading conditions while the RVE analysis needs to solve the system for every different loading conditions. This advantage will greatly accelerate the failure analysis such as constructing the failure envelope, which will be detailed discussed later in this dissertation. It is noted that the real time taken by a computer code depends not only on the theory behind the code but also many other factors and it is not easy to compare the efficiency of two computer codes.

2.2 Two-step Homogenization for Textile Composites

A two-step homogenization approach is used to obtain the effective properties of textile composites. To use MSG, we need to identify SG, which is similar as other micromechanics approaches to identifying RVE. However, SG is different from RVE

because SG is defined as the smallest mathematical building block of the structure. For example, in order to get 3D material properties, RVE is required to be a 3D domain but the SG can be one-dimensional (1D), 2D or 3D domains. As will be shown later, the yarn properties can be obtained by a 2D SG instead of a 3D RVE which can reduce the computational time without loss of accuracy. For textile composites, the SG is relatively easy to identify since most textile composites are made by repeating a fixed pattern. At microscale level, we compute the effective properties of the yarn which is composed of the fibers and matrix using a 2D SG. Then we use the effective properties of the yarns and matrix to compute the effective properties of the textile composite. As mentioned in the last section, another advantage of MSG is that it can easily relieve the periodicity in any directions but still obtain the complete set of 3D elastic properties. For the thin structures made by textile composites, it is not realistic to assume the periodicity in the thickness direction. Such problems can be easily solved in a systematic way using MSG. The general procedure for the two-step homogenization approach using MSG is shown in Figure 2.3.

2.2.1 Geometry Modeling of Textile Composites

TexGen is an open source software for the geometric modeling of textile composites that was developed at the University of Nottingham [69]. A yarn path in TexGen is described by a number of discrete positions. Spline interpolation is used to interpolate these points to get the accurate yarn path [70]. An analytical form of the area of a power ellipse has been used to create the cross section of yarns [71]. TexGen can generate ABAQUS mesh files and assign local orientation for each element, which is very important for accurate modeling of textile composites. We have implemented the extended MSG into SwiftComp$^{\text{TM}}$, a general-purpose multiscale constitutive modeling code. Exploiting the geometric capabilities of TexGen and constitutive modeling capabilities of SwiftComp$^{\text{TM}}$, TexGen4SC provides a fast and easy way to compute the effective properties of textile composites. A screenshot of this new software Tex-
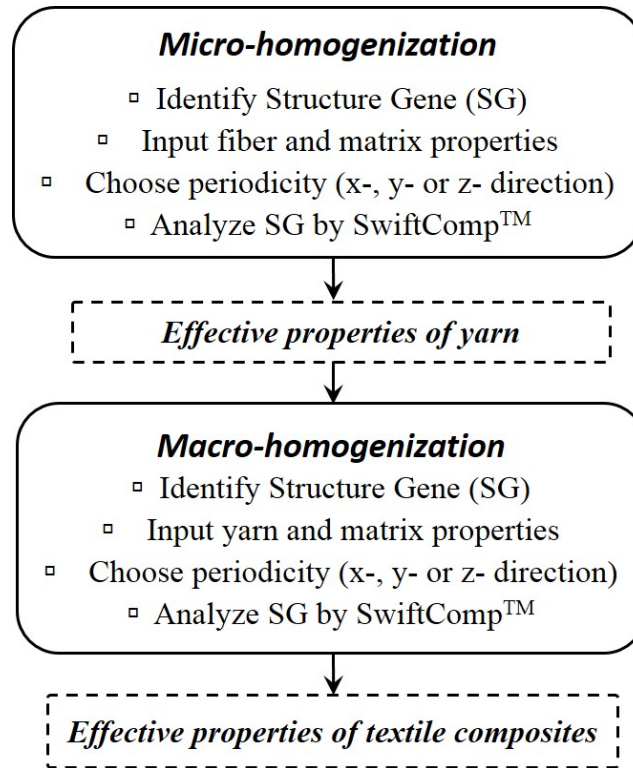
Figure 2.3. Two-step homogenization of textile composites

Gen4SC is shown in Figure 2.4. All the numerical examples used in this section were generated and analyzed by TexGen4SC. A short introduction of TexGen4SC is given in Appendix B.

2.2.2 Micro-homogenization for Yarns

Each yarn, embedded in woven composites, consists of many fibers and the matrix material. In these yarns, fibers are densely packed and bonded together by the matrix material. They are commonly modeled as unidirectional composites. The complete set of 3D elastic properties of yarns can be determined by MSG using a 2D SG because the heterogeneity is only in two directions. It is emphasized here that although the analysis domain is 2D, the strain energy of this 2D SG is expressed in terms of the 3D strain field which enables us to compute a 6×6 stiffness matrix as the complete set of
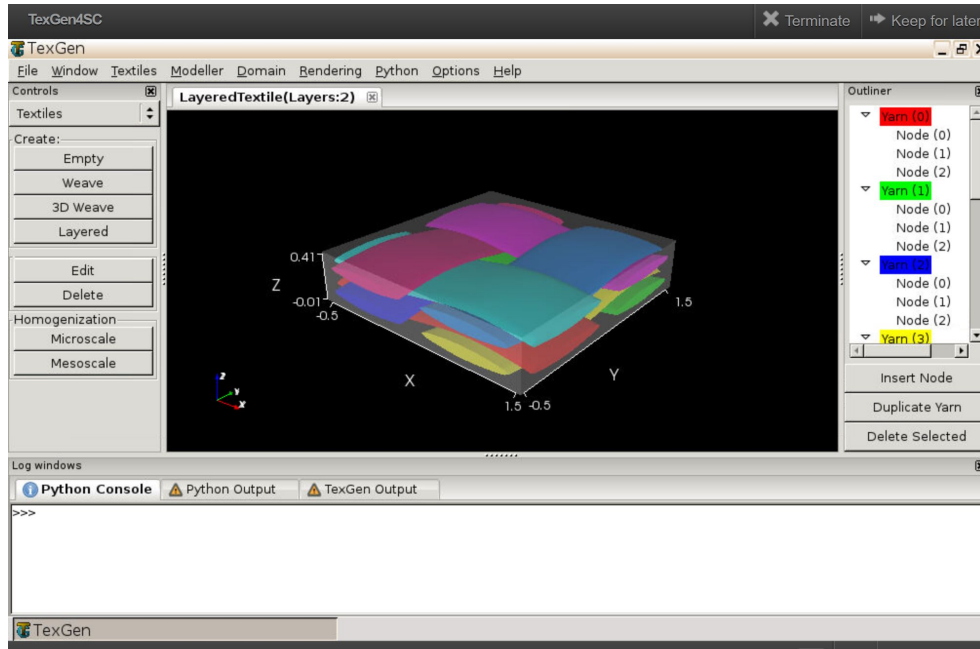
Figure 2.4. TexGen4SC on the cloud through cdmHUB.org

3D properties. As shown in the following example, MSG can compute 3D properties using a 2D SG with the same accuracy as that of 3D RVE analysis in a more efficient manner.

To evaluate the MSG-based yarn model, a data set for carbon fiber (T-300) and epoxy resin-3601 is taken from [72]. These properties are presented in Table 2.1. The fiber volume ratio in the yarn is considered 80%. The hexagonal shaped 2D SG which contains 824 four-node quadrilateral elements is shown in Figure 2.5. The effective properties of the yarn are computed based on this model using SwiftComp$^{\text{TM}}$.

To compare the accuracy of elastic constants obtained using MSG, 3D FEA analysis of a yarn RVE is conducted in the commercial code Abaqus 6.13 as shown in Figure 2.5, which has the same fiber volume ratio as of the 2D SG. This yarn RVE is extruded based on 2D SG with just one element in the fiber direction, and discretized to generate periodic mesh using 8-noded hexahedral elements (C3D8). After a convergence study, the finite element mesh consists of 824 C3D8 elements. The elastic
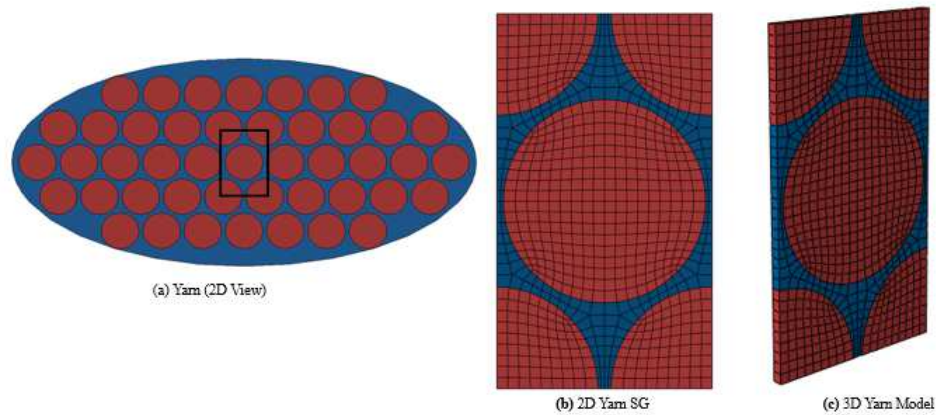
Figure 2.5. 2D SG and 3D RVE for the yarn model

Table 2.1. Mechanical properties of the constituents for epoxy 3601/carbon T-300 plain woven composite

Elastic constants	Matrix	Fiber
E_1 (GPa)	4.51	208.8
$E_2{=}E_3$ (GPa)	4.51	43
$G_{12}{=}G_{13}$ (GPa)	1.7	7.42
G_{23} (GPa)	1.7	7.42
$\nu_{12}{=}\nu_{13}$	0.38	0.2
ν_{23}	0.38	0.499

properties of the yarn RVE are determined by applying PBCs using six independent steps.

Table 4.3 compares the elastic constants predicted by MSG and 3D FEA, and "Diff1" in the table is defined as

$$\text{Diff1} = \frac{\|\text{MSG (PBCs) results - 3D FEA results}\|}{\text{3D FEA results}} \times 100\% \qquad (2.35)$$

An excellent agreement is seen in all nine constants. The percentage difference is less than one percent in all the cases. However, MSG is 10 times more efficient than

3D FEA for this case which is expected as MSG uses only one 2D analysis while RVE analysis requires six 3D analyses.

Table 2.2. Comparison between MSG and 3D FEA results

	2D SG	3D FEA	Diff1 (%)
Number of elements	824	824	
Computational time (s)	0.208	3	
E_1 (GPa)	167.702	167.702	0.000%
E_2 (GPa)	22.762	22.702	0.264%
E_3 (GPa)	22.762	22.702	0.264%
G_{12} (GPa)	5.101	5.104	0.059%
G_{13} (GPa)	5.101	5.104	0.059%
G_{23} (GPa)	5.136	5.129	0.136%
ν_{12}	0.230	0.231	0.217%
ν_{13}	0.230	0.231	0.217%
ν_{23}	0.490	0.490	0.000%

2.2.3 Macro-homogenization for Textile Composites

Once the properties of yarns are obtained from micro-homogenization analysis, we are ready to perform a marco-homogenization analysis to compute the properties of the textile composites. For macro-homogenization of the textile composites, 3D SG models with periodicity in all three directions, denoted as MSG (PBCs), and only in the in-plane directions, denoted as MSG (aPBCs), are created and analyzed. The effective properties of several common textile composites are predicted in the following sections. Since SG is defined as the smallest mathematical building block of a structure, the SG model should be chosen in a way that the entire structure can be reconstructed by repeating this SG along different directions. For example, if SG has periodicity in all three directions, then the entire textile composites can be reconstructed by repeating this SG in all three directions. If we consider aPBCs

along the thickness direction, then the original textile composites can be obtained by repeating SG in x and y direction. Textile composites are often made by repeating a fixed pattern, which can be easily identified as the corresponding SG. Figures 2.6 - 2.8 show the typical 2D woven fabric composites and the corresponding SG, and Figures 2.9 -2.10 show the SG for different 3D woven fabric composites. In order to demonstrate the accuracy and efficiency of MSG, the same models with identical mesh size and element type are used for 3D RVE analysis by Abaqus 6.13. The difference of the results using MSG and 3D RVE with PBCs in three directions are compared using "Diff1" defined as in Eq. (2.35). The difference between MSG (aPBCs) and 3D RVE analysis with PBCs is compared using "Diff2" defined as

$$\text{Diff2} = \frac{\|\text{MSG (aPBCs) results - 3D FEA results}\|}{\text{3D FEA results}} \times 100\% \qquad (2.36)$$

Plain woven composites

The typical plain weave and the corresponding SG is shown in Figure 2.6. The SG contains 2 warp yarns and 2 weft yarns. The yarn spacing is 1 unit and yarn width is 0.8 unit. The fabric thickness is 0.2 unit and the yarn has an elliptical cross section. The 3D model contains 16,000 C3D8 elements generated using TexGen4SC. Table 2.3 presents the results using MSG with aPBCs in the thickness direction and with PBCs in all three directions. The 3D RVE analysis results are compared with MSG results.

As observed from Table 2.3, all the nine engineering constants computed using MSG (PBCs) agree well with 3D FEA results, and all the differences are within 1%. However, MSG (PBCs) is about 15 times faster than 3D FEA. The results obtained using MSG (aPBCs) are smaller than the corresponding results using MSG (PBCs) except G_{12} and ν_{12}. G_{12} is the same as 3D FEA result and very close to MSG (PBCs) result, and ν_{12} is almost twice of those predicted using MSG (PBCs) and 3D FEA. Removing the periodic boundary conditions along the thickness direction significantly
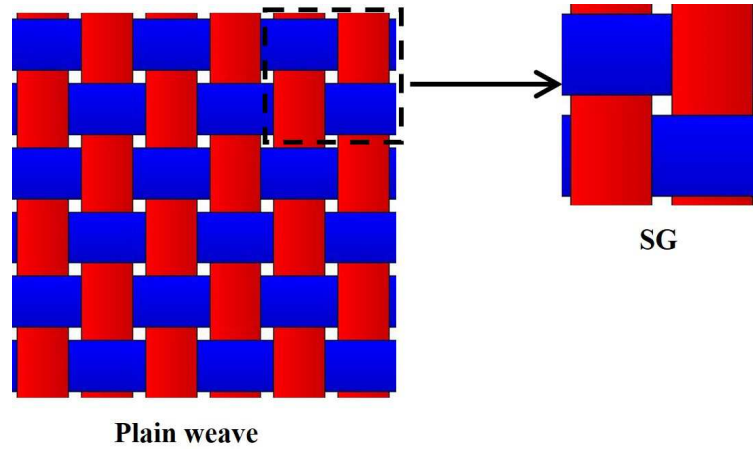
Figure 2.6. plain weave and its SG

Table 2.3. MSG and 3D FEA results for plain woven composites

	MSG (aPBCs)	MSG (PBCs)	3D FEA	Diff1 (%)	Diff2 (%)
Computational time (s)	16.038	10.782	160		
$E_1=E_2$ (GPa)	43.041	50.261	49.952	0.619%	13.835%
E_3 (GPa)	13.350	14.983	14.905	0.523%	10.433%
G_{12} (GPa)	3.414	3.416	3.414	0.059%	0.000%
$G_{13}=G_{23}$ (GPa)	2.913	3.140	3.133	0.223%	7.022%
ν_{12}	0.257	0.138	0.137	0.730%	87.591%
$\nu_{13}=\nu_{23}$	0.386	0.424	0.424	0.000%	8.962%

affects all of the elastic constants except in-plane shear modulus. The computational time of MSG (aPBCs) is about 10 times faster than 3D FEA.

Twill woven composites

The 2×2 twill weave and the corresponding SG is shown in Figure 2.7. The SG contains 4 warp yarns and 4 weft yarns. The yarn spacing is 1 unit and yarn width is 0.8 unit. The fabric thickness is 0.4 unit and the yarns have elliptical cross sections. Similarly, the model is generated by TexGen4SC and the effective properties

are computed by invoking SwiftComp$^{\text{TM}}$. The model contains 25,000 C3D8 elements and the results using MSG with both aPBCs and PBCs and 3D RVE analysis are given in Table 2.4.

2X2 twill

SG
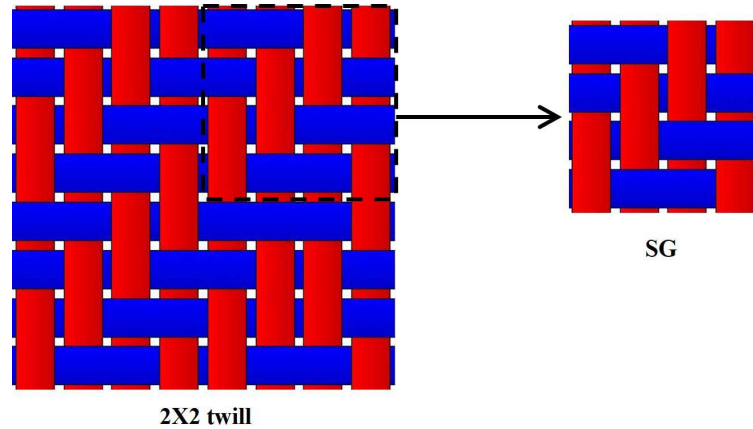
Figure 2.7. 2×2 twill weave and its SG

Table 2.4. MSG and 3D FEA results for 2×2 twill composites

	MSG (aPBCs)	MSG (PBCs)	3D FEA	Diff1 (%)	Diff2 (%)
Computational time (s)	62.563	19.938	217		
$E_1=E_2$ (GPa)	39.815	48.569	48.287	0.584%	17.545%
E_3 (GPa)	13.990	15.572	15.449	0.792%	9.444%
G_{12} (GPa)	3.415	3.445	3.441	0.116%	0.756%
$G_{13}=G_{23}$ (GPa)	3.266	3.513	3.500	0.371%	6.686%
ν_{12}	0.297	0.154	0.153	0.654%	94.118%
$\nu_{13}=\nu_{23}$	0.375	0.428	0.429	0.233%	12.587%

Based on the results, all the nine engineering constants computed using MSG (PBCs) agree well with 3D FEA results, and all the differences are within 1%. By comparing the computational time, MSG (PBCs) approach is about 11 times faster than 3D FEA. The results obtained using MSG (aPBCs) are smaller than the corresponding results using MSG (PBCs) except G_{12} and ν_{12}. G_{12} is slightly smaller than 3D FEA and MSG (PBCs) result, and ν_{12} almost doubles those predictions us-

ing MSG (PBCs) and 3D FEA. Again, we can conclude that removing the periodic boundary conditions along the thickness direction significantly affects all of the elastic constants except in-plane shear modulus. The computational time of MSG (aPBCs) is about 3.5 times faster than 3D FEA.

5-harness satin woven composites

The 5-harness satin weave and the corresponding SG is shown in Figure 2.8. The SG contains 5 warp yarns and 5 weft yarns. The yarn spacing is 1 unit and yarn width is 0.8 unit. The fabric thickness is 0.4 unit and the ellipse cross section is used for the yarn. The model contains 36,000 C3D8 elements and the corresponding results are given in Table 2.5.
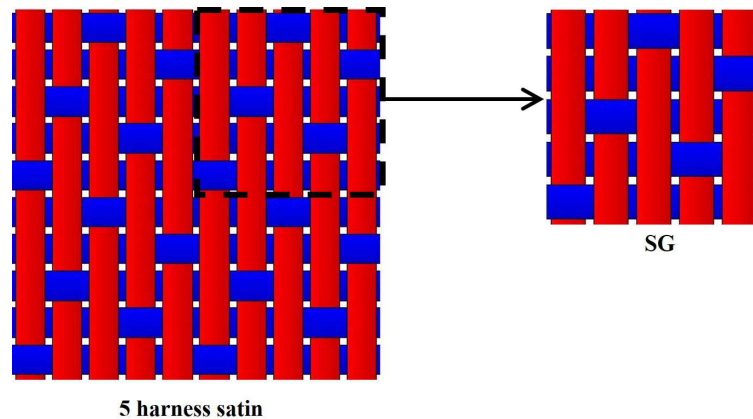
Figure 2.8. 5-harness satin weave and its SG

As observed from the results listed in Table 2.5, all the nine engineering constants computed using MSG (PBCs) agree well with 3D FEA results, and all the differences are within 1%. By comparing the computational time, MSG (PBCs) approach is about 17 times faster than 3D FEA. The results obtained using MSG (aPBCs) are smaller than the corresponding results using MSG (PBCs) except G_{12} and all the Poisson's ratios. MSG (aPBCs) predicts G_{12} slightly smaller than the 3D FEA and MSG (PBCs) result, and ν_{12} much larger than the result using MSG (PBCs) and

Table 2.5. MSG and 3D FEA results for 5-harness satin composites

	MSG (aPBCs)	MSG (PBCs)	3D FEA	Diff1 (%)	Diff2 (%)
Computational time (s)	74.095	25.048	434		
$E_1=E_2$ (GPa)	46.785	51.579	51.340	0.465%	8.872%
E_3 (GPa)	14.264	15.941	15.806	0.854%	9.756%
G_{12} (GPa)	3.493	3.528	3.525	0.085%	0.908%
$G_{13}=G_{23}$ (GPa)	3.281	3.503	3.492	0.315%	6.042%
ν_{12}	0.164	0.116	0.116	0.000%	41.379%
$\nu_{13}=\nu_{23}$	0.438	0.438	0.439	0.228%	0.228%

3D FEA. We can conclude that removing the periodic boundary conditions along the thickness direction significantly affects all of the elastic constants except in-plane shear modulus and two out-of-plane Poisson's ratios (ν_{13} and ν_{23}). The computational time of MSG (aPBCs) is about 6 times faster than 3D FEA.

3D orthogonal woven composites

The previous examples can be considered as 2D or 2.5D model which only contains one layer. In addition to that, 3D woven composites are widely used in recent years due to the improved properties in the transverse direction and high production speed which reduces the manufacturing cost and cycle times. A 3D model of orthogonal woven composites is built as shown in Figure 2.9. The model contains 3 layers with 2 weft yarns in each layer. The weft yarn spacing is 1 unit, yarn width is 0.8 unit and yarn height is 0.1 unit. There are 2 layers with 2 warp yarns in each layer and 1 binder yarn. The warp yarn spacing is 1 unit, yarn width is 0.8 unit and yarn height is 0.1 unit. The cross sections of all the yarns in this model are elliptical cross sections. The model contains 50,000 C3D8 elements and the corresponding results are given in Table 2.6.

As observed from Table 2.6, all the nine engineering constants computed using MSG PBCs agree well with 3D FEA results and all the differences are within 1%.
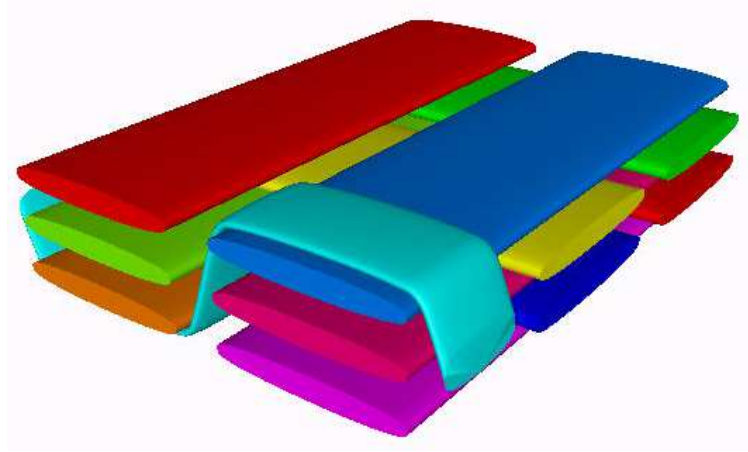
Figure 2.9. SG for 3D orthogonal woven composites

Table 2.6. MSG and 3D FEA results for 3D orthogonal woven composites

	MSG (aPBCs)	MSG (PBCs)	3D FEA	Diff1 (%)	Diff2 (%)
Computational Time (s)	165.253	172.846	783		
E_1 (GPa)	32.757	33.010	32.974	0.109%	0.658%
E_2 (GPa)	51.188	51.229	51.211	0.035%	0.045%
E_3 (GPa)	10.907	11.170	11.126	0.395%	1.968%
G_{12} (GPa)	2.879	2.881	2.880	0.035%	0.035%
G_{13} (GPa)	2.433	2.443	2.433	0.411%	0.000%
G_{23} (GPa)	2.419	2.451	2.449	0.082%	1.225%
ν_{12}	0.0608	0.0618	0.0617	0.162%	1.459%
ν_{13}	0.507	0.496	0.497	0.201%	2.012%
ν_{23}	0.461	0.454	0.456	0.439%	1.096%

By comparing the computational time, MSG (PBCs) approach is about 4.5 times faster than 3D FEA. The results obtained using MSG (aPBCs) are very close to the corresponding results using MSG (PBCs) and the 3D FEA results. Some properties using MSG (aPBCs) such as E_1, E_2, G_{12} and G_{13} are almost the same as the results using MSG (PBCs) and 3D FEA. The out of plane properties $(E_3, G_{23}, \nu_{12}, \nu_{13}, \nu_{23})$ have some slight differences with the largest difference around 2%. The computational time of MSG (aPBCs) is about 4.7 times faster than 3D FEA.

Woven laminates with inter-ply shifts

Inter-ply shifting in textile laminates is a common phenomenon during composites manufacturing. This inter-ply shifting affects the mechanical behavior of laminates. Due to the limitations of experimental work such as manufacturing complexity and small unit cell size, multi-scale modeling is usually used to investigate this effect. Four-ply thick woven laminates of balanced 2/2 twill woven fabric are generated and analyzed using TexGen4SC. The four inter-ply shift configurations [73], named as Periodic, Symmetric, Step, and Stairs were modeled for homogenization, which are presented in Figure 2.10.

1. Periodic: no shift in ply;

2. Symmetric: alternate plies are shifted to two units distance in the warp direction;

3. Step: alternate plies are shifted to one unit distance in the warp direction;

4. Stairs: each ply is shifted to one unit in the warp direction.
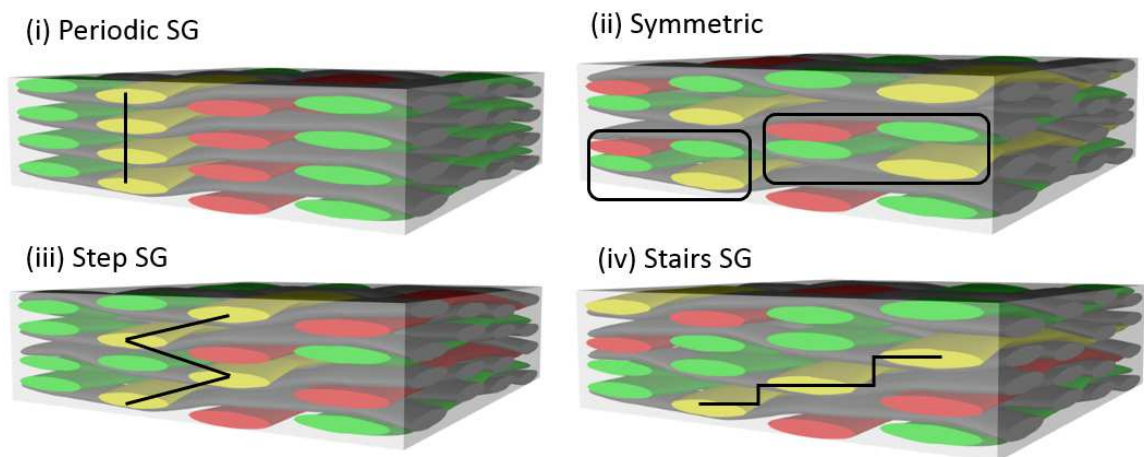
Figure 2.10. SGs for 3D orthogonal woven composites with different inter-ply shifts

Each model was meshed using 194,672 C3D8 elements and the corresponding results are given in Tables 2.7-2.10.

Table 2.7. MSG and 3D FEA results for periodic stacking woven composites

	MSG (aPBCs)	MSG (PBCs)	3D FEA	Diff1 (%)	Diff2 (%)
Computational time (s)	791	1123	2407		
$E_1=E_2$ (GPa)	52.117	53.153	52.737	0.789%	1.176%
E_3 (GPa)	14.174	15.502	15.433	0.447%	8.158%
G_{12} (GPa)	3.412	3.419	3.416	0.088%	0.117%
$G_{13}=G_{23}$ (GPa)	3.121	3.204	3.191	0.407%	2.194%
ν_{12}	0.108	0.096	0.096	0.000%	12.500%
$\nu_{13}=\nu_{23}$	0.446	0.431	0.432	0.231%	3.241%

Table 2.8. MSG and 3D FEA results for symmetric stacking woven composites

	MSG (aPBCs)	MSG (PBCs)	3D FEA	Diff1 (%)	Diff2 (%)
Computational time (s)	657	1146	2368		
$E_1=E_2$ (GPa)	54.649	54.870	54.380	0.901%	0.495%
E_3 (GPa)	14.099	15.360	15.295	0.425%	7.820%
G_{12} (GPa)	3.399	3.400	3.396	0.118%	0.088%
$G_{13}=G_{23}$ (GPa)	3.201	3.327	3.312	0.453%	3.351%
ν_{12}	0.064	0.065	0.065	0.000%	1.538%
$\nu_{13}=\nu_{23}$	0.468	0.445	0.445	0.000%	5.169%

Based on the results listed in these four tables, we can observe that all the nine engineering constants computed using MSG (PBCs) agree well with 3D FEA results and all the differences are within 1%. In terms of efficiency, MSG (PBCs) in all the four examples are about two times faster than 3D FEA. Although these four models have different architectures, in-plane modulus using MSG (aPBCs) (E_1, E_2 and G_{12}) are almost the same as the results using MSG (PBCs) and 3D FEA. It can also be observed that the effects to the transverse Young's modulus E_3 remain similar among these four different architectures. The differences of other properties predicted by

Table 2.9. MSG and 3D FEA results for step stacking woven composites

	MSG (aPBCs)	MSG (PBCs)	3D FEA	Diff1 (%)	Diff2 (%)
Computational time (s)	1122	1121	2461		
$E_1=E_2$ (GPa)	53.433	54.196	53.775	0.785%	0.636%
E_3 (GPa)	14.156	15.460	15.393	0.435%	8.036%
G_{12} (GPa)	3.407	3.412	3.409	0.088%	0.059%
$G_{13}=G_{23}$ (GPa)	3.167	3.267	3.253	0.430%	2.644%
ν_{12}	0.086	0.080	0.080	0.000%	7.500%
$\nu_{13}=\nu_{23}$	0.457	0.438	0.439	0.228%	4.100%

Table 2.10. MSG and 3D FEA results for stairs stacking woven composites

	MSG (aPBCs)	MSG (PBCs)	3D FEA	Diff1 (%)	Diff2 (%)
Computational Time (s)	1110	1142	2356		
$E_1=E_2$ (GPa)	54.699	55.085	54.623	0.846%	0.139%
E_3 (GPa)	14.168	15.486	15.418	0.441%	8.107%
G_{12} (GPa)	3.406	3.410	3.407	0.088%	0.029%
$G_{13}=G_{23}$ (GPa)	3.183	3.295	3.279	0.488%	2.928%
ν_{12}	0.065	0.066	0.066	0.000%	1.515%
$\nu_{13}=\nu_{23}$	0.467	0.444	0.444	0.000%	5.180%

different methods vary with respect to the inter-ply shifts. The computational time of MSG (aPBCs) in the four models is 2 to 3 times faster than 3D FEA.

2.2.4 Results and Discussions

All the meshes of the woven composite examples studied above are generated by TexGen4SC, and the voxel mesh is used to avoid distorted elements. However, the number of elements of a voxel mesh is required to be high to achieve accurate representation of the textile geometry [74]. This limitation results in considerable computation resources and time in 3D RVE analysis. However, we can conclude from the above examples that MSG computational time is much faster than 3D RVE

analysis with the same mesh size. The percentage difference between MSG (PBCs) and 3D FEA is less than one percent in all properties in all the examples. In other words, MSG can provide the results as accurate as 3D RVE analysis using FEA with greatly improved computational efficiency.

In addition, the homogenized properties with aPBCs considering finite thickness effect are also computed using MSG. The difference of the results between MSG (aPBCs) and MSG (PBCs) is more obvious for 2D or 2.5D woven composites than complex 3D woven composites. For the results of 3D woven composites using MSG (aPBCs), the in-plane properties of 3D SG with different architectures are almost the same as the corresponding results using MSG (PBCs) and 3D FEA, but the out-of-plane properties and Poisson's ratios have relatively larger difference comparing with MSG (PBCs) and 3D FEA results. This behavior is easy to understand since we only relieve the periodicity in the thickness direction which should not have much effects on the in-plane direction if the analysis domain is relatively thick. If the textile composites is very thick, then the boundary conditions along the thickness direction will not noticeably affect the in-plane properties, which explains why plain weave, 2×2 twill and 5 harness satin composites have larger differences between the results obtained by PBCs and aPBCs. To further illustrate this point, addition numerical tests are performed from 2-layer to 5-layer plain woven composites with aPBCs. The results, normalized by 3D FEA results, are shown in Figure 2.11. The in-plane Young's moduli E_1 and E_2 are converging to one with the increased layers, which means E_1 and E_2 are converging to the results obtained using 3D FEA using PBCs. Although E_3 is also converging to 3D FEA using PBCs, the difference is still relatively large and the converging speed is much slower than E_1 and E_2. For the shear moduli shown in Figure 2.11(b), G_{12} obtained using MSG (aPBCs) is the same as 3D FEA results and does not change with the increased layers. G_{13} and G_{23} exhibit a slow convergence to the 3D FEA results. For the Poisson's ratios in Figure 2.11(c), ν_{12} has very large difference compared with 3D FEA results when there is only one layer, then it rapidly converges to 3D FEA results, which implies that ν_{12} is sensitive to the

boundary effects in the thickness direction. ν_{13} and ν_{23} converge to 3D FEA results when there are two layers. The convergence behavior of engineering constants with respect to increased layers using MSG (aPBCs) also agrees well with the observations in the literature [75].
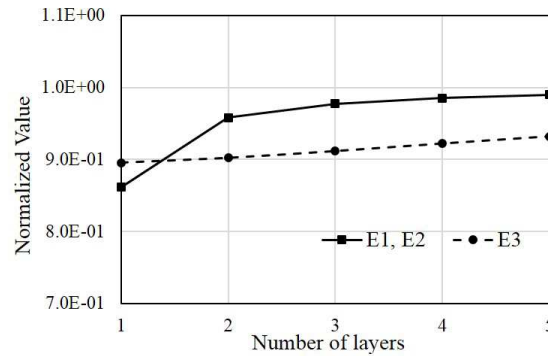
(a) Young's modulus
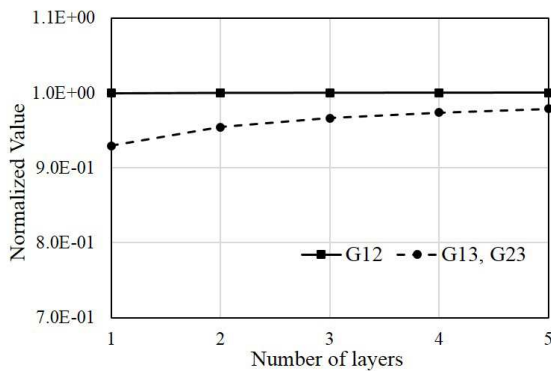
(b) Shear modulus
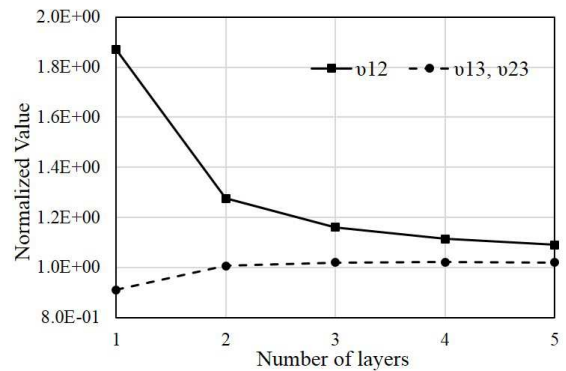
(c) Poisson's ratio

Figure 2.11. Normalized engineering constants using MSG (aPBCs) with different layers

The above results and discussions show that MSG (aPBCs) can provide reasonable results and predict the finite thickness effects and inter-ply shift effects. The out-of-plane properties and Poisson's ratio obtained using MSG (aPBCs) show distinct differences compared with 3D RVE analysis using PBCs. All the effects are accurately captured using MSG (aPBCs) which are important for design and analysis of thin structures made of textile composites.

2.3 Multiscale Structural Analysis

In finite element analysis, there are three types of commonly used elements: solid elements, shell elements, and beam elements. The 3D effective properties can be directly input into FEA software to define a solid element. However, shell and beam elements are also widely used for analyzing thin and slender composite structures. Therefore, MSG beam and plate models have been applied to enable multiscale modeling of slender and thin textile composite structures analysis. The MSG-based multiscale modeling framework is given in Figure 2.12. The original structural analysis has been decoupled into MSG homogenization, macroscopic structural analysis and MSG dehomogemization. The decomposition of the original structural analysis can greatly improve the computational efficiency while maintaining the accuracy. The first step of MSG-based multiscale modeling is to identify the SG based on the heterogeneity of the original structure. Then, the effective elastic constitutive information is computed based on different MSG models with the homogenization analysis. For the MSG solid model, the constitutive information is effective material properties defining solid elements in the structural analysis. For the MSG plate and beam models, the constitutive information is the plate or beam stiffness matrix defining shell or beam elements in the structural analysis. For the macroscopic structural analysis, the constitutive information of the MSG plate model can be directly input into Abaqus using the "General Stiffness Section" for modeling plate structures. The constitutive information of the MSG beam model can be used to solve the beam structural responses analytically [11]. After the structural analysis, the structural responses $\bar{\epsilon}$ based on different MSG models can be obtained, and then the responses are used to recover the local fields in the SG.

2.3.1 MSG-based Beam Structural Analysis

The layered plain weave beam structure and the corresponding SG is given in Figure 2.13. The SG is discretized using 86,400 20-noded brick elements (C3D20).
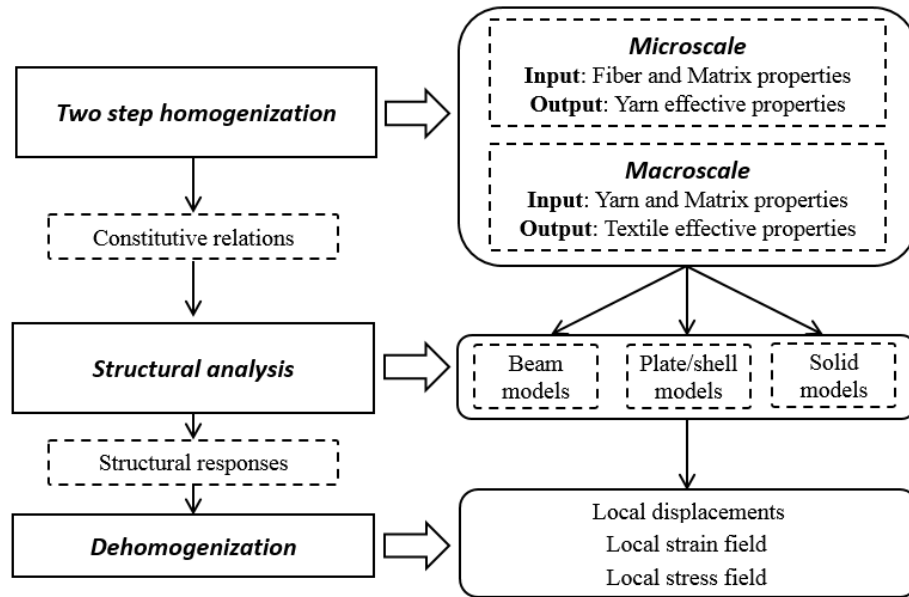
Figure 2.12. MSG-based modeling framework for textile composites

The beam structure is subjected to fixed-free BCs and a uniform pressure is applied at the top surface. A DNS model with all the yarn details has also been created and analyzed to show the accuracy and efficiency of the proposed approach. This 3D structure is discretized using 864,000 20-noded brick elements. Moreover, the homogenized properties of the corresponding woven structure using 3D RVE analysis are computed, and another beam analysis with homogenized properties is carried out in Abaqus to show the loss of accuracy of using homogenized textile composites properties along with beam elements.

The beam structural responses are solved analytically based on the MSG beam model. The reversed form of Eq. (2.26) is

$$
\left\{
\begin{array}{c}
\epsilon_1 \\
\kappa_1 \\
\kappa_2 \\
\kappa_3
\end{array}
\right\}
=
\begin{bmatrix}
S_{11}^b & S_{12}^b & S_{13}^b & S_{14}^b \\
S_{12}^b & S_{22}^b & S_{23}^b & S_{24}^b \\
S_{13}^b & S_{23}^b & S_{33}^b & S_{34}^b \\
S_{14}^b & S_{24}^b & S_{34}^b & S_{44}^b
\end{bmatrix}
\left\{
\begin{array}{c}
F_1 \\
M_1 \\
M_2 \\
M_3
\end{array}
\right\}
\tag{2.37}
$$

It is obvious that the C matrix in the above equation has the relation with the S matrix in Eq. (2.26) as $C = S^{-1}$. For a beam problem, the beam stress resul-
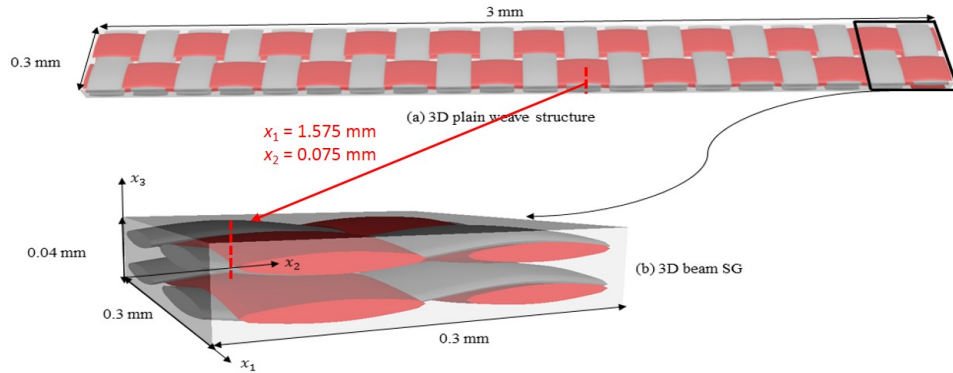
Figure 2.13. Plain woven composite structure and its SG: a) 3D plain woven structure; b) 3D beam SG.

tants can be calculated based on the external loading using the knowledge of undergraduate strength of materials. For example, the stress resultants for a cantilever beam subjected to a uniform pressure along negative x_3 direction can be obtained as $M_2 = \frac{1}{2}qx_1^2 - qLx_1 + \frac{1}{2}qL^2$ with F_1, M_1 and M_3 are zeros. q is the uniform pressure and L is the length of the beam. Based on MSG beam model, the beam stiffness matrix has been computed as well as its inversed form in Eq. (2.37). Then, the beam strain measures can be obtained as $\{\epsilon_1 \quad \kappa_1 \quad \kappa_2 \quad \kappa_3\} = \{C_{13}M_2 \quad C_{23}M_2 \quad C_{33}M_2 \quad C_{34}M_2\}$. If the coupling terms C_{13}, C_{23} and C_{34} are zeros, the strain measures become $\kappa_2 = C_{33}M_2$ which is just a function of x_1. Using the Eq. (2.5) and the boundary conditions such as $u_i(0) = 0$ and $u_i'(0) = 0$ for the cantilever beam, the beam displacements u_i can be computed analytically.

The displacements and the the local stress σ_{11} based on different models are given in Figures 2.14 and 2.15. It is clear that MSG beam model achieves the same accuracy as DNS model while the beam analysis with homogenized properties cannot give good predictions especially for the local stress distribution. In terms of the computing efficiency, MSG-based beam analysis took approximately 2 hours and 4 minutes with one CPU for three steps: homogenization, 1D beam analysis and dehomogenization. However, DNS took 7 hours and 44 minutes with 28 CPUs.
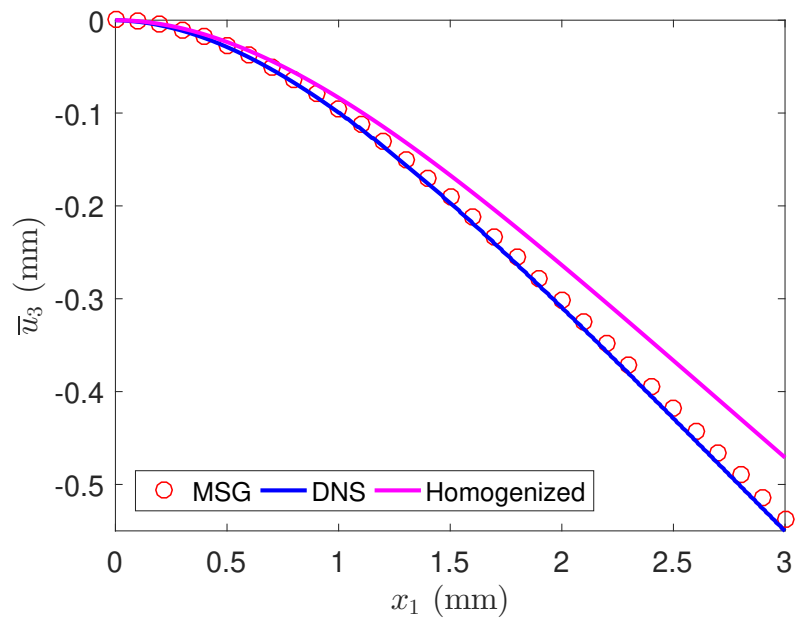
Figure 2.14. Deflection in plain woven beam along x_1 direction
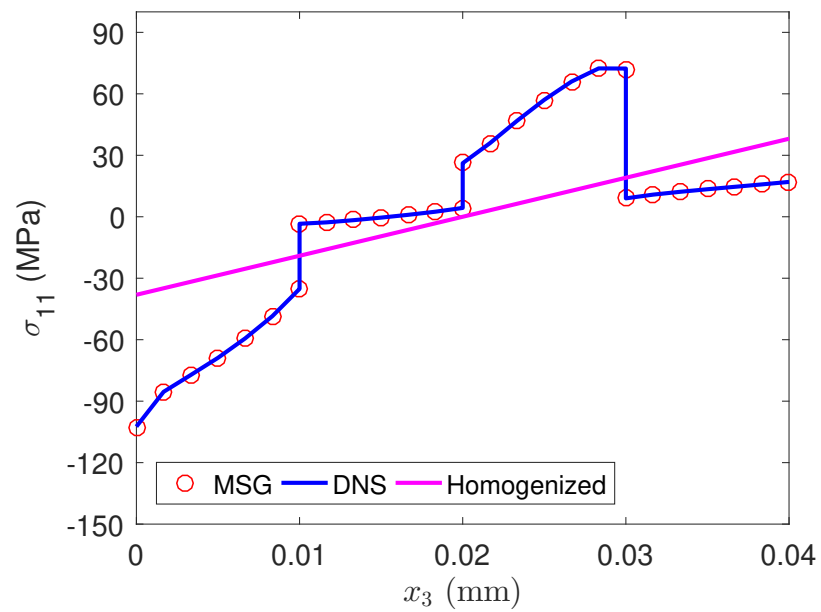
Figure 2.15. Distribution of σ_{11} along a path throughout the thickness

2.3.2 MSG-based Plate Structural Analysis

A 3D orthogonal composite plate structure and the corresponding SG is given in Figure 2.16. The SG is discretized using 12,000 20-noded brick elements (C3D20). The plate structure is subjected to fixed-free BCs and a uniform pressure is applied at the top surface. A DNS model with all the yarn details has also been created and analyzed to show the accuracy and efficiency of the proposed approach. This 3D structure is discretized using 5,760,000 20-noded brick elements. Moreover, the homogenized properties of the corresponding woven structure using 3D RVE analysis are computed, and another plate analysis with homogenized properties is carried out in Abaqus to show the loss of accuracy of using homogenized textile composites properties along with shell elements.
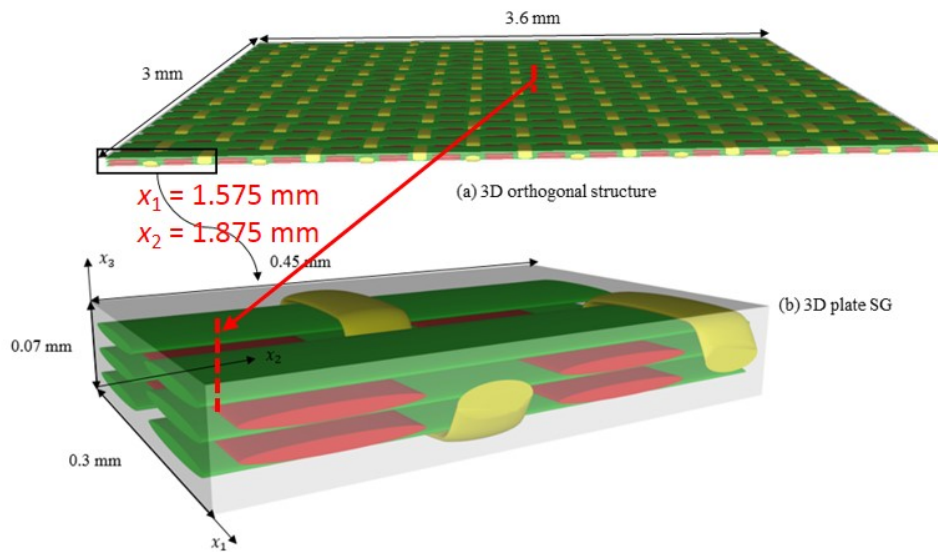
Figure 2.16. 3D orthogonal composite structure and its SG: a) 3D Orthogonal structure; b) 3D plate SG

The displacements and the the local stress σ_{11} based on different models are given in Figures 2.17 and 2.18. It is clear that MSG plate model achieves the same accuracy as DNS model while the plate analysis with homogenized properties cannot give good

predictions especially for the local stress distribution. In terms of the computing efficiency, MSG-based plate analysis took approximately 2 hours and 3 minutes with one CPU for three steps: homogenization, 2D plate analysis and dehomogenization. However, DNS took 20 hours and 2 minutes with 80 CPUs.
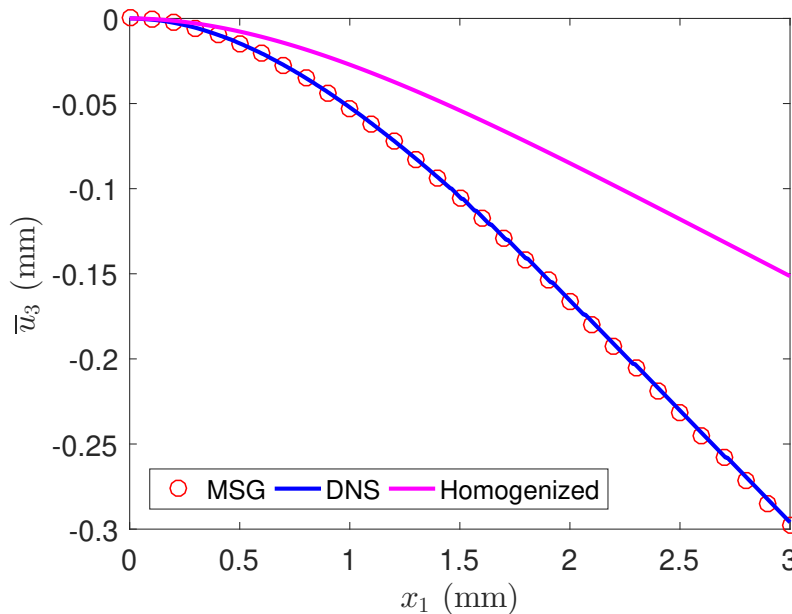
Figure 2.17. Deflection in 3D orthogonal plate along x_1 direction

2.3.3 MSG-based Structural Analysis in MSC.Nastran

MSC.Nastran is a widely used FEA software in structural analysis [76], especially in the aerospace industry. Finite element constitutive modeling modules for analyzing composite structures using shell and beam elements are highly sought-after as these elements provide better computational efficiency than solid elements and more accurate results in some cases [11]. The software includes built-in constitutive modeling functions such as PCOMP and PBMSECT that allow simulation of laminated composite plate and beam structures using CLPT. These models have been proven to be powerful tools for the analysis of traditional fiber reinforced laminates. In order
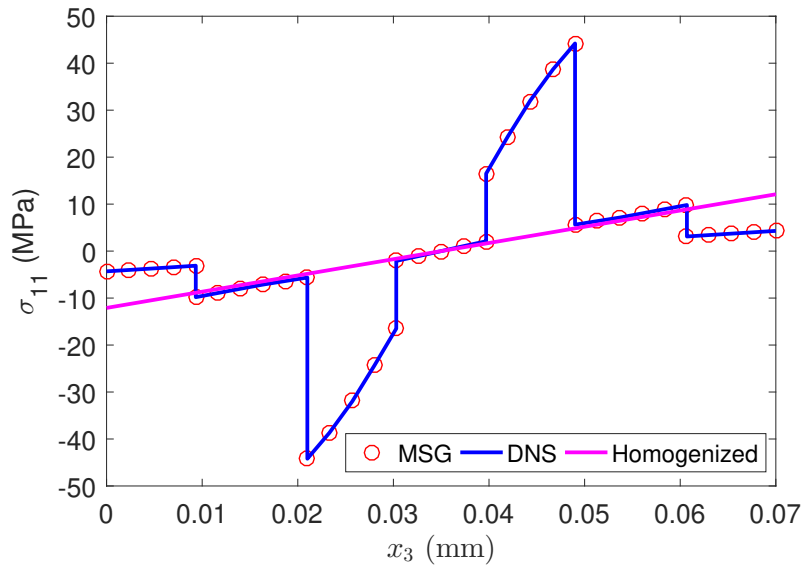
Figure 2.18. Distribution of σ_{11} along a path throughout the thickness

to use these functions for plate and beam modeling, homogenized lamina properties have to be input by users, which can be obtained directly from experimental testing or constitutive modeling at the sub-scale. Although obtaining homogenized material properties from experimental testing remains the standard approach in the industry, multiscale constitutive modeling can provide a lower cost alternative or complement for predicting effective material properties in the preliminary design phase. However, for woven composite material forms, either laminated or non-laminated, effective properties obtained by conventional numerical or analytical multiscale homogenization for the beam and plate elements in MSC.Nastran might cause loss of accuracy. Moreover, conventional structural elements in the composite structural design are widely used due to their simplicity. Therefore, there is a need to enhance modeling capability of conventional elements for complex woven composite structures without loss of accuracy.

SwiftComp$^{\text{TM}}$ has been integrated into MSC.Nastran to serve as a multiscale constitutive modeling module to provide effective material and element properties for MSC.Nastran shell and beam elements (e.g. CQUAD4, CQUAD8 and CBEAM).

A graphical user interface (GUI) has been developed for MSC.Nastran to incorporate the constitutive modeling and to enable the automation of the information passing between constitutive modeling and structural analysis (Figure. 2.19). In order to reduce the modeling efforts for creating complex microstructures of woven composites, TexGen [69] has been integrated into the GUI to provide rapid textile composite microstructure generation for constitutive modeling. More details of the MSC.Patran/Nastran-SwiftComp GUI are given in the Appendix B.
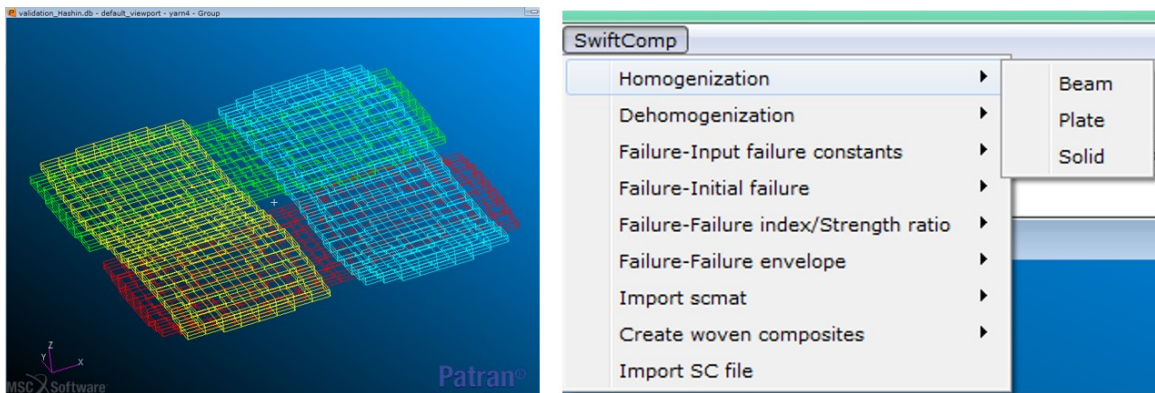
Figure 2.19. MSC.Patran-SwiftComp$^{\text{TM}}$ GUI

For isotropic plate and shell elements such as CQUAD4 and CQUAD8, only one set of 2D material properties can be input. The constitutive equation for a 2D solid can be expressed using Eq. (2.38), which is available in most FEA codes.

$$
\left\{
\begin{array}{c}
\sigma_{11} \\
\sigma_{22} \\
\sigma_{12}
\end{array}
\right\}
=
\begin{bmatrix}
G_{11} & G_{12} & G_{13} \\
G_{12} & G_{22} & G_{23} \\
G_{13} & G_{23} & G_{33}
\end{bmatrix}
\left\{
\begin{array}{c}
\varepsilon_{11} \\
\varepsilon_{22} \\
2\varepsilon_{12}
\end{array}
\right\}
\tag{2.38}
$$

However, due to the heterogeneity of composite plates, one set of material properties cannot capture all possible mechanical behaviors. Therefore, $\boldsymbol{A}$, $\boldsymbol{B}$ and $\boldsymbol{D}$ matrices are the most widely used constitutive information for modeling composite plate structures, and they can be directly input into commercial software like

Abaqus and Ansys. The $\boldsymbol{A}$, $\boldsymbol{B}$ and $\boldsymbol{D}$ matrices in the plate model represent the in-plane behaviors, membrane-bending couplings, and bending behaviors, respectively. In MSC.Nastran, three sets of 2D material properties are used to define PSHELL element properties, which can be extracted from $\boldsymbol{A}$, $\boldsymbol{B}$ and $\boldsymbol{D}$ matrices as follows.

$$\boldsymbol{G_a} = \frac{\boldsymbol{A}}{h}; \quad \boldsymbol{G_b} = \frac{\boldsymbol{B}}{h^2}; \quad \boldsymbol{G_d} = \frac{12\boldsymbol{D}}{h^3} \tag{2.39}$$

The linear elastic mechanical behaviors of an isotropic beam can be described using the following stiffness terms: EA, GJ and EI. E is the Young's modulus of the material, A is the area of the cross section, G is the shear modulus, J is the torsional constant, and I is the area moment of inertia of the cross section. If the cross section is described using $x_2 - x_3$ coordinates, then I_{22} and I_{33} are the moment of inertia with respect to x_2 and x_3 axes, and I_{23} is called the product of inertia with respect to the x_2 and x_3 axes. In this section, we define A, J and I as beam sectional properties. The MSC.Nastran PBEAM element properties can directly take the terms in the beam stiffness matrix as given in Eq. (2.40)

$$\boldsymbol{C_b^*} = \begin{bmatrix} EA & 0 & 0 & 0 \\ 0 & GJ & 0 & 0 \\ 0 & 0 & EI_{22} & EI_{23} \\ 0 & 0 & EI_{23} & EI_{33} \end{bmatrix} \tag{2.40}$$

It is easy to see that the values in Eq. (2.40) contain the information for both material properties and the sectional properties. The diagonal terms EA, GJ, EI_{22} and EI_{33} are the extensional stiffness, the torsional stiffness, and bending stiffness about x_2 and x_3, respectively. The off-diagonal terms represent the elastic couplings between different deformation modes [77]. Note Eq. (2.40) also implies the definitions of the diagonal terms. For example, EA is defined by assuming a constant state of strain ϵ_1 with all other curvatures equal to zero, then EA is equal to axial force F_1 divided by ϵ_1. This definition is the same as the axial stiffness definition in [78].

It is easy to see from Eq. (2.40) that the twisting-extension, twisting-bending and extension-bending terms cannot be directly input into PBEAM element properties. However, the extension-bending coupling behaviors can be modeled by taking advantage of the offset function in MSC.Nastran. By default, the beam reference line is centered at the extension center, but the reference line can be moved to a new position by specifying offset values, which can be used to simulate the extension-bending coupling behaviors. If the offset values are specified as (x_{2c}, x_{3c}), a new beam stiffness can be obtained based on the material and sectional properties (see Eq. (2.40)) defined in MSC.Nastran for a CBEAM element with PBEAM properties which can be expressed as

$$
\boldsymbol{C_b} = \begin{bmatrix}
EA & 0 & x_{3c}EA & -x_{2c}EA \\
0 & GJ & 0 & 0 \\
x_{3c}EA & 0 & EI_{22} + x_{3c}^2 EA & EI_{23} - x_{2c}x_{3c}EA \\
-x_{2c}EA & 0 & EI_{23} - x_{2c}x_{3c}EA & EI_{33} + x_{2c}^2 EA
\end{bmatrix}
\tag{2.41}
$$

By comparing Eq. (2.41) with the stiffness matrix computed by SwiftComp$^{\text{TM}}$, we can observe that if the stiffness matrix computed by SwiftComp$^{\text{TM}}$ does not feature extension-twist coupling ($C_{12}^b = 0$) and twisting-bending couplings ($C_{23}^b = C_{24}^b = 0$), we can use CBEAM element with PBEAM properties to carry out the corresponding 1D beam analysis with the corresponding inputs extracted as

$$
EA = C_{11}^b \qquad GJ = C_{22}^b \qquad x_{2c} = \frac{-C_{14}^b}{EA} \qquad x_{3c} = \frac{C_{13}^b}{EA}
$$
$$
EI_{22} = C_{33}^b - x_{3c}^2 EA \qquad EI_{33} = C_{44}^b - x_{2c}^2 EA
\tag{2.42}
$$
$$
EI_{23} = C_{34}^b - x_{2c}x_{3c}EA
$$

In other words, MSC.Nastran CBEAM element cannot capture extension-twist coupling and twisting-bending couplings even if such couplings are contained in the stiffness matrix computed by SwiftComp$^{\text{TM}}$.

Plate stiffness computed based on different BCs of a woven lamina

Laminated plate structures made by 2D woven composites are often modeled using the PCOMP function in MSC.Nastran. This function internally computes A, B and D matrices for PSHELL properties. If the lamina input properties are computed with the RVE approach, instead of being directly measured from experimental testing, loss of accuracy may come from the BCs chosen for the RVE analysis. A 2 by 2 twill woven laminated plate example is used to study the effect of RVE BCs on A, B and D matrices. The yarns and matrix properties are given in Table 2.11. The yarn width, spacing and thickness are 0.8 mm, 1 mm and 0.1 mm respectively.

Table 2.11. Elastic constants of yarns and matrix.

Parameter	Matrix	Yarn
E_1 (GPa)	4.51	126.91
$E_2 = E_3$ (GPa)	4.51	16.49
$G_{12} = G_{13}$ (GPa)	1.70	3.72
G_{23} (GPa)	1.70	3.22
$\nu_{12} = \nu_{13}$	0.38	0.26
ν_{23}	0.38	0.44

A one-step approach and two two-step approaches are used to study the A, B and D matrices of the woven laminated plate. For the one-step approach, the A, B and D matrices are directly computed based on the plate SG using the MSG plate model, which has been shown to have the same accuracy as DNS [11] and serves as the reference model.

However, a plate SG is not always easy to create due to the complex microstructures when off-axis plies exist. For that reason, a two-step approach is preferred for laminated structures with angle plies. In the first step, effective properties of the woven lamina are computed based on the properties of yarns and matrix. In the second step, the lamina properties are used to determine the A, B and D matrices based

on CLPT for the whole laminate. MSC.Nastran PCOMP function serves the purpose of the second step to compute plate stiffness matrix based on the lamina properties and the layup information. However, the woven laminated plate only contains one or two yarns along the thickness direction in each woven lamina, therefore there is no periodicity of yarns in a lamina in the thickness direction. The absence of periodicity poses a challenge when the appropriate BCs have to be applied to the RVE model. To obtain lamina properties, which is crucial for computing the plate stiffness matrix for the structural analysis, two different two-step approaches are studied. The first approach uses the MSG plate model to get the in-plane material properties, which are equivalent to the properties obtained from the RVE analysis with in-plane PBCs [75]. The second model uses MSG solid model with PBCs along x, y and z directions. Both models use CLPT to get the $\boldsymbol{A}$, $\boldsymbol{B}$ and $\boldsymbol{D}$ matrices for the laminate based on the homogenized lamina properties.

The 2×2 twill woven laminated plate is analyzed using the three different approaches mentioned above. Laminated plates with two, six and ten layers are considered. The SG of the two-step approach consists of a single layer woven lamina, whereas the SG of the one-step approach includes all layers that form the woven laminate. The whole constitutive modeling procedure is summarized in Figure 2.20.
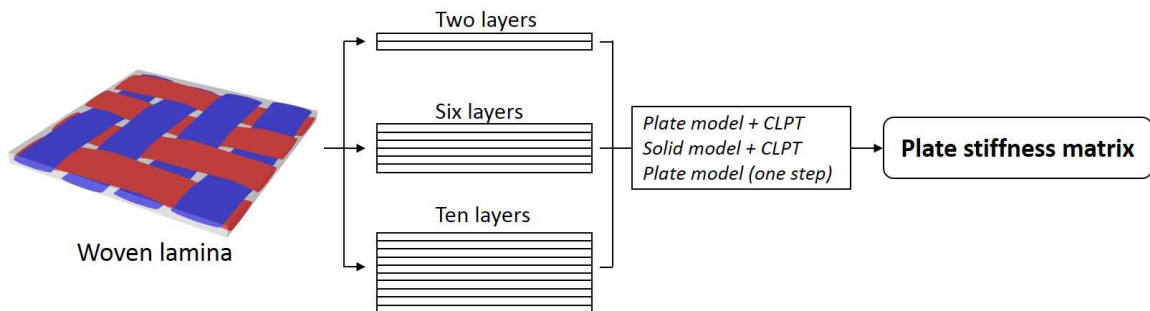
Figure 2.20. Modeling framework for computing woven laminate stiffness matrix

In this example, all the layers are in the same direction, so there are no coupling effects and the B matrix is zero. To better compare the three approaches, the stiffness matrix terms of the two-step approaches are normalized with the corresponding stiffness terms obtained from the one-step approach. Due to the in-plane symmetry, additional relations of values in the plate stiffness matrix can be obtained as $A_{11} = A_{22}$ and $D_{11} = D_{22}$. The results show A_{66} and D_{66} obtained by three models are almost the same, which means these values are insensitive to the out-of-plane boundary conditions and the number of layers. This can be easily explained as A_{66} and D_{66} are computed mainly based on the in-plane shear modulus. Other normalized non-zero values in A and D matrices are plotted in Figure 2.21.

(a) A_{11} (b) A_{12}

(c) D_{11} (d) D_{12}
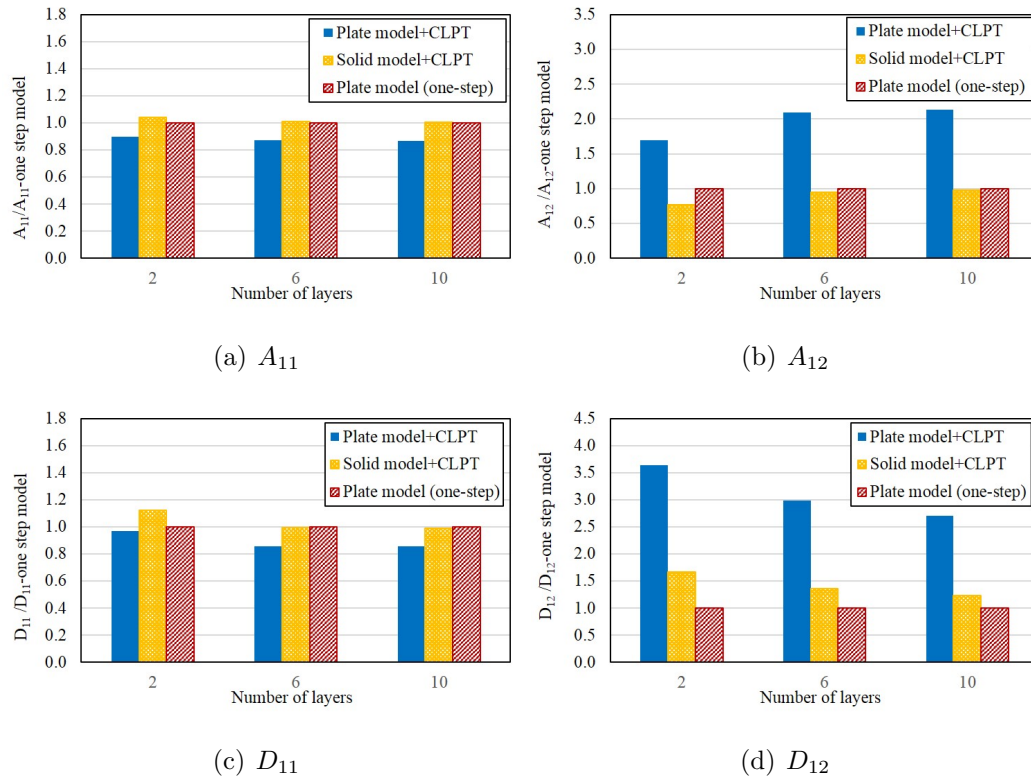
Figure 2.21. Plate stiffness matrix for different layers and models

For the two-step approaches, we can conclude that using MSG solid model to obtain 3D lamina properties provides more accurate results than the ones using MSG

plate model to compute lamina in-plane properties for a woven laminate. By increasing the number of layers, the results obtained by MSG solid model and CLPT have a better agreement with the one-step MSG plate model. However, if the number of layers is small, such as the two layers plate in this example, two-step approach using MSG plate model also provides good predictions for A_{11} and D_{11} as shown in Figures 2.21(a) and 2.21(c). If only one layer is analyzed, two-step MSG plate model will give more accurate results than two-step MSG solid model, because there is no PBCs along thickness direction and additional constrains in solid model would cause loss of accuracy in the prediction. However, if there are many layers, the top and bottom surfaces of the lamina would be constrained by other layers, then the additional constrains from MSG solid model would make the predictions closer to the one-step approach. We can also conclude from Figures 2.21(b) and 2.21(d) that there are still some differences even for large number of layers between two-step MSG solid model and one-step MSG plate model, because the two-step approach assumes that the SG repeats along the thickness infinite many times. On the other hand, one-step MSG plate model approach preserves the finite thickness of the real structure, therefore more accurate results can be expected using the one-step MSG plate model. Hence, if PCOMP function is used to analyze laminated woven structures with multiple layers and homogenized lamina properties are not available from experimental testing, the MSG solid model with PBCs would provide better predictions than the corresponding plate model. Moreover, the one-step approach is always recommended for laminates if the SGs of the laminate plate can be easily created.

MSG-based MSC.Nastran beam analysis with extension-bending coupled behaviors

The conventional beam elements in MSC.Nastran have been powered to consider extension-bending coupling behaviors of textile composite beams such as the 3D orthogonal beam shown in Figure 2.22. The beam stiffness computed from

SwiftComp$^{\text{TM}}$ is converted to beam cross-section properties and a set of isotropic material properties which can be directly used to define a beam element in MSC.Nastran. The offset values, which are used to capture the extension-bending coupling behaviors, are computed based on the beam stiffness from SwiftComp$^{\text{TM}}$. For simple beam problems, the beam structural responses can also be solved analytically [11].

Four different models are used to validate the MSG-powered multiscale beam analysis in MSC.Nastran. Model A uses homogenized properties with MSC.Nastran solid elements to compute the structural responses. Model B uses the beam elements in MSC.Nastran with the properties and offset values computed based on the MSG beam model. Model C directly use MSG beam stiffness matrix to compute the beam responses analytically [11], and Model D uses DNS which can be considered as a reference model. The beam is clamped at one end and free at the other end. The length of the beam is 85.71 mm, and a 5000 N point-load in x_1 direction is applied at the beam free end.
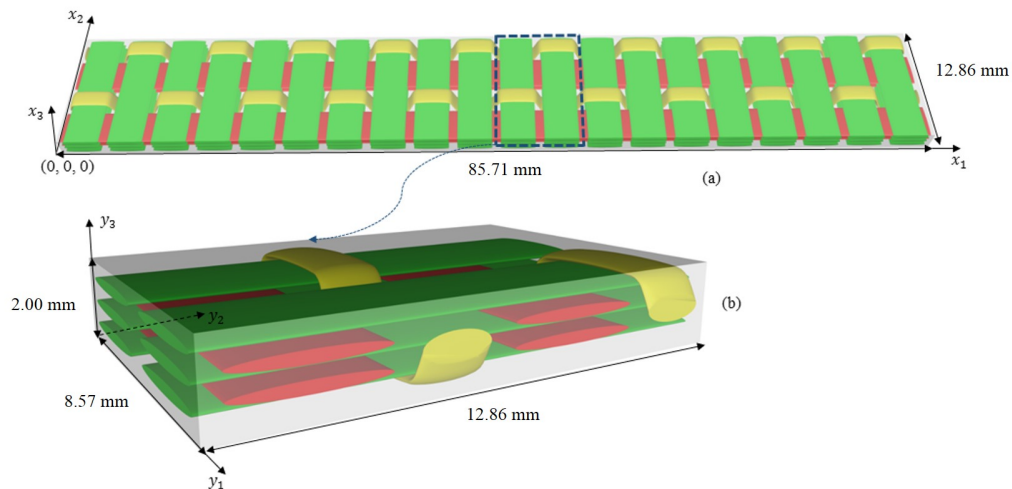
Figure 2.22. The woven beam and its SG

In Model B, the initial beam stiffness matrix is first computed using the MSG beam model with the SG centered at the geometric center (i.e. centroid). The non-

zero components in the 4×4 beam stiffness matrix are: $C_{11}^b = 5.82 \times 10^5$ N, $C_{22}^b = 6.61 \times 10^4$ N $\cdot$ mm^2, $C_{33}^b = 1.02 \times 10^5$ N $\cdot$ mm^2, $C_{44}^b = 7.41 \times 10^6$ N $\cdot$ mm^2, $C_{14}^b = C_{41}^b = 3.58 \times 10^5$ N $\cdot$ mm. The values of the extension-bending coupling term C_{14}^b and C_{41}^b are not negligible, therefore the coupling behaviors should be considered. Using Eq. (2.42), the extension center coordinates (x_{2c}, x_{3c}) of this beam cross section are $(-0.615, 0)$. A new beam stiffness matrix is calculated with respect to the extension center. The non-zero components in the new beam stiffness matrix are: $EA = 5.82 \times 10^5$ N, $GJ = 6.61 \times 10^4$ N$\cdot$mm^2, $EI_{22} = 1.02 \times 10^5$ N$\cdot$mm^2, $EI_{33} = 7.19 \times 10^6$ N$\cdot$mm^2. In order to input sectional area, moments of inertia and torsional stiffness via PBEAM entry, a set of fictitious isotropic material properties are created such that $E = 1$ MPa and $G = 1$ MPa. Then the sectional properties are obtained based on Eq. (2.40): $A = 5.82 \times 10^5$ mm^2, $J = 6.61 \times 10^4$ mm^4, $I_{22} = 1.02 \times 10^5$ mm^4 and $I_{33} = 7.19 \times 10^6$ mm^4. Note that the correct local stress field cannot be obtained from FEA macroscopic level (i.e structural level) since the material properties are fictitious. Instead, the stress field should be obtained using dehomogenization analysis in the MSG beam model [79].

Based on Figure 2.23(a), we can see that all the models give good predictions for the displacements in the x_1 direction. The homogenized properties used in Model A are computed using MSG solid model with aPBCs [80]. The MSG aPBCs model provides better results compared with the commonly used RVE analysis with PBCs, because the non-periodic features in beam transverse directions can be taken into account.

Due to the extension-bending coupling behaviors, the displacements in the x_2 direction are significant as shown in Figure 2.23(b). However, the Model A with homogenized solid elements cannot capture the coupling behaviors, because the heterogeneity of the beam cross section has been removed after smearing yarns and matrix properties. The other three models show a good agreement. Hence, the MSC.Nastran FEM PBEAM property and CBEAM elements can be used to model
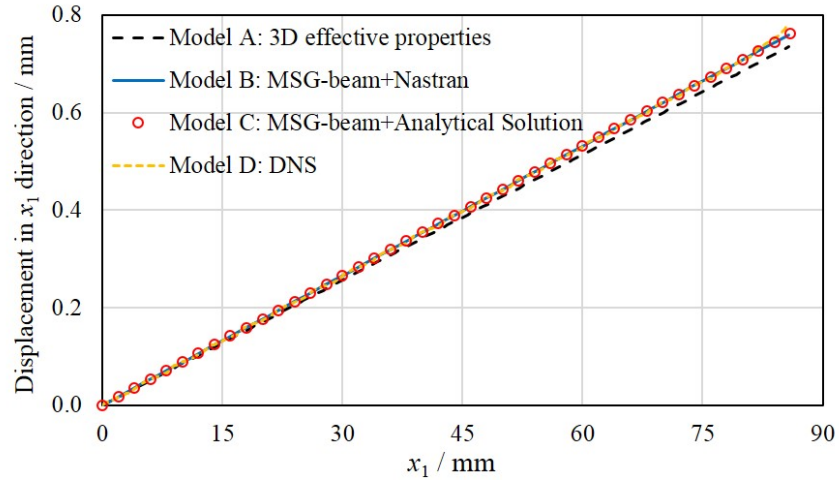
(a) Displacements in x_1 direction
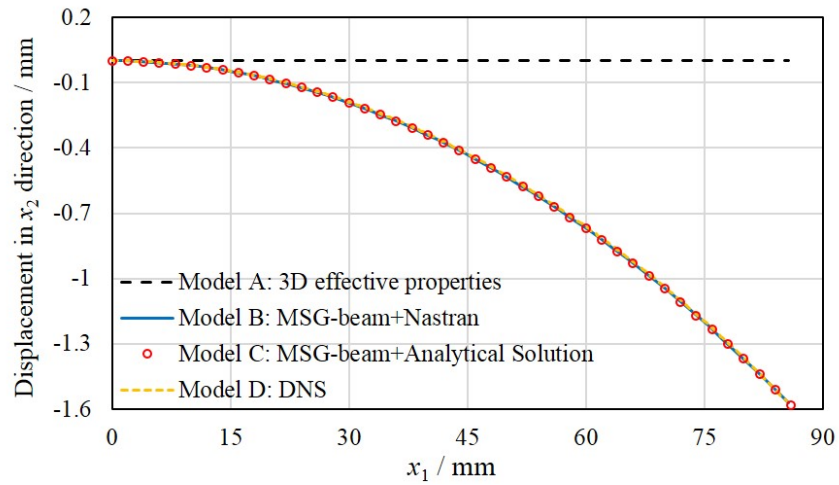
(b) Displacements in x_2 direction

Figure 2.23. Displacements of the 3D woven beam structure

extension-bending coupling behaviors with the help of MSG beam model, which provides beam section inertia and offset values.

2.4   Summary

In this chapter, a novel multiscale modeling approach using MSG is provided for analyzing elastic behavior of textile composite materials and structures considering different micro/mesoscale features.

The MSG solid model is extended to provide a two-step approach to predicting the effective material properties of textile composites. The material orientation along yarn path is captured in the MSG model. Several examples are given to illustrate the proposed approach. The results show that the MSG solid model achieves the same accuracy as the 3D RVE analysis using FEM but the computing time is significantly reduced.

The MSG plate and beam models are used to perform structural analysis for the thin and slender textile composites. Both the structural responses and local stress/strain fields are captured. Compared with the DNS results, the MSG models achieves the same accuracy with a great computational efficiency.

The developed multiscale modeling approach is integrated into the commercial software MSC.Patran/Nastran. The example shows that the beam extension-bending coupling behavior can be well predicted with the help of the MSG beam model using the normal beam elements in the MSC.Patran/Nastran. The developed theory provides a powerful module in the FEM software to perform multiscale structural modeling of complex composites.

3. MULTISCALE VISCOELASTIC ANALYSIS OF TEXTILE COMPOSITES

Copyright permissions have been obtained to reuse the published materials from [12] in this chapter.

3.1 Linear Viscoelastic Theory

The constitutive equations for the linear viscoelastic material can be expressed in the time domain in Eq. (3.1).

$$\boldsymbol{\sigma}(t) = \int_{-\infty}^{t} \boldsymbol{C}(t-\tau) : \frac{d\boldsymbol{\epsilon}}{d\tau} d\tau \tag{3.1}$$

where $\boldsymbol{C}(t)$ is the stress relaxation modulus. The stress relaxation tests are performed at constant strains,

$$\varepsilon_{kl}(t) = \begin{cases} 0 & t < 0 \\ \varepsilon_{kl}^{\text{cst}} & t \geq 0 \end{cases} \tag{3.2}$$

where "cst" means constant values that do not vary with time. Applying the integration by parts to Eq. (3.1), the following expression can be obtained.

$$\sigma_{ij}(t) = \left(C_{ijkl}(0) + \int_{0}^{t} \frac{\partial C_{ijkl}(t-\tau)}{\partial(t-\tau)} d\tau \right) \varepsilon_{kl}^{\text{cst}} \equiv C_{ijkl}(t)\varepsilon_{kl}^{\text{cst}} \tag{3.3}$$

Eq. (3.3) implies that the instantaneous stress values are dependent on the instantaneous values of stress relaxation coefficients when the linear viscoelastic materials are subject to constant strain load [36]. Using this fact to conduct viscoelastic analysis is called the quasi-elastic approach [81].

In this section, matrix is assumed to be isotropic viscoelastic with a constant Poisson's ratio. The fibers are assumed to be linear elastic and transversely isotropic.

A Prony series can be used to represent the relaxation modulus over a wide range of time scale. For the isotropic matrix used in this section, the Young's modulus is represented in terms of the Prony series as:

$$E(t) = E_\infty + \sum_{i=1}^{m} E_i e^{-t/\rho_i} \tag{3.4}$$

where E_∞ is the long-term modulus, E_i are the Prony coefficients, and ρ_i are the relaxation times. Each exponential term is used to represent the variation of the relaxation modulus over a chosen time period, and the number of terms included in the Prony series depends upon the time range of interest for the problem that is considered. For general anisotropic material properties, the relaxation modulus tensor can be expressed in a similar way using the Prony series as:

$$C_{ijkl} = C_{ijkl,\infty} + \sum_{i=1}^{n} C_{ijkl,m} e^{-t/\rho_m} \tag{3.5}$$

3.1.1 MSG-based Solid Model

According to MSG, the displacement of the original heterogeneous body in terms of that of the homogeneous body at the time t can be expressed as

$$u_i(x_1, x_2, x_3, y_1, y_2, y_3, t) = \bar{u}_i(x_1, x_2, x_3, t) + \varepsilon \chi_i(x_1, x_2, x_3, y_1, y_2, y_3, t) \tag{3.6}$$

where u_i represents the displacement field of the heterogeneous body, $\bar{u}_i$ represents the displacement of the homogenized body, and χ_i represents the difference between these two fields, which is known as fluctuating functions in micromechanics.

The instantaneous strain field of the linear viscoelastic body can be expressed as

$$\varepsilon_{ij}(t) = \frac{1}{2}\left(\frac{\partial u_i(t)}{\partial x_j} + \frac{\partial u_j(t)}{\partial x_i}\right) \tag{3.7}$$

Dropping small terms according to the variational asymptotic method (VAM) [66], the strain field of the heterogeneous body can be written as

$$\varepsilon_{ij}(x, y, t) = \bar{\varepsilon}_{ij}(x, t) + \chi_{(i|j)}(t) \tag{3.8}$$

with $\chi_{(i|j)} = \frac{1}{2}\left(\chi_{i|j} + \chi_{i|j}\right)$.

The constraints on the fluctuating functions are defined as

$$\langle\chi_i(t)\rangle = 0 \qquad \langle\chi_{(i|j)}(t)\rangle = 0 \tag{3.9}$$

where $\langle\cdot\rangle$ denotes the average over the domain of a SG. The above constraints imply that the average displacements and strains are the same in the homogenized and original models. MSG uses the principle of minimum information loss (PMIL) to minimize the difference between the transient strain energy of the heterogeneous model and the homogenized model which is

$$\Pi(t) = \langle\frac{1}{2}C_{ijkl}(t)\varepsilon_{ij}(t)\varepsilon_{kl}(t)\rangle - \frac{1}{2}\bar{C}_{ijkl}(t)\bar{\varepsilon}_{ij}(t)\bar{\varepsilon}_{kl}(t) \tag{3.10}$$

To minimize $\Pi(t)$, the homogenized model is considered as given (i.e. $\bar{C}_{ijkl}$ and $\bar{\varepsilon}_{ij}$ cannot be varied with respect to χ_i). Then χ_i can be solved from the following variational statement

$$\min_{\chi_i(t)}\langle\frac{1}{2}C_{ijkl}(t)\varepsilon_{ij}(t)\varepsilon_{kl}(t)\rangle = \min_{\chi_i(t)\in\text{Eq.(3.9)}}\langle\frac{1}{2}C_{ijkl}(t)(\bar{\varepsilon}_{ij}(t) + \chi_{(i|j)}(t))(\bar{\varepsilon}_{kl}(t) + \chi_{(k|l)}(t))\rangle \tag{3.11}$$

It is noted that other constraints such as those due to the periodicity of the microstructure can be added into Eq. (3.9) to solve Eq. (3.11). Let us denote $\bar{\varepsilon}(t) = [\bar{\varepsilon}_{11}(t) \quad \bar{\varepsilon}_{22}(t) \quad \bar{\varepsilon}_{33}(t) \quad 2\bar{\varepsilon}_{23}(t) \quad 2\bar{\varepsilon}_{13}(t) \quad 2\bar{\varepsilon}_{12}(t)]$ and $w(t) = [\chi_1(t) \quad \chi_2(t) \quad \chi_3(t)]$. Then the functional in the variational statement of Eq. (3.11) can be rewritten in the following matrix form as

$$U(t) = \frac{1}{2}\langle(\Gamma_h w(t) + \bar{\varepsilon}(t))^T C(t)(\Gamma_h w(t) + \bar{\varepsilon}(t))\rangle \tag{3.12}$$

with

$$\Gamma_h = \begin{bmatrix} \frac{\partial}{\partial y_1} & 0 & 0 & 0 & \frac{\partial}{\partial y_3} & \frac{\partial}{\partial y_2} \\ 0 & \frac{\partial}{\partial y_2} & 0 & \frac{\partial}{\partial y_3} & 0 & \frac{\partial}{\partial y_1} \\ 0 & 0 & \frac{\partial}{\partial y_3} & \frac{\partial}{\partial y_2} & \frac{\partial}{\partial y_1} & 0 \end{bmatrix}^T \tag{3.13}$$

For 1D or 2D SGs, the derivatives with respect to the corresponding coordinates should vanish in Γ_h. Minimizing $U(t)$ in Eq. (3.12) subject to the constraints, we can

solve the fluctuating functions, and the transient strain energy of the homogenized model can be obtained as

$$U(t) = \frac{1}{2}\bar{\varepsilon}(t)^T\bar{C}(t)\bar{\varepsilon}(t) \tag{3.14}$$

where $\bar{C}(t)$ represents the effective relaxation stiffness matrix for the macroscopic model. It is noted that because $\bar{\varepsilon}$ contains six components, $\bar{C}(t)$ is a 6×6 matrix containing the complete set of 3D properties although the SG could be a 1D, 2D, or 3D domain. It is noted that the homogenized strain field $\bar{\varepsilon}$ is not assumed to be constant with respect to time t in the above derivation, which means the above derivations are not limited to the stress relaxation. If the stress is also time-dependent, then Eq. (3.14) can be written in another form

$$U(t) = \frac{1}{2}\bar{\sigma}(t)^T\bar{S}(t)\bar{\sigma}(t) \tag{3.15}$$

The instantaneous constitutive relations can be expressed as [82]

$$\bar{\sigma}_{ij}(t) = \bar{C}_{ijkl}(t)\bar{\varepsilon}_{kl}(t); \qquad \bar{\varepsilon}_{ij}(t) = \bar{S}_{ijkl}(t)\bar{\sigma}_{kl}(t) \tag{3.16}$$

It is clear $\bar{C}_{ijkl}(t) = \bar{S}_{ijkl}^{-1}(t)$ at the time t. If constant strain loadings are applied, then the first equation in Eq. (3.16) becomes

$$\bar{\sigma}_{ij}(t) = \bar{C}_{ijkl}(t)\bar{\varepsilon}_{kl}^{\text{cst}} \tag{3.17}$$

where the "cst" means constant values that do not vary with time. Eq. (3.17) is often used to study the stress relaxation behaviors of materials. If constant stress loadings are applied, then the second equation in Eq. (3.16) becomes

$$\bar{\varepsilon}_{ij}(t) = \bar{S}_{ijkl}(t)\bar{\sigma}_{kl}^{\text{cst}} \tag{3.18}$$

which is often used to study the creep behaviors of materials.

3.1.2 MSG-based Plate Model

MSG-based Kirchhoff-Love plate model is used at macro-homogenization step. To derive the Kirchhoff-Love plate model for viscoelastic body using MSG, the 3D displacement field can be expressed in terms of the 2D displacement variables admitted by the Kirchhoff-Love plate model as:

$$u_1(x_1, x_2, y_1, y_2, y_3, t) = \bar{u}_1(x_1, x_2, t) - \varepsilon y_3 \bar{u}_{3,1}(x_1, x_2, t) + \varepsilon \chi_1(x_1, x_2, y_1, y_2, y_3, t)$$

$$u_2(x_1, x_2, y_1, y_2, y_3, t) = \bar{u}_2(x_1, x_2, t) - \varepsilon y_3 \bar{u}_{3,2}(x_1, x_2, t) + \varepsilon \chi_2(x_1, x_2, y_1, y_2, y_3, t)$$

$$u_3(x_1, x_2, y_1, y_2, y_3, t) = \bar{u}_3(x_1, x_2, t) + \varepsilon \chi_3(x_1, x_2, y_1, y_2, y_3, t)$$

$$(3.19)$$

where u_i and $\bar{u}_i$ denote the displacements of the original 3D heterogeneous structure and the 2D plate model respectively. In this formulation, there are no apriori assumptions about the kinematics such as the commonly invoked Kirchhoff-Love assumptions. Instead, Eq.(3.19) can be considered as a changes of variables with χ_i denoting the part of 3D displacements which cannot be described using the simple Kirchhoff-Love kinematics.

The 3D strain field at the time t can be written in terms of plate strains and curvatures using Eq. (3.7) as:

$$\varepsilon_{11}(t) = \epsilon_{11}(t) + \varepsilon y_3 \kappa_{11}(t) + \chi_{(1|1)}(t)$$

$$\varepsilon_{22}(t) = \epsilon_{22}(t) + \varepsilon y_3 \kappa_{22}(t) + \chi_{(2|2)}(t)$$

$$\varepsilon_{12}(t) = \epsilon_{12}(t) + \varepsilon y_3 \kappa_{12}(t) + \chi_{(1|2)}(t)$$

$$(3.20)$$

$$\varepsilon_{33}(t) = \chi_{3|3}(t); \qquad \varepsilon_{13}(t) = \chi_{(1|3)}(t); \qquad \varepsilon_{23}(t) = \chi_{(2|3)}(t)$$

where the plate strains and curvatures are defined as:

$$\epsilon_{\alpha\beta}(x_1, x_2, t) = \frac{1}{2}(\bar{u}_{\alpha,\beta}(t) + \bar{u}_{\beta,\alpha}(t)); \ \kappa_{\alpha\beta}(x_1, x_2, t) = -\bar{u}_{3,\alpha\beta}(t) \qquad (3.21)$$

The fluctuating functions for the MSG-based plate model are constrained by $\langle \chi_i(t) \rangle = 0$. It is noted that the in-plane periodicity is also enforced for $\chi_i(t)$. The transient 2D strain energy density defined as:

$$U_{2D}(t) = \frac{1}{2}\langle \sigma_{ij}(t)\varepsilon_{ij}(t) \rangle \qquad (3.22)$$

Substitute the 3D strain field in Eq. (3.20) into Eq. (3.22) and drop small terms according to the VAM. Impose the constraints for fluctuating functions to solve for $\chi_i(t)$. Substitute the obtained fluctuating functions back into Eq. (3.20). The 3D strain field can be expressed in terms of 2D plate strains and curvatures.

The 2D kinetic variables called plate stress resultants are defined as:

$$\frac{\partial U_{2D}(t)}{\partial \epsilon_{11}(t)} = N_{11}(t); \; \frac{\partial U_{2D}(t)}{\partial 2\epsilon_{12}(t)} = N_{12}(t); \; \frac{\partial U_{2D}(t)}{\partial \epsilon_{22}(t)} = N_{22}(t)$$
$$\frac{\partial U_{2D}(t)}{\partial \kappa_{11}(t)} = M_{11}(t); \; \frac{\partial U_{2D}(t)}{\partial 2\kappa_{12}(t)} = M_{12}(t); \; \frac{\partial U_{2D}(t)}{\partial \kappa_{22}(t)} = M_{22}(t)$$

(3.23)

We can get the instantaneous plate constitutive relation to relate the plate stress resultants and strains/curvatures as:

$$\left\{ \begin{array}{c} N_{11}(t) \\ N_{22}(t) \\ N_{12}(t) \\ M_{11}(t) \\ M_{22}(t) \\ M_{12}(t) \end{array} \right\} = \left[\begin{array}{cccccc} A_{11}(t) & A_{12}(t) & A_{16}(t) & B_{11}(t) & B_{12}(t) & B_{16}(t) \\ A_{12}(t) & A_{22}(t) & A_{26}(t) & B_{12}(t) & B_{22}(t) & B_{26}(t) \\ A_{16}(t) & A_{26}(t) & A_{66}(t) & B_{16}(t) & B_{26}(t) & B_{66}(t) \\ B_{11}(t) & B_{12}(t) & B_{16}(t) & D_{11}(t) & D_{12}(t) & D_{16}(t) \\ B_{12}(t) & B_{22}(t) & B_{26}(t) & D_{12}(t) & D_{22}(t) & D_{26}(t) \\ B_{16}(t) & B_{26}(t) & B_{66}(t) & D_{16}(t) & D_{26}(t) & D_{66}(t) \end{array} \right] \left\{ \begin{array}{c} \epsilon_{11}(t) \\ \epsilon_{22}(t) \\ 2\epsilon_{12}(t) \\ \kappa_{11}(t) \\ \kappa_{22}(t) \\ 2\kappa_{12}(t) \end{array} \right\}$$

(3.24)

Here, the 6×6 plate stiffness matrix is composed of the time-dependent $A(t), B(t)$ and $D(t)$ matrices needed for the Kirchhoff-Love plate model.

3.1.3   MSG Two-step Viscoelastic Modeling Framework

The first step in MSG homogenization analysis is to identify SG. In order to obtain effective viscoelastic properties of textile composites, homogenization analysis usually needs to be performed at the micro-scale (yarn) and macro-scale (textile composites).

In micro-homogenization, effective properties of yarns are computed based on fibers and matrix. The microstructure of the yarn is usually idealized in the literature as a square pack as shown in Figure 3.1. One feature of the MSG approach is that the complete set of 3D material properties can be obtained using just 1D or 2D SG,

and dimensionally reduced SG will greatly save the computing time. Since there is no heterogeneity along the fiber direction, the SG of a yarn for micro-homogenization is 2D. Fibers are assumed to be linear elastic and transversely isotropic. The matrix is viscoelastic and isotropic, and the properties will be updated in each time step. These are reasonable assumptions for typical textile composites, but MSG derived in this chapter has no such restrictions. The micro-homogenization will provide the effective viscoelastic properties of yarns in terms of relaxation modulus tensor, which can be used in macro-homogenization of the woven composites.
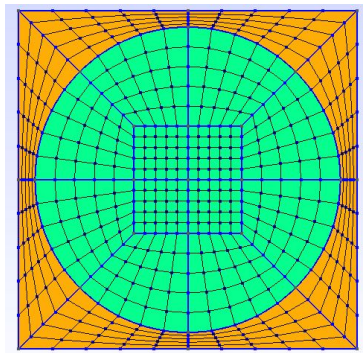
Figure 3.1. 2D SG for yarns
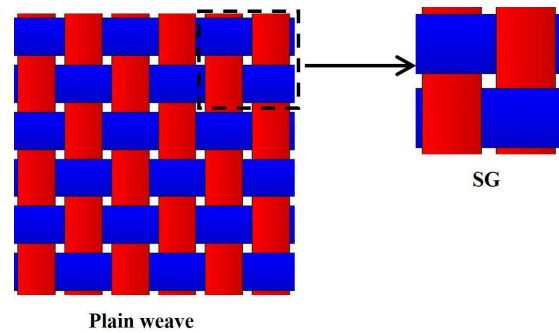
Figure 3.2. Plain weave and its SG

For MSG marco-homogenization of textile composites, unlike unidirectional fiber reinforced composites, both matrix and yarns are viscoelastic materials and the properties need to be updated in each time step. However, properties of yarns are not isotropic based on the micro-homogenization, but most FEA codes cannot directly define non-isotropic viscoelastic properties. Since Eq. (3.3) has been implemented into MSG, the general anisotropic viscoelastic properties can be easily defined.

For thin structures made by textile composites with only several layers, the MSG plate model is used at this homogenization step to get the A, B and D matrices. Because the thin structures do not have many SGs repeating along the thickness direction, A, B and D matrices can provide more accurate predictions than using a solid model with PBCs on the top and bottom surfaces. In addition, woven composite structures are often modeled using plate elements at the structural level, and A, B

Table 3.1. Relaxation times and Prony coefficients for PMT-F4 epoxy

i	∞	1	2	3	4	5	6	7
E_i (MPa)	1000	224.1	450.8	406.1	392.7	810.4	203.7	1486.0
ρ_i (s)	–	1.0e+3	1.0e+5	1.0e+6	1.0e+7	1.0e+8	1.0e+9	1.0e+10

and D matrices are more convenient to use in the structural design. If the woven textile structures are made by many repeated layers, which satisfies the periodicity requirement in the thickness direction, the MSG solid model can be used to compute the relaxation modulus tensor. Therefore, MSG provides more options for handling different woven composites. All the woven composites and the corresponding finite element meshes are generated using TexGen [69].

3.2   2D Plain Woven Composites

In order to verify the accuracy of the proposed approach, the viscoelastic behaviors of 2D plain woven composites are predicted using MSG two-step homogenization. The results at the microscale and mesoscale are compared with 3D RVE analysis using FEA and the experimental data in the literature respectively. The typical plain woven composites and the corresponding SG are shown in Figure 3.2. The fiber volume fraction in each yarn is chosen to be $v_f = 0.64$, and the fiber properties and matrix properties are obtained from the literature [39]. The properties of the fiber are: E_1 = 233,000 MPa, $E_2 = E_3 = 15,000$ MPa, $G_{12} = G_{13} = 8,963$ MPa, $G_{23} = 5,639$ MPa, $\nu_{12} = \nu_{13} = 0.2$ and $\nu_{23} = 0.33$. For the matrix, the relaxation times and Prony coefficients are given in Table 3.1. The matrix properties are expressed in terms of the relaxation times and Prony coefficients in Eq. (3.2), and a constant Poisson's ration 0.33 is assumed.

3.2.1 MSG Micro-homogenization for Yarns

For micro-homogenization, the SG is shown in Figure 3.1 which contains 320 4-noded quadrilateral elements. Only the matrix is defined as viscoelastic and its behaviors can be described based on Eq. (3.2) using the values in Table 3.1. Considering the microstructural symmetry of the yarn, the constitutive equation can be expressed using the relaxation stiffness matrix in the engineering form given in Eq. (3.25).

$$
\left\{
\begin{array}{c}
\sigma_{11} \\
\sigma_{22} \\
\sigma_{33} \\
\sigma_{23} \\
\sigma_{13} \\
\sigma_{12}
\end{array}
\right\}
=
\left[
\begin{array}{cccccc}
C_{11} & C_{12} & C_{12} & 0 & 0 & 0 \\
C_{12} & C_{22} & C_{23} & 0 & 0 & 0 \\
C_{12} & C_{23} & C_{22} & 0 & 0 & 0 \\
0 & 0 & 0 & C_{44} & 0 & 0 \\
0 & 0 & 0 & 0 & C_{55} & 0 \\
0 & 0 & 0 & 0 & 0 & C_{55}
\end{array}
\right]
\left\{
\begin{array}{c}
\varepsilon_{11} \\
\varepsilon_{22} \\
\varepsilon_{33} \\
2\varepsilon_{23} \\
2\varepsilon_{13} \\
2\varepsilon_{12}
\end{array}
\right\}
\tag{3.25}
$$

In order to verify the results based on MSG solid model, a 3D RVE model is built in Abaqus 6.13. The materials are defined by the build-in viscoelastic functions in the time domain using the Prony series given in Table 3.1. PBCs are applied to the RVE in three directions, and the mesh size is kept the same in the planar directions as for the 2D SG shown in Figure 3.1. Five separate analyses are used to determine the C_{11}, C_{12}, C_{22}, C_{23}, C_{44} and C_{55} in relaxation stiffness matrix in Eq. (3.25). Each analysis consisted of two steps, defined with the option *VISCO in Abaqus. To get the relaxation stiffness matrix, a unit strain is applied to the RVE over a short time period (0.1 s). In the second step, the strain remains constant and lasts 10^{10} s. The values in relaxation stiffness matrix are plotted in Figure 3.3. The Prony coefficients of relaxation modulus for yarns are obtained using Levenberg-Marquardt algorithm in Matlab [83], which are given in Table 3.2, and the fitting curves are also given in Figure 3.3.

It is easy to conclude from Figure 3.3 that all the values in the relaxation stiffness matrix based on the MSG solid model agree well with ones obtained from the 3D

(a) C_{11}

(b) C_{12}

(c) C_{22}

(d) C_{23}

(e) C_{44}

(f) C_{55}
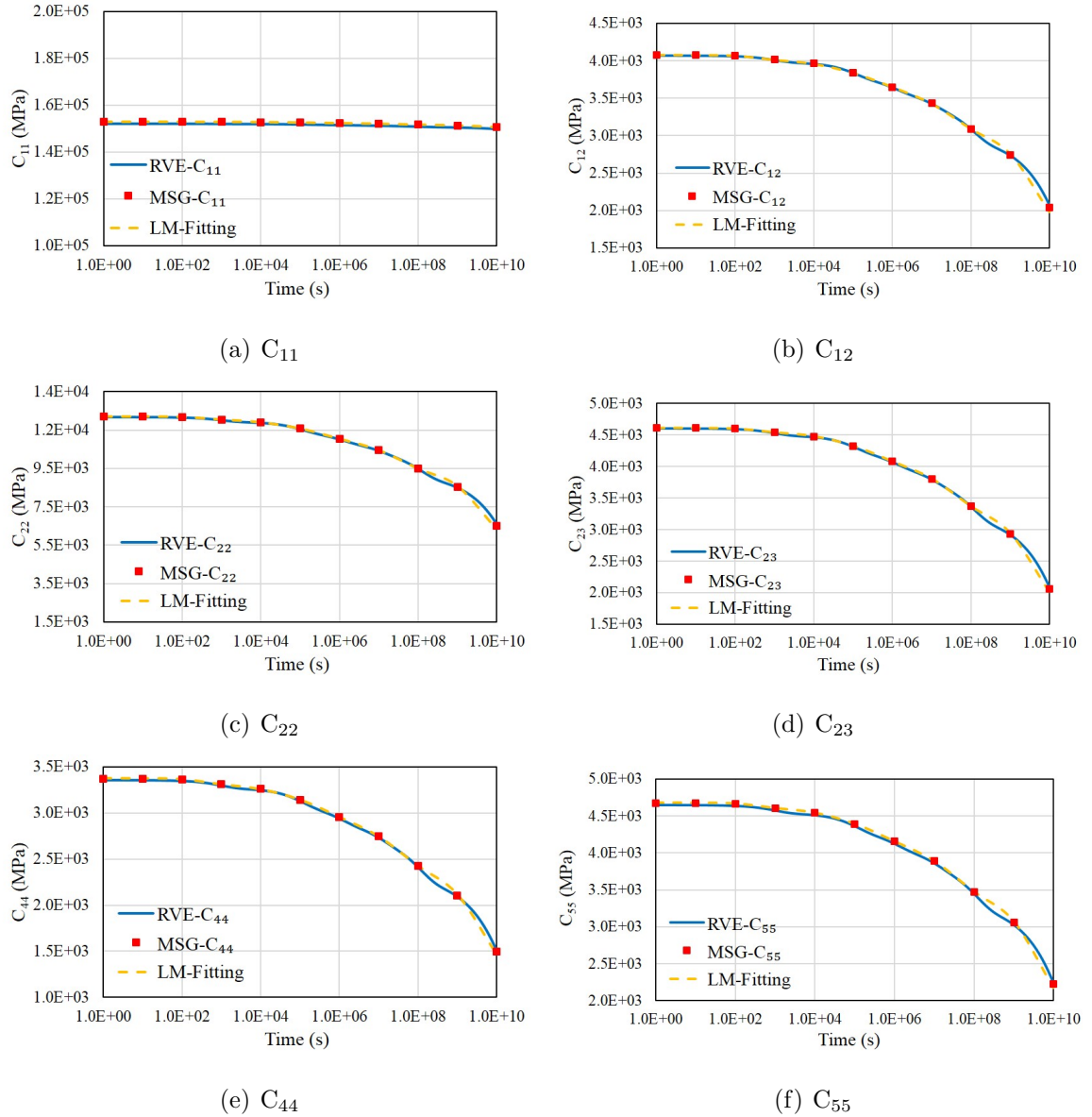
Figure 3.3. The effective relaxation stiffness of the yarn

RVE analysis. In other words, the MSG solid model using a 2D SG can reproduce the results of 3D RVE analysis using FEA without applying complicated boundary conditions. In terms of efficiency, the RVE analysis toke 50 seconds to complete the analysis while MSG toke 7.1 seconds to complete the analysis with the same number of time steps. We can also see that the time has almost negligible impact on the C_{11} because the behavior in the fiber direction is dominated by the time-independent

Table 3.2. Relaxation times and Prony coefficients for yarns

k	ρ_k (s)	$C_{11,k}$	$C_{12,k}$	$C_{22,k}$	$C_{23,k}$	$C_{44,k}$	$C_{55,k}$
∞	–	150200.0	1477.0	4839.0	1393.0	1046.0	1584.0
1	1.0e+3	132.9	100.0	245.6	105.9	100.0	110.9
2	1.0e+5	258.7	190.2	510.6	234.0	175.6	234.8
3	1.0e+6	242.6	176.9	542.1	255.5	190.8	231.9
4	1.0e+7	245.0	221.5	503.1	229.8	190.3	241.9
5	1.0e+8	528.0	434.8	1353.7	613.2	427.2	564.2
6	1.0e+9	100.0	100.0	100.0	100.0	100.0	100.0
7	1.0e+10	1205.6	1378.6	4117.7	1679.1	1143.5	1609.1

behavior of the fibers. Other terms in relaxation stiffness matrix show time-dependent behaviors as the values decrease with the increased time.

In order to demonstrate that the viscoelastic solid model using MSG also computes the instantaneous creep compliance matrix, which is the inverse of the relaxation matrix at the same time. The same RVE model with PBCs is analyzed by applying the constant stress instead of the constant strain. Similar to the analysis for stress relaxation, five analyses are performed to get the values in creep compliance matrix. The results of the RVE analysis are plotted with the creep compliance matrix obtained using MSG viscoelastic solid model as shown in Figure 3.4. The creep compliance matrix of the MSG solid model is obtained by inversing the relaxation stiffness matrix at the same time. The results based on the MSG solid model and 3D RVE model agree well, therefore the instantaneous creep compliance matrix can be directly obtained by inversing the relaxation matrix at the same time.

3.2.2 MSG Macro-homogenization for Woven Composites

For macro-homogenization, the model contains two different materials: yarns and matrix. Based on the analysis in the previous section, both yarns and matrix are
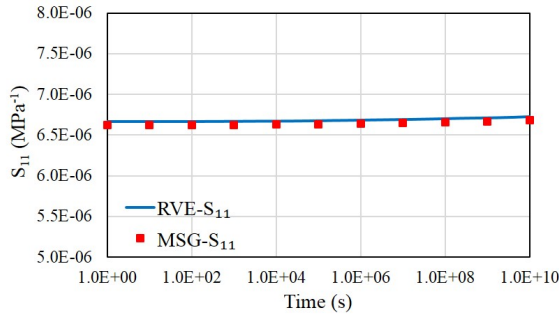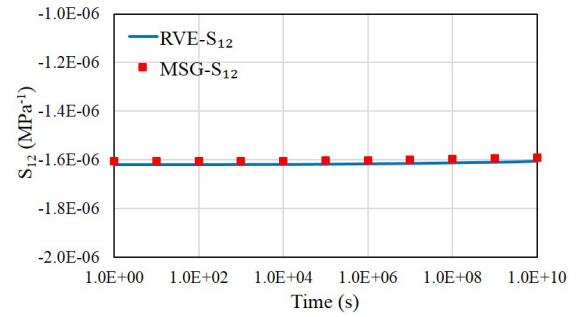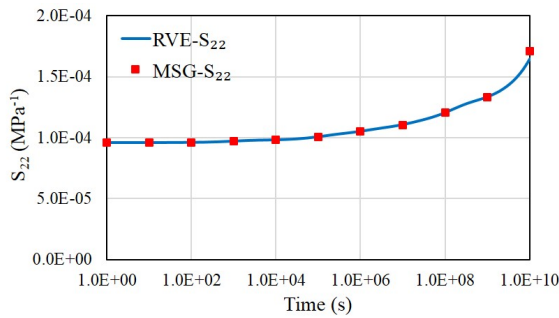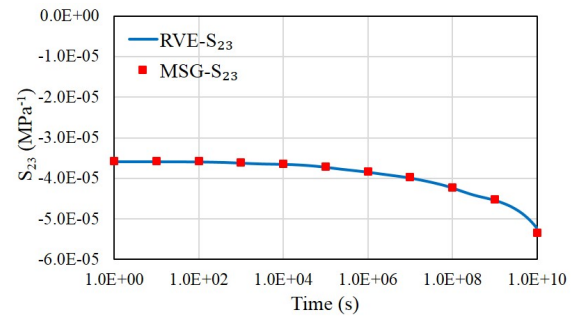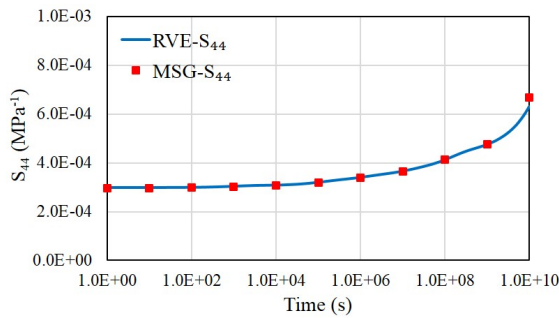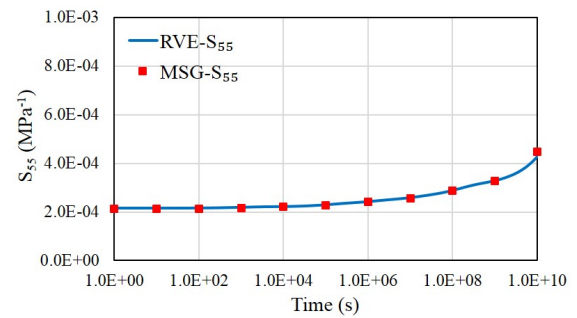
Figure 3.4. The effective creep compliance of the yarn

viscoelastic materials and the corresponding properties vary with time. For this example, there is only one layer in the plain woven fabric, which means the material is not periodic along the thickness direction. Therefore, the time-dependent plate stiffness matrix should be used to represent viscoelastic behavior of this woven composites. To verify the accuracy of the viscoelastic behaviors predicted by using the

MSG plate model, MSG results are compared with the experimental data from the Ref. [39]. The experimental data is obtained based on uniaxial tension and four-point bending creep test of single-ply ±45 lamina. The results based on MSG plate model in the SG coordinate are translated to the experimental coordinate. The thickness and width of the yarns in the MSG model are 0.06 mm and 0.90 mm respectively. The yarn spacing is 1.75 mm and the thickness of the fabric is 0.12 mm. In order to eliminate the mesh dependence on the results, two different mesh sizes are applied for this model using 8-noded solid elements, which contain 50,000 and 168,750 elements respectively. The properties of matrix and yarns are given in the previous sections. The stretching and bending compliance of this plain woven fabric with time are given in Figures 3.5 and 3.6. The MSG solid models with PBCs and aPBCs are also used to analyze the same SG using 50,000 elements. As mentioned in the previous sections, anisotropic viscoelastic properties can be easily defined in MSG models without any user-defined subroutines. The homogenized properties based on the MSG solid model are used to compute the A and D matrices of the plate model, and the results are plotted in Figures 3.5 and 3.6.
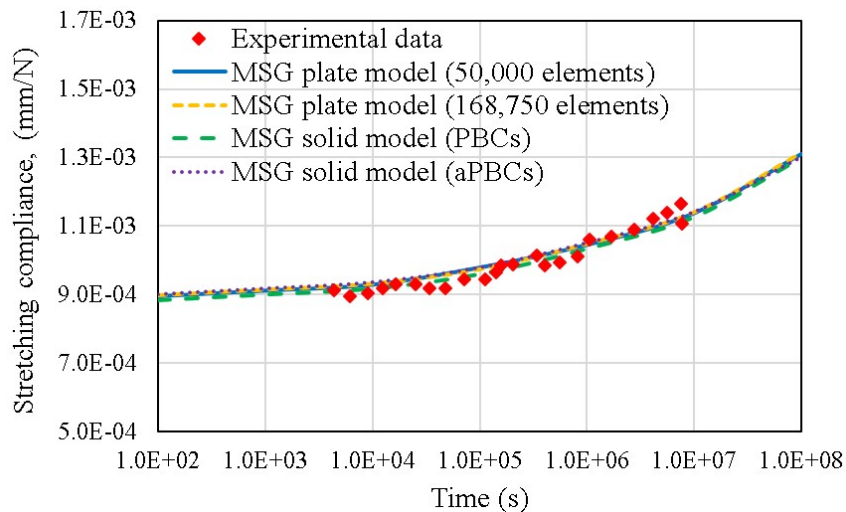
Figure 3.5. Longitudinal stretching compliance of plain woven composites
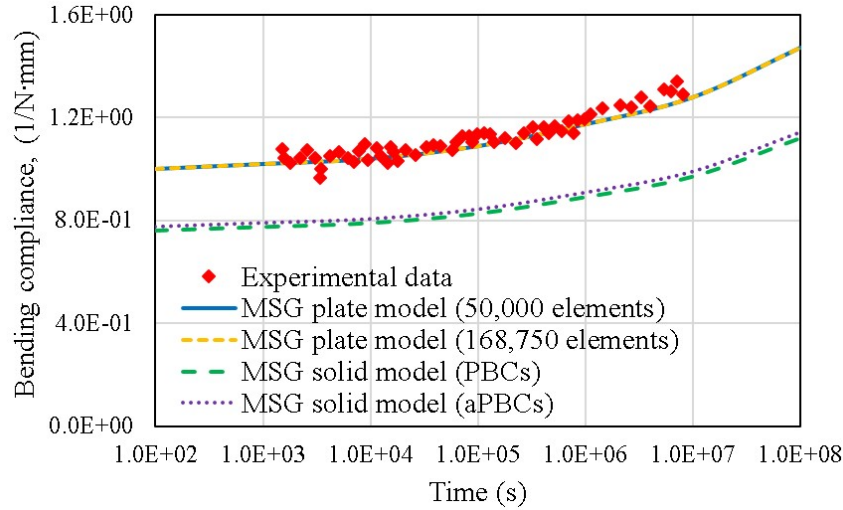
Figure 3.6. Longitudinal bending compliance of plain woven composites

The results of MSG plate model agree well with the experimental data, which means the MSG plate model can provide reasonable predictions for the viscoelastic behaviors of woven composites. In addition, the results based on two different meshes are identical which means the results are converged. The results of MSG solid model based on PBCs and aPBCs for the stretching compliance are almost the same as the results of MSG plate model, because stretching compliance mainly reflects the in-plane behaviors and the in-plane periodicities are considered in both the MSG plate and the solid model. However, big differences of bending compliance are shown in Figure 3.6, which represents the out-of-plane behaviors. For the MSG solid models with PBCs and aPBCs, the bending compliance based on aPBCs is slight better than the results based on PBCs due to the relief of the periodic conditions in the thickness direction, because the experimental sample only contains one layer. However, the MSG solid model still homogenizes the heterogeneity of the plate in the thickness direction which brings inaccuracy in the predicted bending behaviors, but MSG plate model can keep the heterogeneity which gives accurate predictions compared with the experimental data as shown in Figures 3.5 and 3.6.

3.3 Parametric Studies

3.3.1 Model Parameters

In this section, the method proposed is used to study the effects of different weave patterns on the viscoelastic behaviors of general woven composites. The plain woven composites shown in the last section is still used in this section. Two other commonly used woven composites named 2×2 twill woven composites and 3D orthogonal woven composites are also analyzed. The SGs for these two woven composites are given in Figures 3.7 and 3.8.
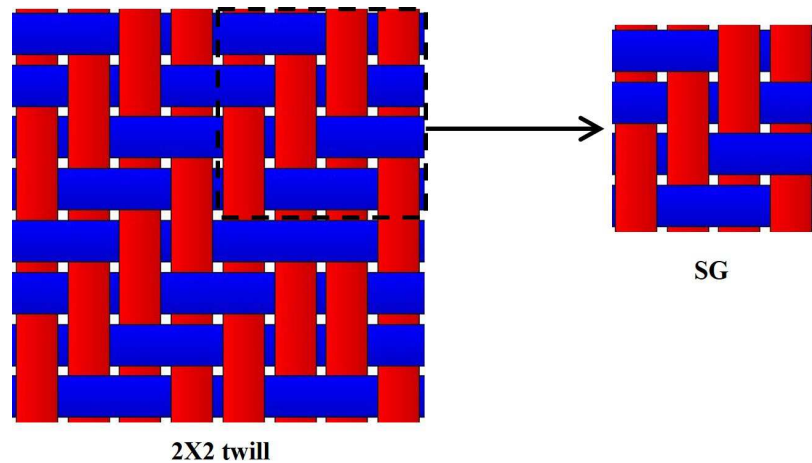
Figure 3.7. 2×2 twill weave and its SG
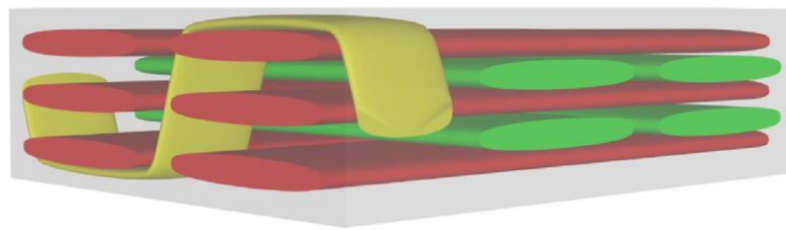
Figure 3.8. SG for 3D orthogonal woven composites

The viscoelastic properties of yarns are obtained using MSG micro-homogenization from the last section. The same yarn volume faction $v_f = 0.52$ is used in all woven

composites examples, and the weft and warp yarns have the same geometry shape. For the plain and twill woven composites, yarn width is 0.68 mm, yarn thickness is 0.1 mm and yarn spacing is 1 mm. For weft and warp yarns in 3D orthogonal woven composites, yarn width is 0.8 mm, yarn thickness is 0.1 mm and yarn spacing is 1 mm, and for the binder yarn, yarn width is 0.4 mm and yarn thickness is 0.05 mm. The plain woven and twill woven composites are made by three layers so that the total thickness of the three woven examples is the same, and the same fiber volume fraction in all fabrics is achieved with the above parameters.

The reference surfaces of the SGs are chosen to be the middle plane surfaces, so the B matrix is zero due to the symmetric of the SGs. In other words, there are no extension-bending couplings for these three SGs. Since the weft and warp yarns are assumed to be the same geometry shapes, the following relations can be obtained for plain and twill woven fabric: $A_{11} = A_{22}$ and $D_{11} \approx D_{22}$. The relations are not true due to the binder yarn for 3D orthogonal woven composites. The viscoelastic behaviors in weft (red yarns in Figure 3.8) and warp (green yarns in Figure 3.8) directions of 3D woven fabric would be different.

3.3.2 Results and Discussion

Figure 3.9 shows the in-plane relaxation coefficients of three different woven fabrics, which reveals plate force relaxation behaviors. Based on Eq. (3.24), Figure 3.9 illustrates the changes of the in-plane forces under the constant in-plane plate strains over the time. The subscript "11" represents the warp direction and "22" represents the weft direction. Figure 3.9(a) indicates the relaxation behaviors of in-plane normal forces. 3D orthogonal woven example shows less relaxation effects than the other two examples. Relaxations of normal forces in warp and weft directions are different in 3D woven example, and the normal force along weft direction shows less relaxation effects. In the warp direction, plain woven shows the most relaxation while 3D woven shows the least relaxation effects. The coupling behaviors between in-plane normal

forces are give in Figure 3.9(b), and the coupling means a constant unit plate strain applied in the weft direction would cause the force A_{12} in the warp direction. An interesting observation is that A_{12} increases with the time in the plain and twill woven examples, which means the larger normal force is needed to maintain the initial strain in the transverse direction. However, 3D orthogonal woven exhibits an oppose trend. Figure 3.9(c) shows the viscoelastic behaviors of in-plane shear forces, and all the woven examples show the same relaxation effects over the time.
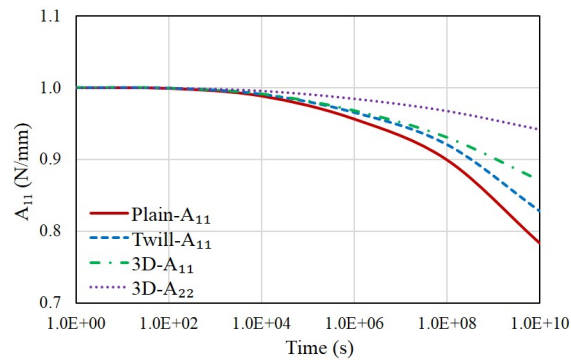
(a) A_{11}
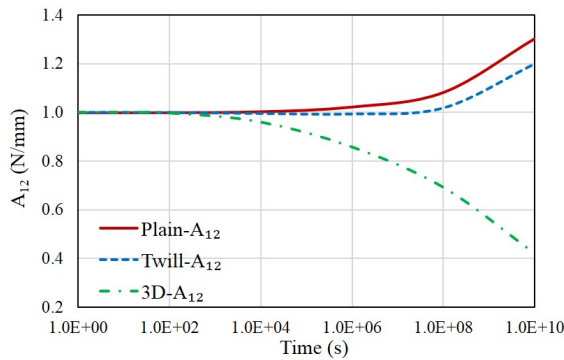
(b) A_{12}
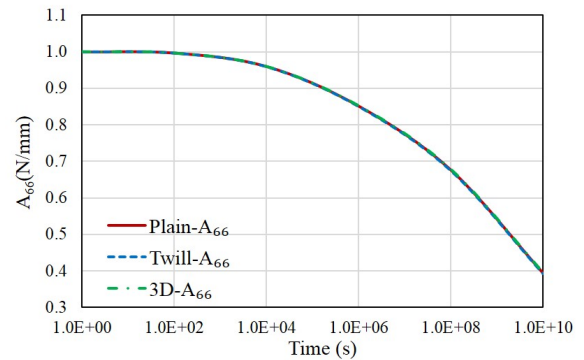
(c) A_{66}

Figure 3.9. In-plane relaxation coefficients

Figure 3.10 shows the bending relaxation coefficients of three different woven composites, which reveals plate bending moment relaxation effects. Based on Eq. (3.24), Figure 3.10 illustrates the changes of the bending moments under the constant plate

curvatures over the time. Figure 3.10(a) indicates the relaxation behaviors of bending moments along the weft and warp direction. Unlike the relaxation of in-plane forces, twill woven example shows less relaxation effects than the other two examples in the warp direction, but 3D orthogonal woven example shows less relaxation effects in the weft direction. The coupling behaviors between bending moments are give in Figure 3.10(b). The coupling behaviors for bending moments mean that a constant unit plate curvature applied in the weft direction leads to D_{12} moment in the warp direction. All the coupling induced bending moments decreases with time and the plain woven example shows the least relaxation effects over the other two examples. Figure 3.10(c) shows the viscoelastic behaviors of M_{12}, and all the woven examples show the same relaxation effects over the time.
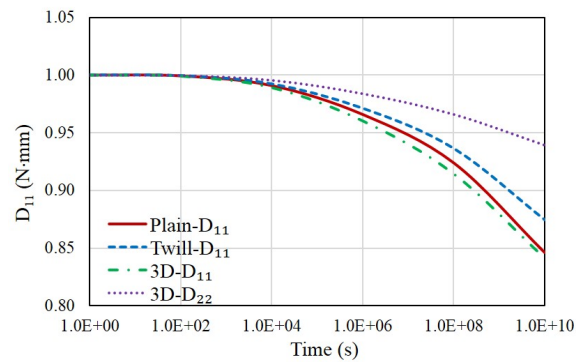

(a) D_{11}
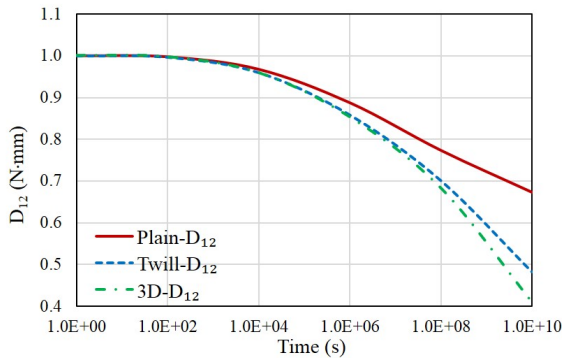
(b) D_{12}
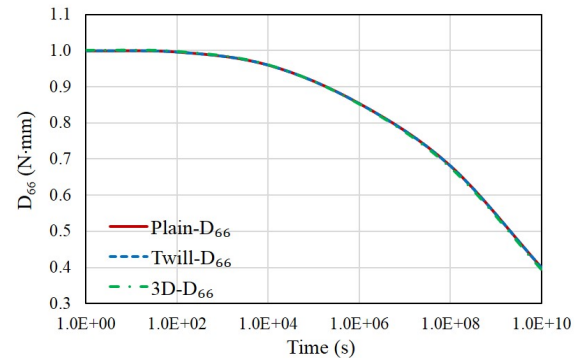
(c) D_{66}

Figure 3.10. Out-of-plane relaxation coefficients

Based on the above results, if the relaxation effects are the design parameters to be minimized. 3D orthogonal woven composites are the preferable materials if the relaxation of in-plane forces are the main concerns in the design. If the bending moments are the main loading cases in the design, 3D orthogonal woven composites can provide better long-term performance in the weft direction while the warp direction has poor long-term performance. 2×2 twill woven composites might provide the balanced performance in both directions for the structures under long-term bending moments.

3.4 Summary

In this chapter, a new multiscale approach based on MSG is proposed to study the viscoelastic behaviors of textile composites. MSG two-step homogenization is carried out at microscale (yarn) and macroscale (woven composites). At the microscale level, homogenized viscoelastic properties of yarns are computed considering elastic fibers and viscoelastic matrix properties using the MSG solid model. At the macroscale level, the viscoelastic yarn and matrix are used to compute the overall viscoelastic behaviors of textile composites, which are expressed in terms of A, B and D matrices using the MSG plate model. In order to validate the proposed model, a 3D RVE model is created using Abaqus 6.13 at microscale, and the viscoelastic properties are computed by applying PBCs using FEA. The viscoelastic behaviors at macroscale using the MSG plate model are validated using the experimental data in the literature. All the results based on the proposed approach agree well with the reference results, and MSG approach is much more efficient than the RVE analysis. Plain woven, 2×2 twill woven and 3D orthogonal woven composites are analyzed using the proposed method. With the same thickness and fiber volume fraction, the long-term in-plane behavior of 3D orthogonal woven is more stable than plain woven and 2×2 twill woven fabric. For the long-term bending behaviors, 3D orthogonal woven example has better performance in the weft direction while 2×2 twill woven example gives

more balanced performance along weft and warp directions. The proposed approach can be used in the textile composite structures design when the long-term behaviors due to material viscoelastic properties are concerned.

4. MULTISCALE THERMOELASTIC ANALYSIS OF TEXTILE COMPOSITES

MSG has been developed as a multiscale and multiphysics approach for constitutive modeling of composite structures. In this chapter, the variational statement of the MSG models has been modified to capture the pointwise temperature loads. Moreover, thermal stress resultants are derived from the MSG plate and beam models to describe the thermal-induced mechanical behaviors of thin and slender textile composite structures. Copyright permissions have been obtained to reuse the published materials from [13] in this chapter.

4.1 MSG Thermoelastic Constitutive Modeling

The kinematics of the MSG models are defined in the Chapter 2. To account for the thermoelastic behavior of composites, the variational statement must be modified.

4.1.1 MSG Variational Statement

We can define the thermal stress tensor β_{ij} in terms of the elasticity tensor C_{ijkl} and thermal expansion tensor α_{kl} as:

$$\beta_{ij} = C_{ijkl}\alpha_{kl} \tag{4.1}$$

Then, the linear constitutive equation can be expressed as:

$$\sigma_{ij} = C_{ijkl}\varepsilon_{kl} - \beta_{ij}\theta \tag{4.2}$$

where θ can be considered as the thermal load that denotes the difference between the actual temperature and the reference temperature.

Using the strain measures defined in Eq. (2.12), the Helmholtz free energy density can be expressed as [68]:

$$U = \frac{1}{2\omega} \left\langle \Gamma^T C \Gamma - 2\beta\Gamma\theta + c_v \frac{\theta^2}{T_0} \right\rangle \tag{4.3}$$

where ω denotes the volume of the domain spanned by y_k. c_v is the specific heat per unit volume at constant volume, T_0 is the reference temperature at which the constituent material is stress free. MSG minimizes the free energy loss of the original model and homogenized model. Since the free energy of the homogenized model is independent of the fluctuating functions. The problem is equivalent to minimize Eq. (4.3) with respect to the fluctuating functions. The variational statement is:

$$\delta\frac{1}{2\omega} \left\langle \Gamma^T C \Gamma - 2\beta\Gamma\theta + c_v \frac{\theta^2}{T_0} \right\rangle = 0 \tag{4.4}$$

Plugging Eq. (2.12) into Eq. (4.4), the following equation can be obtained

$$\delta\frac{1}{2\omega} \left\langle (\Gamma_h\chi + \Gamma_\epsilon\bar{\epsilon})^T C (\Gamma_h\chi + \Gamma_\epsilon\bar{\epsilon}) - 2\beta (\Gamma_h\chi + \Gamma_\epsilon\bar{\epsilon})\theta + c_v \frac{\theta^2}{T_0} \right\rangle = 0 \tag{4.5}$$

4.1.2 Finite Element Implementation

In general, a numerical technique such as the finite element method is used to solve the variational statement in Eq. (4.5). To this end, the fluctuating functions χ over SG can be expressed as:

$$\chi(x_k, y_j) = S(y_j)V(x_k) \tag{4.6}$$

where S are the standard shape functions depending on the type of elements. V is what we need to solve for as the nodal values. Plugging Eq. (4.6) into Eq. (4.5), we obtain the following discretized version of the variational statement:

$$\delta\frac{1}{2\omega} \left(V^T E V + 2V^T D_{h\epsilon}\bar{\epsilon} + \bar{\epsilon}^T D_{\epsilon\epsilon}\bar{\epsilon} - 2V^T D_{h\theta} - 2D_{\epsilon\theta}\bar{\epsilon} + \frac{D_{\theta\theta}}{T_0} \right) = 0 \tag{4.7}$$

where

$$E = \left\langle (\Gamma_h S)^T C(\Gamma_h S) \right\rangle, \quad D_{h\epsilon} = \left\langle (\Gamma_h S)^T C\Gamma_\epsilon \right\rangle, \quad D_{\epsilon\epsilon} = \left\langle \Gamma_\epsilon^T C\Gamma_\epsilon \right\rangle$$
$$D_{h\theta} = \left\langle (\Gamma_h S)^T \beta\theta \right\rangle, \quad D_{\epsilon\theta} = \left\langle \beta\Gamma_\epsilon\theta \right\rangle, \quad D_{\theta\theta} = \left\langle c_v\theta^2 \right\rangle \tag{4.8}$$

There are two modifications in the variational statement in Eqs. (4.7) and (4.8) compared with the statement in [84]. First, the current statement has been generalized to consider different models (i.e. solid, plate and beam) by introducing the general strain expression in Eq. (2.12). Second, the thermal load θ can be pointwisely distributed in the SG while the θ was assumed to be constant in the original variational statement in [68]. By removing the constant θ assumption, MSG models can be used for various temperature distribution cases.

Performing the variation in Eq. (4.7) subjected to the constraints based on different MSG models as well as other constrains (e.g. $\chi_i^+ = \chi_i^-$ if there is a periodic boundary condition in y_i direction) if needed, we can obtain the following linear system:

$$EV = -D_{h\epsilon}\bar{\epsilon} + D_{h\theta} \tag{4.9}$$

The solution V can be symbolically expressed as:

$$V = V_0\bar{\epsilon} + V_\theta \tag{4.10}$$

where $V_0 = -E^{-1}D_{h\epsilon}$ and $V_\theta = E^{-1}D_{h\theta}$.

Based on Eq. (4.10), the free energy density can be rewritten as:

$$U = \frac{1}{2}\bar{\epsilon}^T\bar{C}\bar{\epsilon} - \bar{\epsilon}^T\hat{\beta} + \hat{c}_v \tag{4.11}$$

where

$$
\begin{aligned}
\bar{C} &= \frac{1}{\omega}(V_0^T D_{h\epsilon} + D_{\epsilon\epsilon}) \\
\hat{\beta} &= \frac{1}{\omega}\left[\frac{1}{2}(V_0^T D_{h\theta} - D_{h\epsilon}^T V_\theta) + D_{\epsilon\theta}\right] \\
\hat{c}_v &= \frac{1}{2\omega}\left[\frac{D_{\theta\theta}}{T_0} - V_\theta^T D_{h\theta}\right]
\end{aligned}
\tag{4.12}
$$

Eq. (4.12) gives effective thermoelastic properties of the macroscopic structural model. For the Euler-Bernoulli beam model, $\bar{C}$ could be a fully populated 4×4 stiffness matrix. For the Kirchhoff-Love plate/shell model and Cauchy continuum model, $\bar{C}$ could be a fully populated 6×6 stiffness matrix. $\hat{\beta}$ is effective thermal induced stresses or stress resultants depends on the MSG models. $\hat{c}_v$ is the energy

density contributed by the effective specific heat. The above constitutive information can be used to perform beam, plate or solid structural analysis. For example, the effective CTEs can be obtained using MSG solid model based on Eq. (4.1). If the MSG plate model is used, the corresponding constitutive relation can be written as:

$$
\begin{Bmatrix} N_{11} \\ N_{22} \\ N_{12} \\ M_{11} \\ M_{22} \\ M_{12} \end{Bmatrix} = \begin{bmatrix} A_{11} & A_{12} & A_{16} & B_{11} & B_{12} & B_{16} \\ A_{12} & A_{22} & A_{26} & B_{12} & B_{22} & B_{26} \\ A_{16} & A_{26} & A_{66} & B_{16} & B_{26} & B_{66} \\ B_{11} & B_{12} & B_{16} & D_{11} & D_{12} & D_{16} \\ B_{12} & B_{22} & B_{26} & D_{12} & D_{22} & D_{26} \\ B_{16} & B_{26} & B_{66} & D_{16} & D_{26} & D_{66} \end{bmatrix} \begin{Bmatrix} \epsilon_{11} \\ \epsilon_{22} \\ 2\epsilon_{12} \\ \kappa_{11} \\ \kappa_{22} \\ 2\kappa_{12} \end{Bmatrix} - \begin{Bmatrix} N_{T_{11}} \\ N_{T_{22}} \\ N_{T_{12}} \\ M_{T_{11}} \\ M_{T_{22}} \\ M_{T_{12}} \end{Bmatrix} \tag{4.13}
$$

where $\bar{C}$ is expressed in terms of the ABD matrix, and the thermal induced stress resultants of the MSG plate model are:

$$
\hat{\beta} = [N_{T_{11}} \quad N_{T_{22}} \quad N_{T_{12}} \quad M_{T_{11}} \quad M_{T_{22}} \quad M_{T_{12}}]^T \tag{4.14}
$$

Similarly, if the MSG beam model is used, the corresponding constitutive relation can be written as:

$$
\begin{Bmatrix} F_1 \\ M_1 \\ M_2 \\ M_3 \end{Bmatrix} = \begin{bmatrix} C_{11}^b & C_{12}^b & C_{13}^b & C_{14}^b \\ C_{12}^b & C_{22}^b & C_{23}^b & C_{24}^b \\ C_{13}^b & C_{23}^b & C_{33}^b & C_{34}^b \\ C_{14}^b & C_{24}^b & C_{34}^b & C_{44}^b \end{bmatrix} \begin{Bmatrix} \epsilon_1 \\ \kappa_1 \\ \kappa_2 \\ \kappa_3 \end{Bmatrix} - \begin{Bmatrix} F_{T_1} \\ M_{T_1} \\ M_{T_2} \\ M_{T_3} \end{Bmatrix} \tag{4.15}
$$

where $\bar{C}$ is expressed in terms of a 4×4 stiffness matrix, and the thermal induced stress resultants of the MSG beam model are:

$$
\hat{\beta} = [F_{T_1} \quad M_{T_1} \quad M_{T_2} \quad M_{T_3}] \tag{4.16}
$$

After the structural analysis, the global structure responses $\bar{\epsilon}$ can be used to recover the local stress and strain field. The fluctuating function can be obtained as:

$$
\chi = SV_0\bar{\epsilon} + SV_\theta \tag{4.17}
$$

Plug Eq. (4.17) into Eq. (2.12), the local strain field can be obtained as:

$$\Gamma = (\Gamma_h SV_0 + \Gamma_\epsilon)\bar{\epsilon} + \Gamma_h SV_\theta \tag{4.18}$$

Based on the 3D constitutive relations in Eq. (4.2) for each constituent material, the local stress field can be recovered as:

$$\sigma = C\Gamma - \beta\theta \tag{4.19}$$

4.2 MSG-based Multiscale Thermoelastic Modeling Framework

The overall modeling framework of MSG-based multiscale thermoelastic structural analysis is given in Figure 4.1. The original structural analysis has been decoupled into MSG homogenization, macroscopic structural analysis and MSG dehomogemization. The decomposition of the original structural analysis can greatly improve the computational efficiency while maintaining the accuracy. The first step of MSG-based multiscale modeling is to identify the SG based on the heterogeneity of the original structure and the pointwise temperature load. Then, using the homogenization analysis, the effective thermoelastic constitutive information is computed based on different MSG models. For the MSG solid model, the constitutive information is effective material properties and CTEs. For the MSG plate and beam models, the constitutive information is the plate or beam stiffness matrix and thermal induced stress resultants.

For the macroscopic thermoelastic structural analysis, since the temperature load has already been taken into account during the constitutive modeling, the thermal stress or thermal induced stress resultants can be directly used in the structural analysis with temperature load $\Delta T = 1$. The thermoelastic constitutive information of the MSG plate model can be directly input into Abaqus using the "General Stiffness Section" for modeling plate structures. The thermoelastic constitutive information of the MSG beam model can be used to solve the beam structural responses analytically [11].
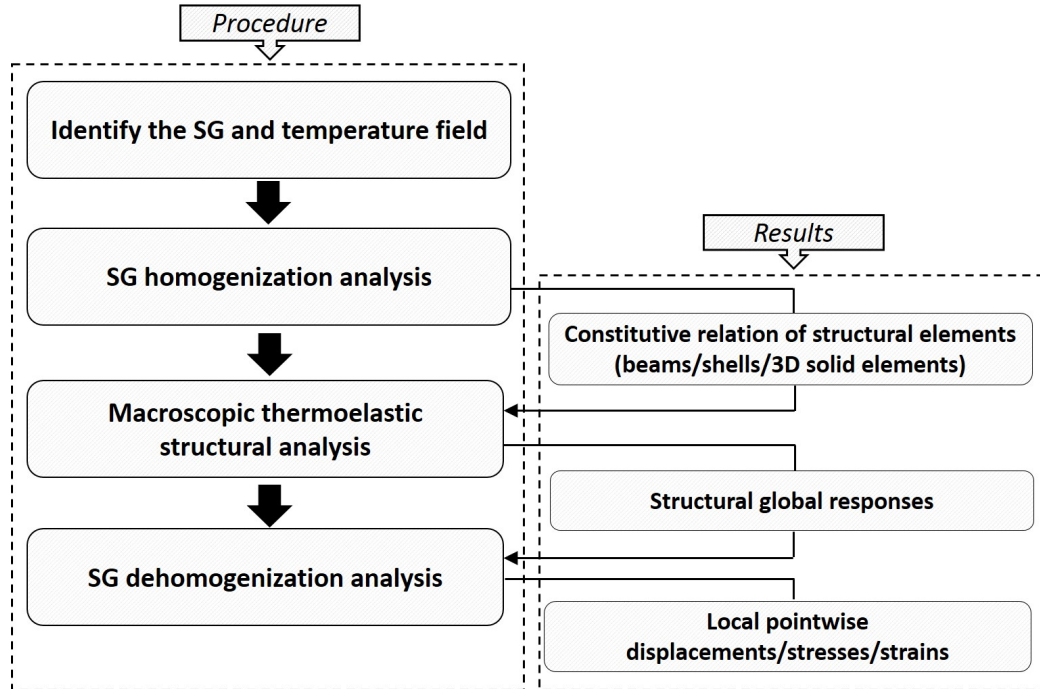
Figure 4.1. MSG-based multiscale thermoelastic modeling framework

After the structural analysis, the structural responses $\bar{\epsilon}$ based on different MSG models can be obtained, and then the responses are used to recover the local fields in the SG. In the next section, several numerical examples are used to demonstrate the accuracy and efficiency of the proposed approach.

4.3   Numerical Examples

Woven numerical examples are analyzed in this section to show the accuracy and efficiency of the proposed MSG thermoelastic models. The fiber and matrix properties used in the examples are given in Table 4.1.

Based on the MSG solid model, a square packed SG with fiber volume fraction $V_f = 0.64$ is used to obtain the effective thermoelastic properties for the yarn, which will be used in the examples in this chapter. The accuracy and efficiency of using MSG solid model in predicting effective elastic properties and CTEs of unidirectional (UD)

Table 4.1. Thermomechanical properties of fiber and matrix [85]

Properties	T300 carbon fiber	Epoxy resin
E_1 (GPa)	230.00	3.45
$E_2 = E_3$ (GPa)	40.00	3.45
$G_{12} = G_{13}$ (GPa)	24.00	1.28
G_{23} (GPa)	14.30	1.28
$\nu_{12} = \nu_{13}$	0.26	0.35
ν_{23}	0.40	0.35
α_{11} (ppm/°C)	-0.70	63.00
$\alpha_{22} = \alpha_{33}$ (ppm/°C)	10.00	63.00

Table 4.2. Effective thermomechanical properties of the lamina and yarn

Properties	lamina and yarn
E_1 (MPa)	1.484×10^5
$E_2 = E_3$ (MPa)	1.437×10^4
$G_{12} = G_{13}$ (MPa)	5.133×10^3
G_{23} (MPa)	3.398×10^3
$\nu_{12} = \nu_{13}$	0.286
ν_{23}	0.342
α_{11} (ppm/°C)	-0.108
$\alpha_{22} = \alpha_{33}$ (ppm/°C)	31.975

composites are shown in the previous work [86]. The results of effective thermoelastic properties are given in Table 4.2.

To study the efficiency of the proposed method, all the MSG and FEA analyses in this chapter are performed in a Windows workstation with 128 GB RAM and 2.70GHz CPU. For the structural analysis of composite structures, MSG approach decouples the analysis into constitutive modeling (homogenization and dehomogenization) and structural analysis of homogenized body. As the SG in constitutive modeling and

homogenized body in the structural modeling requires much fewer degrees of freedom, the computing time of MSG is much less than the corresponding DNS using FEA.

4.3.1 Effective CTEs for a Plain Woven Composite

To get the overall effective properties of textile composites, a two-step homogenization approach is usually used [10]. The first step is to get effective yarn properties which are given in Table 4.2. Once yarn properties are obtained, we can perform the second step homogenization based on yarn and matrix properties. In multiscale modeling using a solid model, a RVE is considered as a point at the structural level, therefore a constant temperature load is often applied to determine the effective thermoelastic properties [42]. In this example, the effective elastic properties and CTEs of a plain weave unit cell are computed using the MSG solid model. To prove the accuracy and efficiency of the MSG solid model, a 3D RVE model is also used to analyze the same plain weave unit cell. The unit cell contains 50,000 C3D8 elements. The PBCs and a constant temperature load are applied to get the effective thermoelastic properties.

As observed from the results given in Table 4.3, the differences of the engineering constants and CTEs based on MSG and RVE models are within 1%. In terms of the computing time, the MSG model only took 83 seconds while 3D RVE model took 963 seconds using a single CPU. Therefore, for predicting the effective thermoelastic properties of composites, MSG solid model can achieve the same accuracy as 3D RVE model while the computational efficiency has been greatly improved.

4.3.2 Layered 2D Woven Beam

A two-layer plain weave composite beam is analyzed using the MSG beam model. The length is 20 mm, the width is 2 mm and the thickness is 0.4 mm. The woven beam structure and its SG are shown in Figure 4.2. This beam structure is subjected to fixed-free boundary conditions, and the temperature load is $\Delta T = (-50 - 200 \times x_3)$

Table 4.3. Comparison of effective thermoelastic properties between
MSG and 3D RVE results

	MSG solid model	3D FEA	Diff (%)
Computational time (s)	83	963	
$E_1=E_2$ (GPa)	4.266	4.256	0.235%
E_3 (GPa)	9.313	9.288	0.269%
G_{12} (GPa)	3.128	3.127	0.032%
$G_{13}=G_{23}$ (GPa)	2.455	2.452	0.122%
ν_{12}	0.145	0.145	0.000%
$\nu_{13}=\nu_{23}$	0.390	0.390	0.000%
$\alpha_{11}=\alpha_{22}$ (ppm/°C)	6.010	6.004	0.100%
α_{33} (ppm/°C)	65.681	65.630	0.078%

°C, where x_3 varies from -0.2 to 0.2 mm. The length, width and thickness of the SG are 2 mm, 2 mm, and 0.4 mm respectively. The 20-noded brick element is used to discretize the SG and the DNS model. There are 32,000 and 320,000 elements for the SG and the DNS model respectively. The width of warp and weft yarns is 0.8 mm, yarn spacing is 1 mm and yarn height is 0.1 mm.

After homogenization analysis using the MSG beam model, the non-zero components in the beam stiffness matrix are: $C_{11}^b = 2.944 \times 10^4$ N, $C_{22}^b = 1.137 \times 10^2$ N · mm², $C_{33}^b = 3.989 \times 10^2$ N · mm², $C_{44}^b = 8.525 \times 10^3$ N · mm². The non-zero thermal induced stress resultants are: $N_{T_1} = -10.59$ N, $M_{T_2} = -0.593$ N · mm, $M_{T_3} = 1.584 \times 10^{-3}$ N · mm. Based on Eq. (4.15), the beam strain measures can be computed analytically for composite beam structures subjected to thermal loads. The displacements in x_3 direction based on the MSG-beam model as well as the results from DNS are plotted in Figure 4.3.

The significant local stresses (σ_{11} and σ_{22}) computed using the MSG beam model are compared with the results from the DNS model. The contour plots of the SG are shown in Figures 4.4(a) and 4.5(a). The matrix part is hidden for a better view of
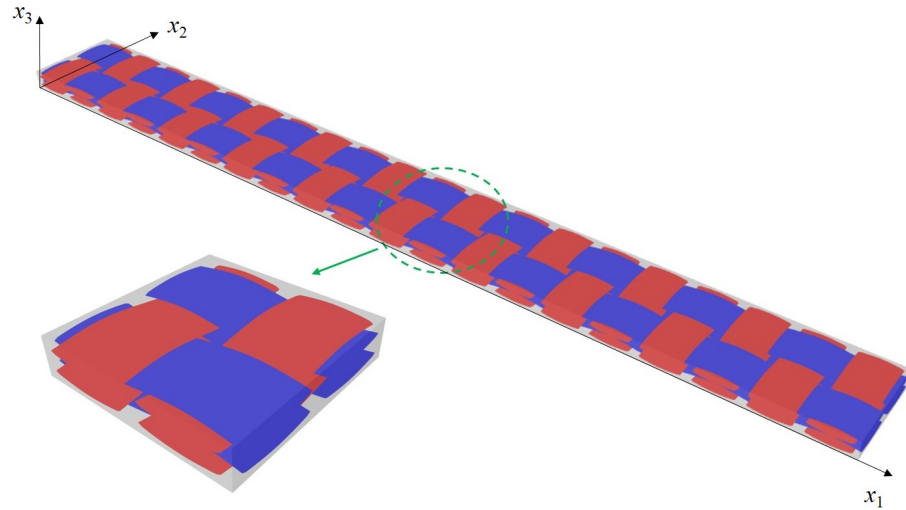
Figure 4.2. Layered plain weave beam and its SG
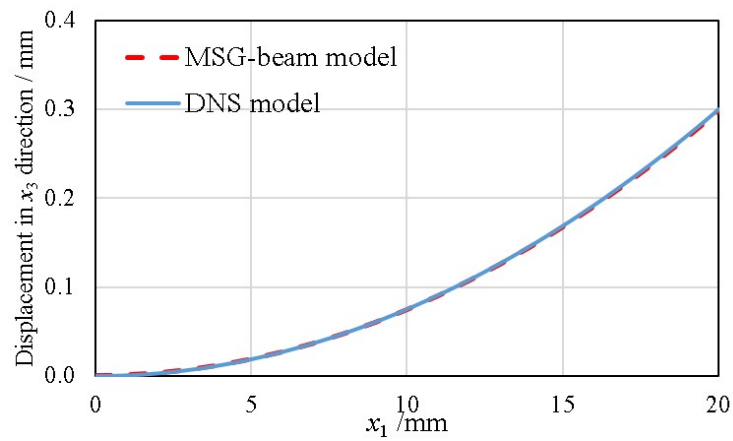
Figure 4.3. Displacement in x_3 direction predicted using the DNS ad MSG beam modal

stress fields in yarns. The stress distributions along the thickness direction at location (9.5 mm, 0.5 mm) are plotted and compared with the results of the DNS model as shown in Figures 4.4(b) and 4.5(b). The path of the stress distribution is highlighted using a red line in the contour plots.

The comparison with DNS results gives evidence that the MSG beam model can accurately predict the local stress distribution in different yarns. Due to the com-
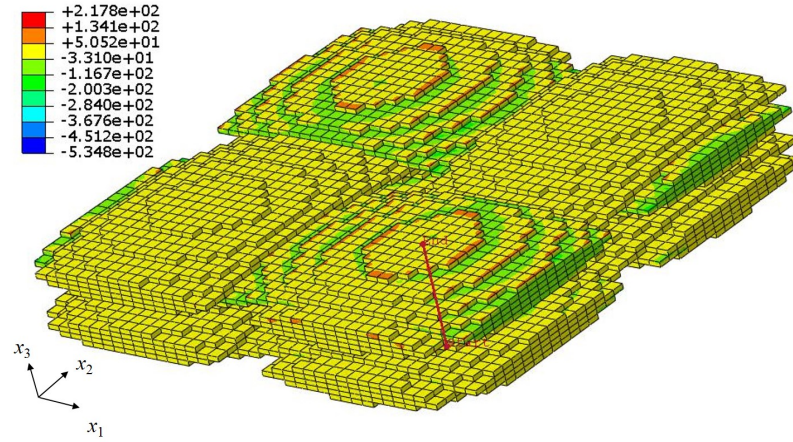
(a) σ_{11} contour plot
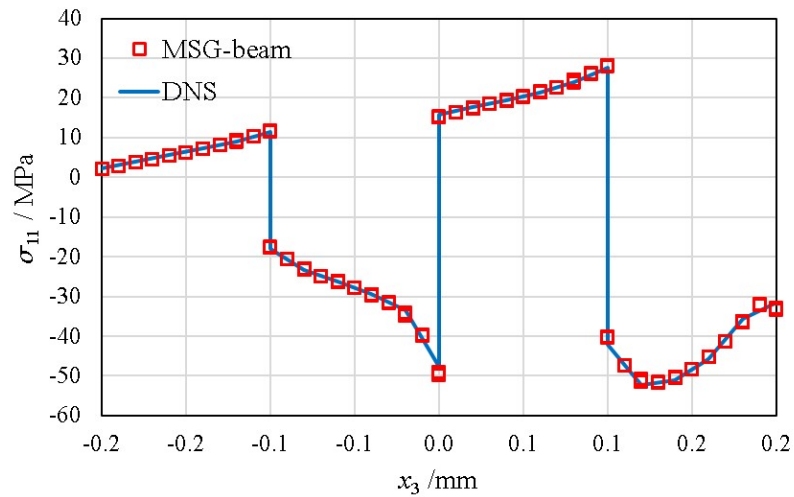
(b) σ_{11} through the path

Figure 4.4. σ_{11} distribution in the SG and the comparison with the DNS model

plexity of the microstructure in woven composites, the local stress distribution can be complex as shown in Figures 4.4 and 4.5. For the computing time, the MSG beam model took 16.2 minutes with 1 CPU for the entire analysis including homogenization (15.0 minutes) and dehomogenization (1.2 minutes), while DNS took 25 minutes with 16 CPUs.
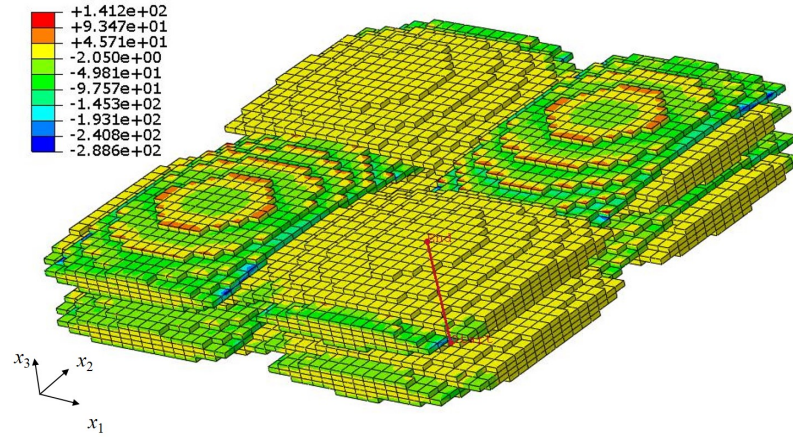
(a) σ_{22} contour plot
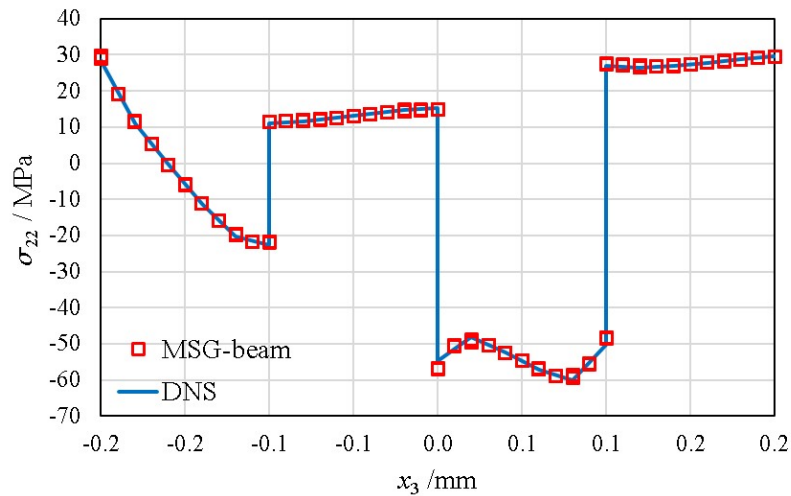
(b) σ_{22} through the path

Figure 4.5. σ_{22} distribution in the SG and the comparison with the DNS model

4.3.3 3D Orthogonal Woven Plate

Due to the complexity of 3D woven composites, using traditional methods such as the CLPT to predict plate stiffness matrix may introduce great loss of accuracy, but the MSG plate model can give accurate prediction for both structural responses and local fields under mechanical loads. With the developed thermoelastic functions in MSG models, the displacements and local fields under temperature loads can also

be accurately predicted. The original woven plate structure and its 3D SG is shown in Figure 4.6. For the plate structure, the length is 20 mm, width is 21 mm, and thickness is 0.6 mm. For the SG, the dimensions are 2 mm × 3 mm × 0.6 mm. Like the beam example, 20-noded brick elements are used in the SG model and DNS model. The SG contains 16,000 elements, and the DNS model contains 1,120,000 elements. The warp and weft yarns have the same dimensions. The yarn width is 0.8 mm, yarn spacing is 1 mm and yarn height is 0.1 mm. The width and height of the binder yarns is 0.4 mm and 0.05 mm.
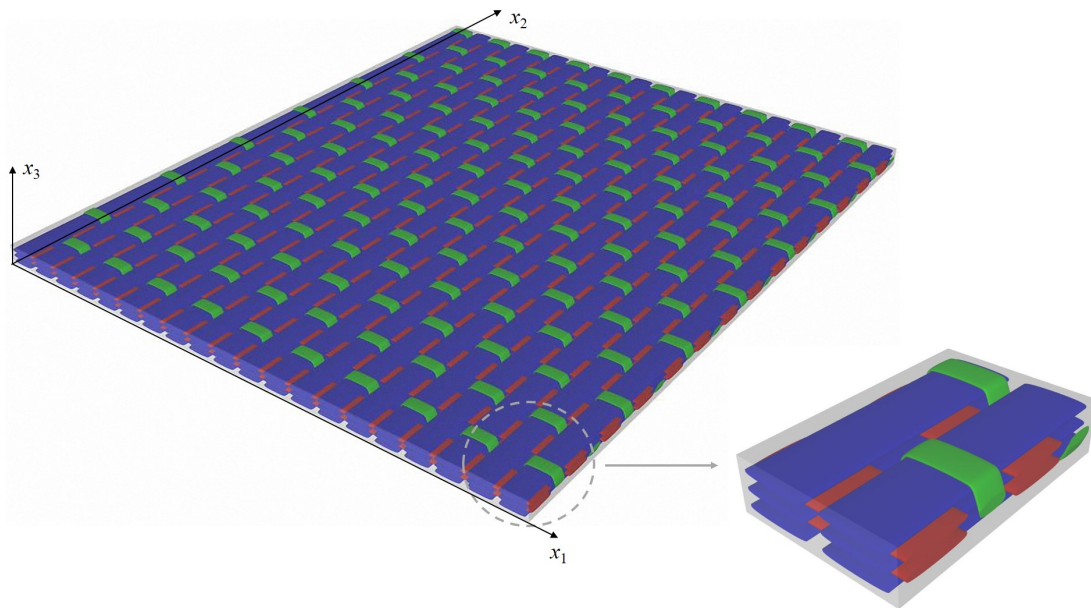
Figure 4.6. 3D orthogonal plate and its SG

Linear temperature load through the thickness

The plate is subjected to clamped-free boundary conditions and a linear temperature load along the thickness direction $\Delta T = (-50 - 100 \times x_3)$ °C. The reference surface of the plate is the middle plate surface, therefore x_3 varies from -0.3 to 0.3 mm. The non-zero components of the plate stiffness matrix are $A_{11} = 1.755 \times 10^4$ N/mm, $A_{22} = 3.300 \times 10^4$ N/mm, $A_{12} = A_{21} = 1.512 \times 10^3$ N/mm, $A_{66} =$

1.709×10^3 N/mm, $D_{11} = 2.873 \times 10^2$ N·mm, $D_{22} = 8.599 \times 10^2$ N·mm, $D_{12} = D_{21} = 3.911 \times 10^1$ N·mm, $D_{66} = 4.607 \times 10^1$ N·mm. The non-zero thermal induced stress resultants are $N_{T_{11}} = -10.26$ N/mm, $N_{T_{22}} = -8.486$ N/mm, $M_{T_{11}} = -0.632$ N, $M_{T_{22}} = -0.509$ N. All the constitutive information can be input into Abaqus S8R elements through the "General Stiffness Section" function for the 2D macroscopic plate analysis. The displacements in the x_3 direction based on the MSG and DNS model are plotted in Figure 4.7.
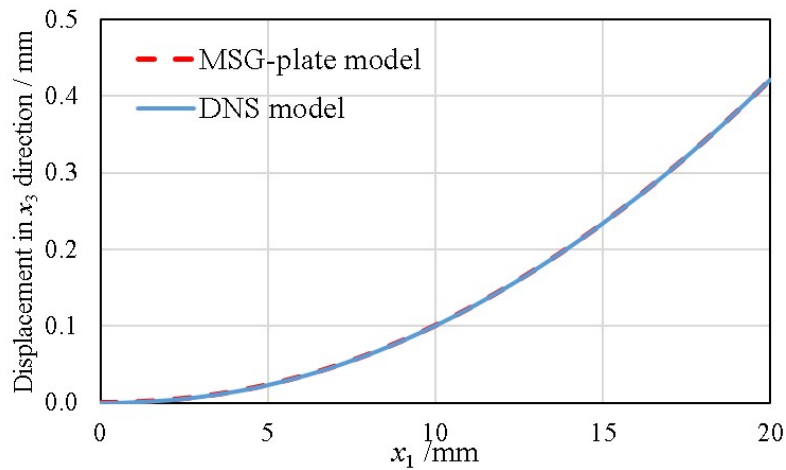
Figure 4.7. Displacement in x_3 direction predicted using the DNS ad MSG plate modal

The contour plots of significant local stresses σ_{11} and σ_{22} of the SG are shown in Figures 4.8(a) and 4.9(a). The matrix part is hidden for a better view of stress fields in yarns. In order to demonstrate the accuracy of the proposed model, the stress distribution along the thickness direction at location (9.5 mm, 9.45 mm) are plotted and compared with the results of the DNS model as shown in Figures 4.8(b) and 4.9(b). The path of the stress distribution is also highlighted using a red line in the contour plots.

Based on the verification against DNS results, the MSG plate model can accurately capture the structural displacements and local stress fields subjected to the linear temperature load through the thickness direction. In terms of the computing time,
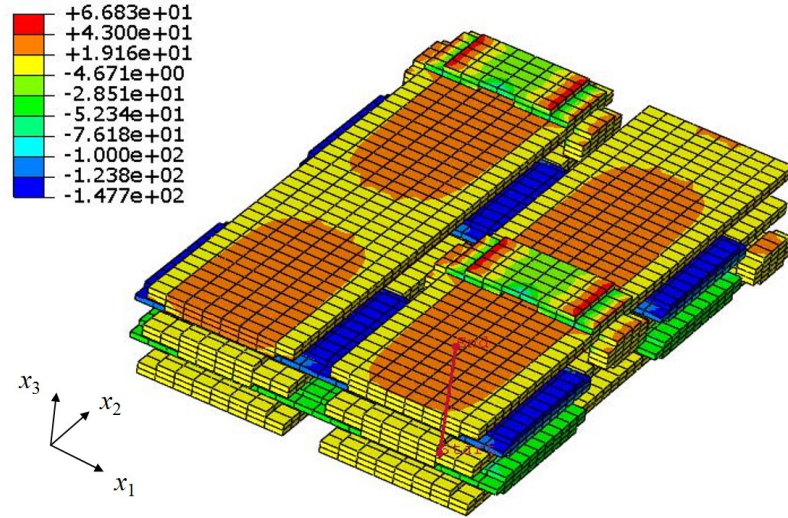
(a) σ_{11} contour plot
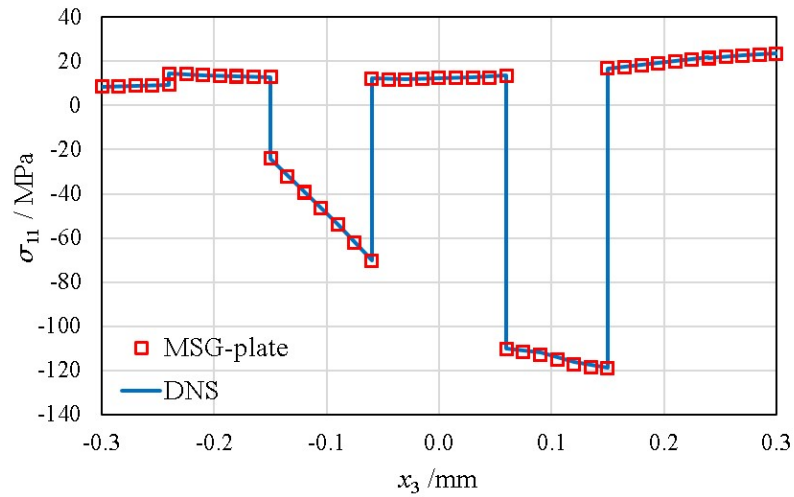
(b) σ_{11} through the path

Figure 4.8. σ_{11} distribution in the SG and the comparison with the DNS model

the MSG plate model took 3.41 minutes with 1 CPU for the entire analysis including homogenization (183.59 seconds), plate analysis (5.00 seconds) and dehomogenization (16.13 seconds). On the other hand, DNS took 271.0 minutes with 24 CPUs.
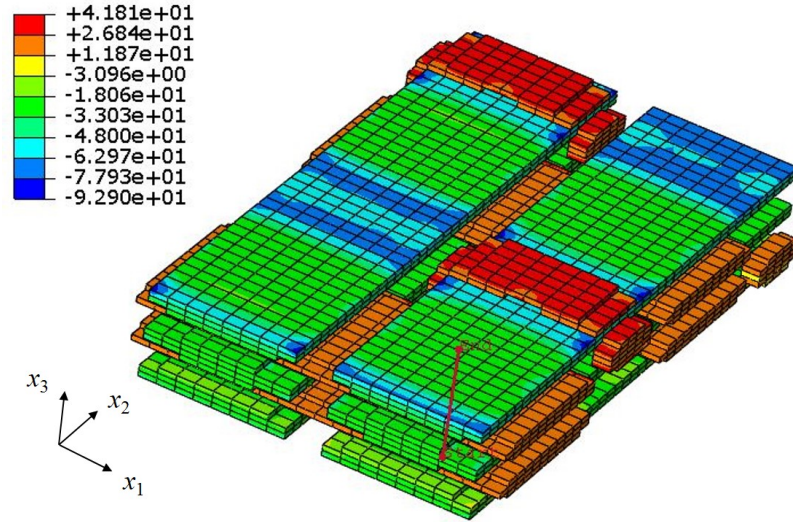
(a) σ_{22} contour plot
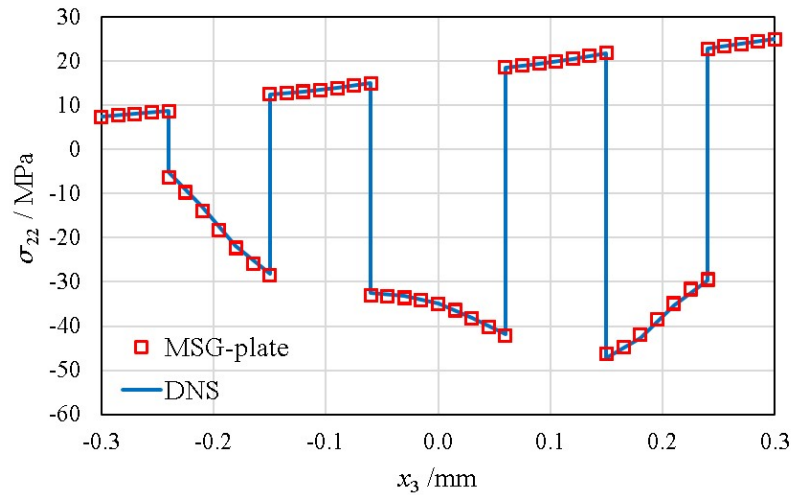
(b) σ_{22} through the path

Figure 4.9. σ_{22} distribution in the SG and the comparison with the DNS model

Pointwise temperature load through the thickness

The previous composite structures examples are subjected to an assumed linearly distributed temperature load along the thickness. In general, the temperature distribution is not always linear through the thickness. Therefore, a heat conduction analysis is carried out firstly to obtain the temperature field in the woven plate. The

bottom and top surfaces are subjected to a uniform temperature of 20 °C and -30 °C respectively. The thermal conductivity of the fiber and matrix are taken from the reference [87]. For the fiber, the thermal conductivities in the longitudinal and transverse directions are 10.2 W/m/°C and 1.256 W/m/°C respectively. The thermal conductivity of the matrix is 0.18 W/m/°C. To obtain the thermal conductivities of yarns, the 2S square packed SG is used based on the MSG solid model for the conductivity homogenization [84]. The resulting thermal conductivities in the longitudinal and transverse directions of the yarns are 6.592 W/m/°C and 0.532 W/m/°C respectively. The heat conduction analysis of the woven plate is performed using Abaqus, and the mesh is kept the same as the model for the thermoelastic analysis.

Figure 4.10(a) shows the contour plot of temperature distribution in a SG, which is taken from the plate structure at $x_1 = 8$ mm to 10 mm and $x_2 = 9$ mm to 12 mm. The temperature field will be used as the load to perform the MSG-based composite plate modeling. The temperature field along the path at the location (9.5 mm, 9.45 mm) is also plotted in Figure 4.10(b). The temperature distribution along the plate thickness is not linear due to the different thermal conductivities of yarns and matrix.

Based on the pointwise temperature distribution from the heat conduction analysis, the MSG plate model is used to perform the thermoelastic analysis of the woven plate. The new non-zero thermal induced stress resultants are $N_{T_{11}} = -5.139$ N/mm, $N_{T_{22}} = -4.243$ N/mm, $M_{T_{11}} = -0.449$ N, $M_{T_{22}} = -0.372$ N. The significant local stresses σ_{11} and σ_{22} of the SG along the path are shown in Figures 4.11(a) and 4.11(b).

The above example shows that the MSG plate model can be used to capture the local stress distribution of complex woven structures under pointwisely distributed temperature loads with the same accuracy of a DNS model.
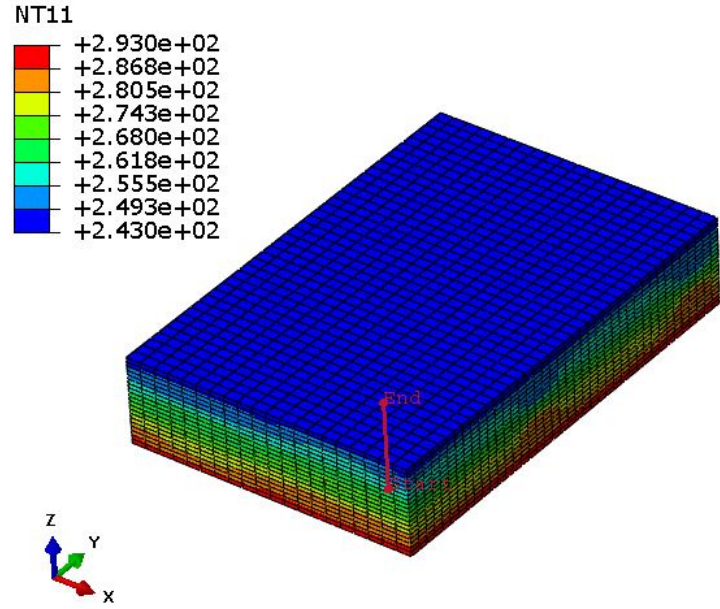
(a) Temperature contour plot
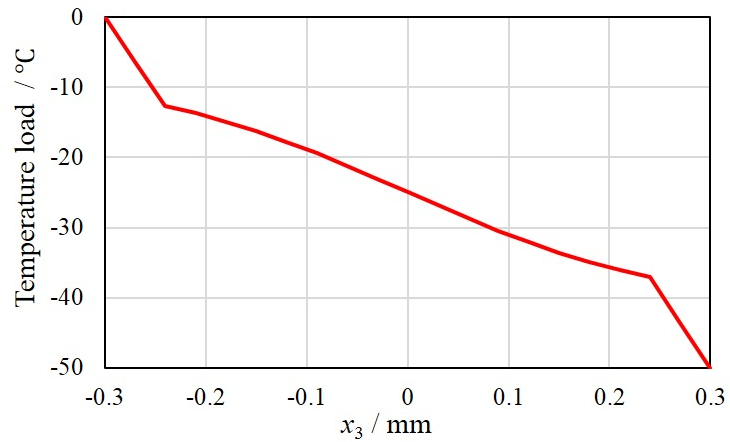
(b) Temperature through the path

Figure 4.10. Temperature distribution in the SG and along the plate thickness

4.4 Summary

In this chapter, a unified multiscale approach for the thermoelastic modeling of composite structures is developed. MSG models have been extended to capture the thermoelastic behaviors of beam, plate and solid structures. With the MSG solid

(a) σ_{11}
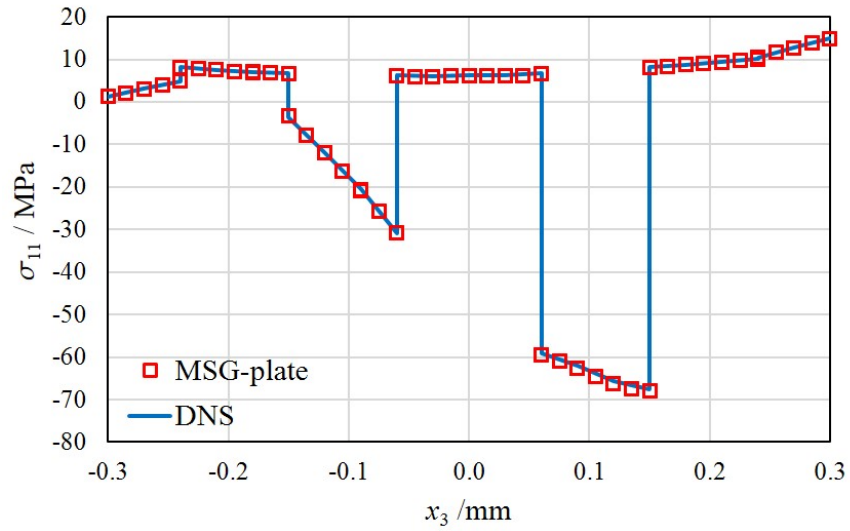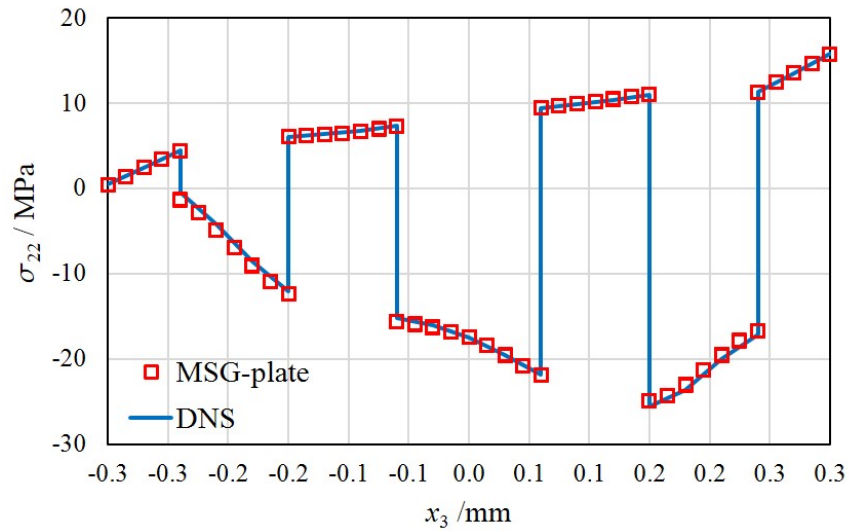
(b) σ_{22}

Figure 4.11. Stress distribution in the SG and the comparison with the DNS model

model, effective thermoelastic properties can be predicted with the same accuracy as 3D FEA while the computing time can be greatly reduced. With the MSG plate and beam models, thermal induced stress resultants are derived to capture the thermoelastic behaviors of thin and slender composite structures. Both structural responses and local stress fields subjected to pointwisely distributed temperature loads can be

predicted. MSG plate and beam models can achieve similar accuracy as DNS models. The analysis approach proposed in this chapter can be used in the high fidelity thermoelastic modeling of composite structures in place of DNS to reduce modeling and computing time.

5. INITIAL FAILURE ANALYSIS OF TEXTILE COMPOSITES

In composite structural analysis and design, initial failure analysis is used to determine the point where a progressive failure material model should be used to capture the nonlinear behavior of a structure following failure onset. As the first step in a progressive failure analysis (PFA), an accurate prediction of failure initiation is crucial for determining the ultimate failure of a structure. To predict the initial failure strength, various failure criteria have been proposed to study the traditional unidirectional (UD) fiber reinforced composites [88,89]. However, compared with traditional UD laminates, textile composites usually have more complex microstructures due to the yarn crimp, which increases the difficulty of accurately predicting the local stress and strain fields.

In this chapter, a meso-micro coupled approach is proposed to study the failure initiation of textile composite structures taking the advantage of the efficiency and accuracy of the MSG models [64]. MSG is extended to perform failure initiation analysis at the microscale based on fiber and matrix failure criteria subject to the mesoscale yarn stress field which is computed through the MSG dehomogenization analysis at the mesoscale [11]. As shown in previous studies [10,12], MSG offers better computation efficiency while keeps the same accuracy as 3D FEA in analyzing textile composite structures. For the thin and slender textile composite structures made by 3D woven composites, the MSG plate and beam models are used to compute the initial strength constants in terms of structural loads, which can be directly obtained from structural level to capture the non-uniform stress along the plate thickness or beam cross-section. Note that instead of predicting ultimate failure strength using PFA,

the present work only focuses on the prediction of initial failure strength constants of textile composites and failure initiation behaviors at fiber and matrix level.

5.1 MSG-based Initial Failure Analysis

5.1.1 Strength Ratio

The initial failure load (initial strength) of a structure, P_{cr}, is defined as the load under which the maximum failure index among all the points is equal to 1. If the stress analysis is linear, for an arbitrary load P, there is a corresponding 3D stress field σ_{ij}. Then, we can compute the failure index for each point based on this stress field. Suppose that the initial failure load is $P_{cr} = \alpha P$, then the corresponding stress field is $\alpha \sigma_{ij}$. If the failure criterion is linear with respect to the stress field, such as the max stress failure criterion, we will have

$$f(\alpha \sigma_{ij}) = \alpha f(\sigma_{ij}) \tag{5.1}$$

where $f(\cdot)$ is the function of the failure criterion. According to the failure criterion, we require $\alpha f = 1$. Thus, we have

$$\alpha = \frac{1}{f} \tag{5.2}$$

Denote the smallest α among all the points as α_{min}, the initial failure load can be computed as

$$P_{cr} = \alpha_{min} P \tag{5.3}$$

α is called the strength ratio. If we let P equal to 1, then α_{min} is the initial failure load. If the failure criterion contains quadratic terms of the stress components such as Tsai-Wu failure criterion [90], α can be obtained by solving a quadratic equation. In this chapter, the initial strength constants of different textile composite structures are computed using the MSG solid and plate models by solving the strength ratio with the P equal to 1.

5.1.2   Strength Constants in Terms of Structural Loads

In the composite structural design, shell and beam finite elements are often used to model thin and slender structures. Instead of applying stress or strain fields at the structural level, plate stress resultants (i.e. plate forces and moments) or beam stress resultants (i.e. beam forces and moments) are often used as structural loads. For MSG plate and beam models, the structural modeling is performed using the plate constitutive relations, where the structural strains (i.e. plate and beam strain measures) can be obtained. Then, the 3D stress and strain fields at the SG level can be recovered through MSG dehomogenization analysis. This process enables predicting failure initiation using 3D stress or strain fields while the failure strength constants can be expressed in terms of structural loads. This feature will provide more straightforward information for the structural design. In addition, another benefit of using structural loads as failure strengths is to account for the non-uniform stress state in the RVE or SG model. For example, Figure 5.1(a) shows a constant stress state which is often used in current approaches to compute the corresponding strength constant (tensile strength in x direction). In this case, the RVE is considered as a point of the homogenized structure, and a uniform stress state for a point is a valid assumption. However, for some thin structures made of 3D woven composites, the thickness of the RVE is the same as the thickness of the original structure. Thus, a constant stress state cannot be used in the thickness direction of the RVE. As shown in Figure 5.1(b), a RVE of a thin textile composite structure can subject to a linear stress distribution under a bending load. For such thin textile structures, plate stress resultants are better to use as failure strength constants. More details of the significance of capturing the non-uniform stress distribution have been discussed by Karkkainen and Sankar [55, 56].

(a) Uniform stress state (b) Non-uniform stress state
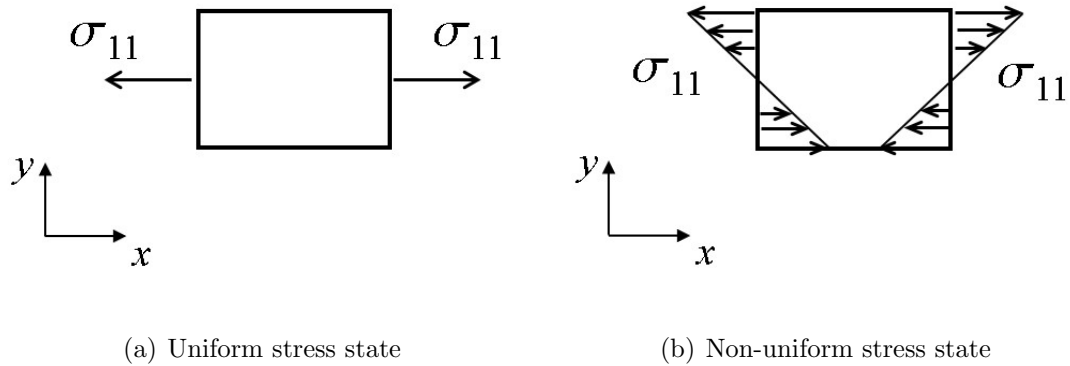
Figure 5.1. Different stress states in solid and plate models

5.2 MSG-based Meso-micro Scale Coupled Initial Failure Analysis

MSG models can predict local stress/strain fields with excellent trade off between computational efficiency and accuracy [79, 86], which is critical for performing initial failure analysis for a full meso-micro scale coupled analysis. Although extensive studies have focused on the failure of the yarn and matrix at the mesoscale level, investigating the failure at the microscale (i.e. the fiber and matrix) could potentially reveal more insights of failure mechanisms at the fiber and matrix level. In this chapter, a mesoscale model, which represents the macroscopic structural behaviors, is first created and subjected to the external load P. The maximum principal stress criterion is used to compute the strength ratio α_1 of the matrix, while no failure criterion is applied to yarns. Instead, the stress field in each finite element representing the yarns is computed and subsequently used to perform the initial failure analysis at the microscale. The minimum strength ratios of matrix and fiber within the yarn are obtained as α_2 and α_3. At last, the initial strength of the textile composites is computed as αP where $\alpha = \min\{\alpha_1, \alpha_2, \alpha_3\}$. The whole analysis procedure is illustrated using a plain woven SG in Figure 5.2. For the initial failure analysis, we assume that no damage occurs before the initial failure. Since the stress concentration is often associated with damage, the stress field computed at each Gaussian point is averaged over the element to reduce the effects of the stress concentration.
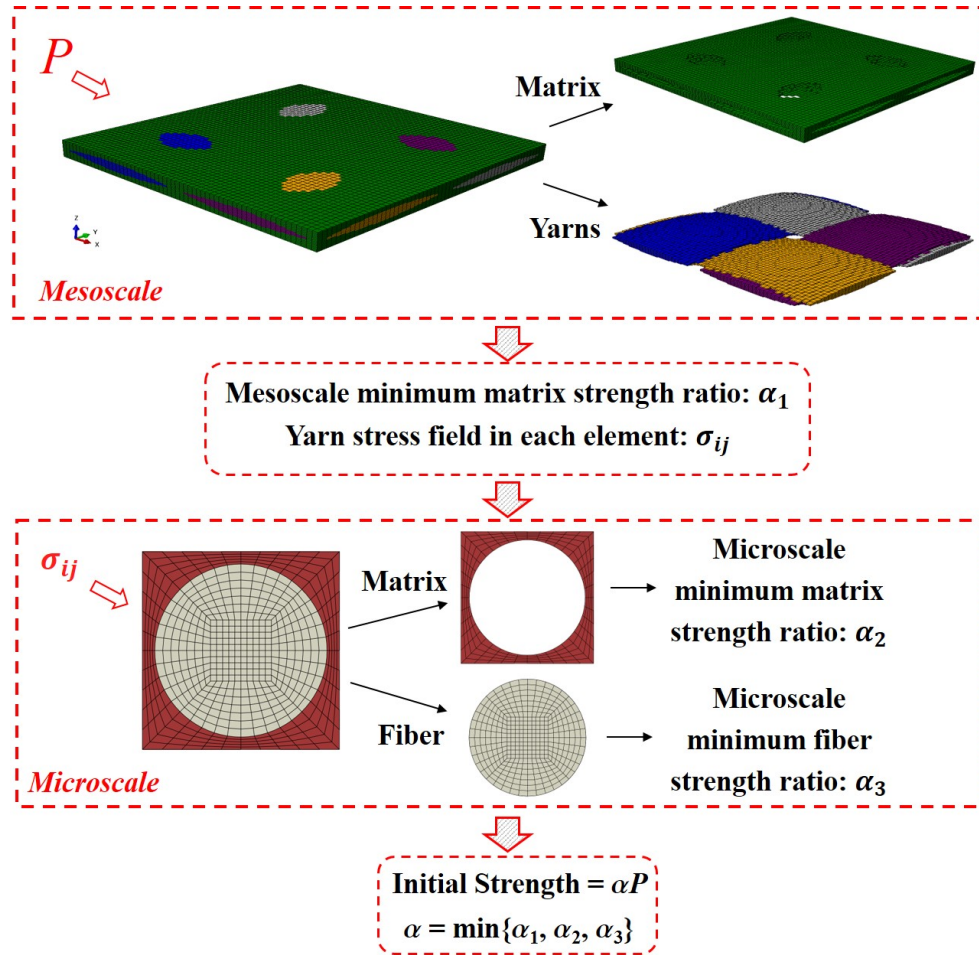
Figure 5.2. Coupled meso-micro scale initial failure analysis

For the MSG models, the analysis is decoupled into homogenization and initial failure analysis. The homogenization analysis solves the unknown fluctuating functions of the SG, and the initial failure analysis will directly use the external loads along with the solved fluctuating functions to get the local stress and strain fields. In other words, there is no need to factorize the system stiffness matrix for the MSG initial failure analysis which is the most time consuming part in the entire analysis.

Generally speaking, there are 12 strength constants for a textile composites determined by 12 loading cases. The tensile strengths X, Y, Z and the compressive strengths X', Y', Z' in the three material principal directions (x_1, x_2, x_3 respectively),

and the shear strengths R, T, S in the three principal planes of symmetry (x_2-x_3, x_1-x_3, x_1-x_2 respectively). Note the shear strengths can be sign dependent due to the antisymmetric configuration of textile composites.

5.3 Numerical Examples

The two-scale initial failure analysis of a plain woven and a 3D orthogonal woven composites example will be carried out in this section. The microscale analysis will be performed using a square pack microstructure as shown in Figure 5.2. As mentioned in the previous section, failure criteria will be applied to matrix and fiber. The maximum principal stress criterion is used for matrix, and the following failure criterion is used for the fiber [91].

$$f = \frac{\sigma_{11}}{X} = 1, \qquad \text{if} \quad \sigma_{11} > 0$$
$$f = \frac{|\sigma_{11}|}{X'} = 1, \qquad \text{if} \quad \sigma_{11} < 0$$

(5.4)

where X and X' are the tensile and compressive strength of the fiber. The material properties and strength constants of the fiber and matrix are given in Table 5.1.

Table 5.1. Elastic and strength constants of fiber and matrix [92]

Material	E_1 (MPa)	E_2 (MPa)	G_{12} (MPa)	G_{23} (MPa)	ν_{12}	X (MPa)	X' (MPa)
Fiber	230000	15000	15000	7000	0.20	25000	2000
Matrix	4200	4200	1567	1567	0.34	69	250

In order to perform a mesoscale analysis, effective elastic constants of the yarn are computed using MSG solid model as given in Table 5.2. The accuracy and efficiency of using MSG solid model to compute effective properties has been studied in [86].

Table 5.2. Elastic constants of the yarn

Material	E_1 (MPa)	$E_2 = E_3$ (MPa)	$G_{12}=G_{13}$ (MPa)	G_{23} (MPa)	$\nu_{12}=\nu_{13}$	ν_{23}
Yarn	139700	9537	4700	3060	0.252	0.259

5.3.1 Plain Woven Lamina

Plain woven composites are often used in laminate structures. For laminate structures, effective woven lamina properties are usually computed first, which are later used to construct the plate stiffness matrix using CLPT. Since plain woven composites are often used as a homogeneous layer, a solid model is needed to compute the effective properties as well as the failure strength constants in terms of stress or strain measures. A plain woven SG is shown in Figure 5.3. The MSG solid model is used to perform homogenization and failure analysis at mesoscale. The PBCs in x, y, and z directions are applied. The plain woven composites only have 6 different strength constants because of the symmetry in x and y direction. To be more specific, $X = Y$, $X' = Y'$ and $R = T$ and there is no sign dependent in shear strengths. The width, spacing and thickness of yarns in this example is 1.65 mm, 1.8 mm and 0.25 mm respectively. The MSG mesoscale model contains 72,000 20-node brick elements. The MSG microscale model contains 580 8-node 2D quadrilateral elements. In terms of the computing time, $t_{meso} = 3{,}484$ s and $t_{micro} = 2$ s for RVE models. For the MSG models, $t_{meso-homo} = 816.64$ s, $t_{meso-fail} = 100.9$ s, $t_{micro-homo} = 0.15$ s, and $t_{micro-fail} = 0.1$ s. The number of yarn elements is 45,875. Hence the computing time for 6 strength constants is 158.7 hours and 8.1 hours based on RVE and MSG analysis respectively. The MSG-based multiscale initial failure analysis shows significant computational efficiency over the RVE-based analysis. Table 5.3 lists the predicted initial failure strength constants as well as the difference between them. The results based on RVE and MSG analysis agree well and all the differences are with 1%.
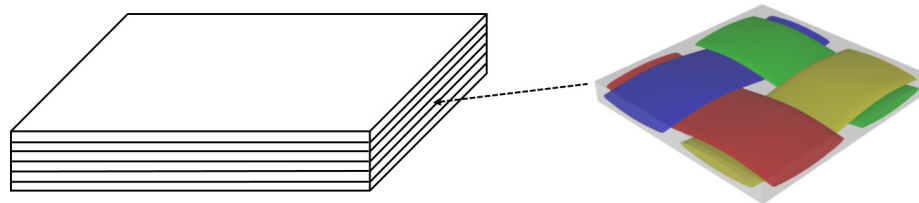
Figure 5.3. Woven laminate and the plain woven SG

Table 5.3. Initial strength constants (MPa)

Model	$X=Y$	$X'=Y'$	Z	Z'	$R=S$	T
MSG	149.81	294.25	39.91	144.60	22.94	19.10
RVE	150.35	292.09	39.93	144.70	22.95	19.11
Diff (MSG vs RVE)	0.36%	0.74%	0.05%	0.07%	0.04%	0.05%

To have a better understanding of the initial failure at microscale, the contour plots of the strength ratio under in-plane loading cases of microscale models are given in Figure 5.4. The red color represents the small strength ratio which corresponds to the large stress level. For the microscale models, RVE model uses a 3D domain while MSG model uses 2D domain, but the distribution of strength ratio in both models agree well. In addition, matrix has relatively smaller strength ratio, which means the first point failure of textile composites tends to occur at the matrix in the yarns. This conclusion is in accordance with previous conclusions by other researchers [93].

5.3.2 3D Orthogonal Woven Plate

3D woven composites are often used in thin composite structures. Due to the binder yarns, it is not easy to use a two-step approach with CLPT to construct plate stiffness matrix as the approach used in plain woven laminate structures. Instead, the plate stiffness should be directly computed based on the mesoscale model of the 3D woven composites. As such mesoscale models often have the same thickness as the original composite structures, MSG plate model is used to perform homogenization and failure analysis, which can capture the non-uniform stress distribution along the thickness of the structure. A homogeneous plate structure with shell elements and the corresponding 3D orthogonal woven SG are shown in Figure 5.5. The SG is analyzed using the proposed two-scale approach, and the microscale model is the same as in the plain woven example. A RVE plate model based on 3D FEA is also carried out

(a) RVE-X

(b) MSG-X

(c) RVE-X'

(d) MSG-X'
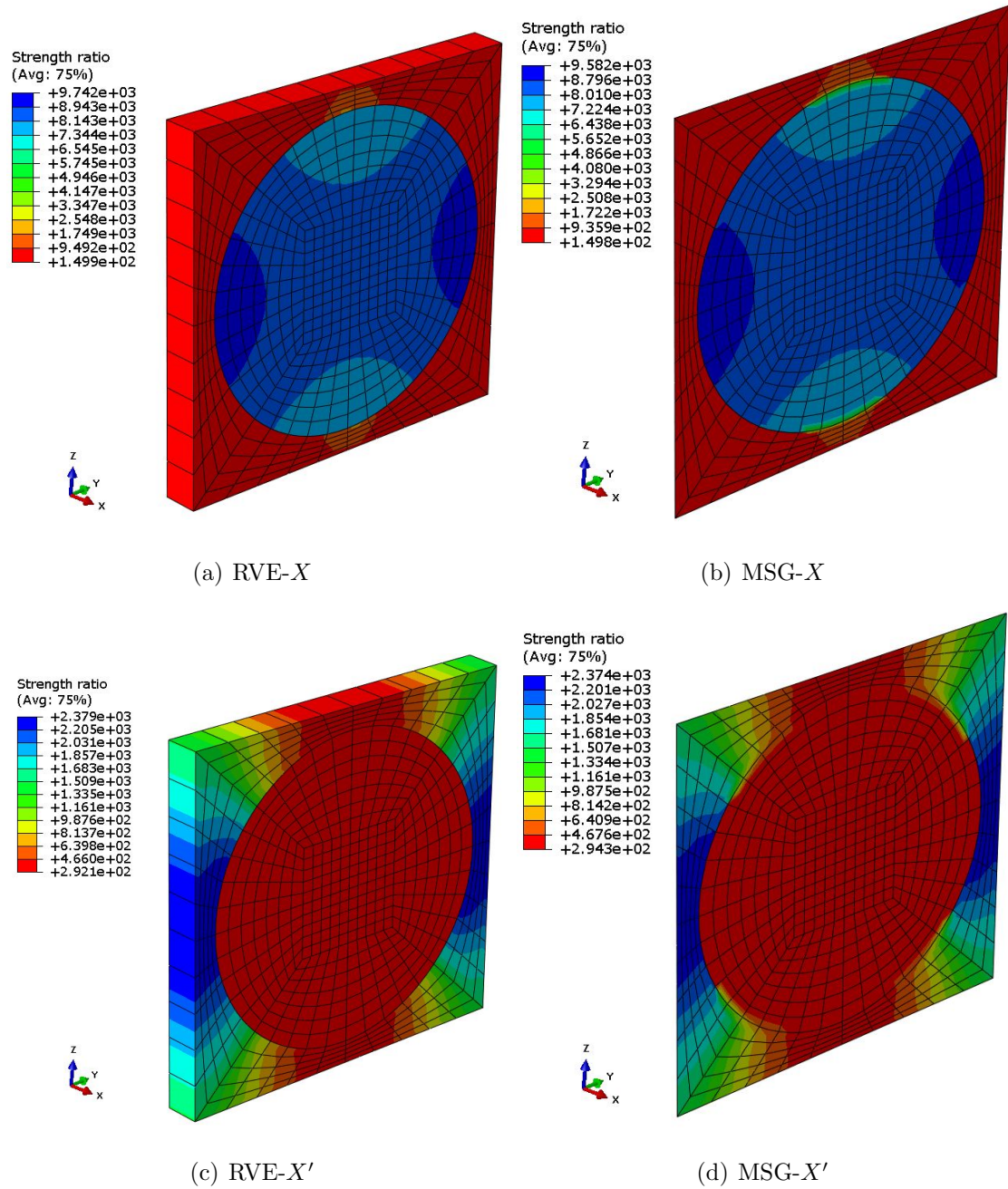
Figure 5.4. Strength ratio under the loads in x direction

which is subjected to the BCs described in [55]. The RVE plate model is analyzed using the Abaqus micromechanics plugin function of SIMULIA [94].

The strength constants are in terms of plate stress resultants $\{\boldsymbol{N}, \boldsymbol{M}\}$ to capture the non-uniform stress distribution which is critical for textile composites.
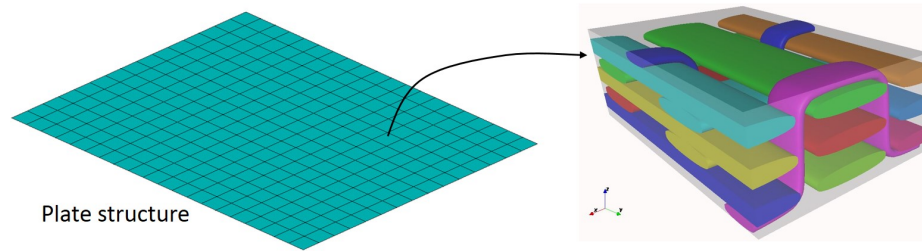
Figure 5.5. Beam structure and the corresponding SG

The initial failure strength constants computed by the MSG plate model are listed in the Table 5.4. The superscripts "+" and "-" indict the loading direction. "+" means the load applied in the positive direction while "-" means the load applied in the negative direction. Due to the geometric configuration of this 3D woven composites, the in-plane shear strength and out-of-plane bending strength constants do not depend on the direction of the loads. It is clear that the results based on the MSG plate model agrees well with the results based on the RVE plate model.

Table 5.4. Initial strength constants for MSG and RVE plate model

Model	N_{11}^{+} (N/mm)	N_{11}^{-} (N/mm)	N_{22}^{+} (N/mm)	N_{22}^{-} (N/mm)	N_{12} (N/mm)	M_{11} (N)	M_{22} (N)	M_{12} (N)
MSG	118.86	263.63	221.97	672.63	40.61	25.37	83.00	17.70
RVE	118.85	263.76	221.95	672.62	40.61	25.37	83.00	17.70

For this orthogonal woven plate model, 8 loading cases are needed to determine all the strength constants. For a single loading case, the mesoscale and microscale RVE model took 4,414 seconds and 2 seconds. For the MSG plate mesoscale model, it took 530.23 seconds for homogenization and 85.60 seconds for failure analysis. For the MSG microscale model, it took 0.15 seconds for homogenization and 0.1 second for failure analysis. In this example, the woven SG contains 28,365 yarn elements and

the computing time for 8 strength constants of this orthogonal woven SG is 135.9 hours and 6.6 hours based on RVE and MSG models respectively.

5.4 Summary

MSG models have been extended to perform initial failure analysis of textile composite structures. Three failure functions are available in the current MSG models: initial failure strength, failure index/strength ratio, and failure envelope. A two-scale approach is proposed to predict initial failure strength of solid- and plate-like textile composite structures. Compared with traditional initial failure predictions at mesoscale, the two-scale model is able to capture the failure behavior of the fiber and matrix instead of the yarn and matrix. The strength constants of the plain and 3D orthogonal woven composites are predicted using the MSG solid and plate models. The results based on MSG models are compared with those from RVE models using 3D FEA, which shows that the two-scale MSG models achieve the same accuracy as RVE models but the computing time is significantly reduced. Moreover, the MSG plate model is able to capture the non-uniform stress along the thickness of textile composite structures, which provides useful information for the design and analysis of thin textile composite structures using shell elements.

6. MACHINE LEARNING ACCELERATED FAILURE ANALYSIS

As shown in the previous chapter, the scale coupled approach is very computationally expensive. In practice, failure analysis is carried out using a non-coupled multiscale modeling approach. For example, the microscale modeling with fiber and matrix is first carried out to compute the effective strength constants of yarns under different loading conditions. At the mesoscale, failure criteria such as Tsai-Wu and Hashin are then assumed for yarns using the effective strength constants, and the failure initiates once the criterion is met. Subsequently, a damage evolution law and a stiffness degradation algorithm are applied to predict the nonlinear behavior of the composite material during failure progression. Therefore, choosing an appropriate failure criterion is crucial in determining the overall failure behavior. However, experimental evidence shows that the current failure criteria are still not mature enough to give an accurate prediction of failure initiation [7]. In addition, most of the existing failure criteria are developed for the unidirectional fiber reinforced lamina. There is limited evidence that these failure criteria can be safely applied to yarns which are often in more complex stress states due to the yarn crimp in fabrics. Copyright permissions have been obtained to reuse the published materials from [15] in this chapter.

Artificial neural network (ANN) approach can be used to construct a surrogate model that can improve the computational efficiency in some expensive simulations [95, 96]. Moreover, ANN can also be used as an universal approximation theorem tool [63] to approximate any functions when its explicit mathematical formulation is unknown or does not exist. The current failure criteria used in composites are mainly based on postulated polynomial functions of stress or strain fields with coefficients to be determined from experiments or sub-scale numerical models. Taking

advantage of ANN, a failure criterion can be directly constructed using appropriate inputs and outputs, thereby avoiding the possible inaccuracies associated with postulated polynomial expressions.

6.1 Basic Feed-forward Neural Network Model

A feed-forward deep learning neural network is used to construct the failure criterion for the yarn. A typical configuration of a multilayer feed-forward network is given in Figure 6.1. The units in each layer are called neurons. $\boldsymbol{X} = \{x_1, x_2, ..., x_n\}$ is defined as the input neurons and $\boldsymbol{Y} = \{y_1, y_2, ..., y_m\}$ is defined as the output neurons.
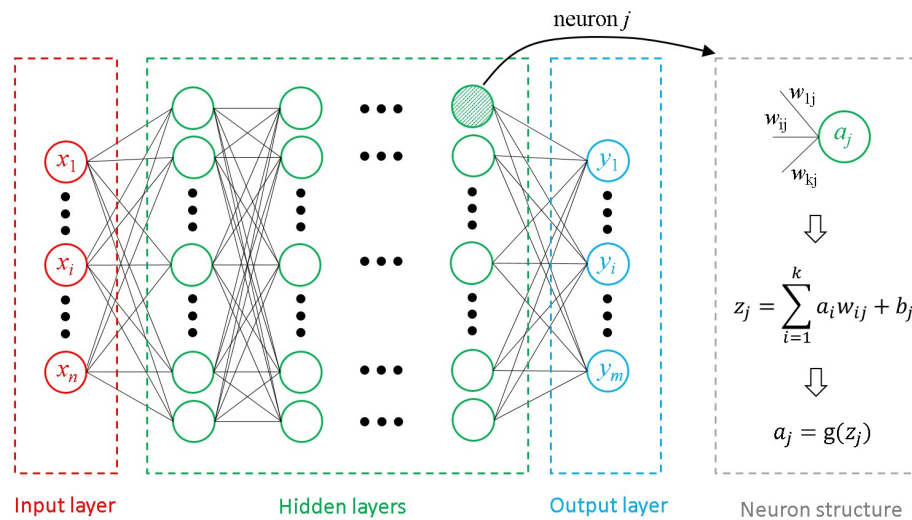
Figure 6.1. Architecture of a multilayer feed-forward network

For every connection between neurons in the $(l-1)^{th}$ layer and l^{th} layer, there is a weight parameter w_{ij} to measure the influence of each of the preceding neurons in the $(l-1)^{th}$ layer. A bias term b_j is used in each neuron in the lth layer to cover a wider range [97]. Each neuron receives input from the preceding neurons. Each input from the preceding neurons is multiplied by the corresponding weight. For a given

neuron j, the bias b_j is added to the sum of the weighted neural inputs as shown in Eq. (6.1)

$$z_j = \sum_{i=1}^{n} a_i w_{ij} + b_j \tag{6.1}$$

Next, an activation function is used to compute a scalar value for each neuron in the current layer using z_j. This scalar constitutes the input that each neuron provides to the next layer. In this chapter, ReLU function [61] is used as the activation function, which has been shown to have a better training performance with deep networks compared to other activation functions [98]. The ReLU function is given in Eq. (6.2)

$$g(z) = \max(z, 0) \tag{6.2}$$

The weights and biases are called trainable variables, which means that they are updated during the training to minimize a loss function. Constructing the failure criterion is considered as a regression problem, and the loss function is defined as the mean square error (MSE):

$$L = \frac{1}{2n} \sum_{i=1}^{n} (y^{(i)} - \hat{y}^{(i)})^2 \tag{6.3}$$

where n is the number of training samples, $y^{(i)}$ is the actual output in the training samples and $\hat{y}^{(i)}$ is the predicted output using the trained model. The gradient descent method is commonly used in the neural network to find the minimum of the loss function [62]. The weights and biases can be updated using the following equations:

$$w_{ij}^{new} = w_{ij}^{old} - \eta \frac{\partial L}{\partial w_{ij}^{old}} \tag{6.4}$$

$$b_{j}^{new} = b_{j}^{old} - \eta \frac{\partial L}{\partial b_{j}^{old}} \tag{6.5}$$

where η is called the learning rate, which is also updated during the training process using the adaptive gradient method [99]. To find the derivatives in Eqs. (6.4) and (6.5), a backpropagation method is often used, which can be summarized into four equations [100]:

$$\boldsymbol{\delta}^L = (\boldsymbol{a}^L - \boldsymbol{y}) \odot g\prime(\boldsymbol{z}^L) \tag{6.6}$$

$$\boldsymbol{\delta}^l = ((\boldsymbol{w}^{l+1})^T \boldsymbol{\delta}^{l+1}) \odot g\prime(\boldsymbol{z}^l) \tag{6.7}$$

$$\frac{\partial L}{\partial b_j^l} = \delta_j^l \tag{6.8}$$

$$\frac{\partial L}{\partial w_{jk}^l} = a_k^{l-1} \delta_j^l \tag{6.9}$$

where δ denotes the error of the layer, the superscript L denotes the output layer and l denotes the hidden layers. Eqs. (6.6) and (6.7) are in matrix form. For example, $\boldsymbol{a}^L$ contains the output values which can be expressed in the vector $[a_1^L \quad a_2^L \quad ... \quad a_m^L]^T$. The "$\odot$" denotes the elementwise product of two vectors. The detailed proof of Eqs. (6.6)-(6.9) can be found in [100]. An open source Tensorflow python library [101] is used to train the DNN model proposed in this chapter.

6.2 Constructing Yarn Failure Criterion

6.2.1 Multiscale Failure Analysis

A multiscale modeling approach is often used to decouple the failure analysis to the mesoscale and microscale. In general, a point at macroscale model can be considered as a mesoscale model including the matrix and homogenized yarns [14], and a point inside a yarn can be modeled by a microscale model with the matrix and fibers (Figure 6.2). Note that the stress gradients of the woven mesoscale model has been neglected so that the strength constants can be expressed as 3D stress or strain measures for the macroscale laminate analysis. A two-step approach is often used to perform multiscale modeling of textile composites [10]. In the first step, effective yarn stiffness and strength constants are computed at the microscale level based on fiber and matrix properties and their corresponding failure criteria. In the second analysis step, performed at the mesoscale, the effective strength constants from the microscale modeling are used in the yarn failure criterion to predict yarn failure. The yarn failure criterion in conjunction with the matrix failure criterion allows to determine the failure initiation of textile composite material, which provides the initial failure strengths of the woven ply in the macroscale laminate analysis.
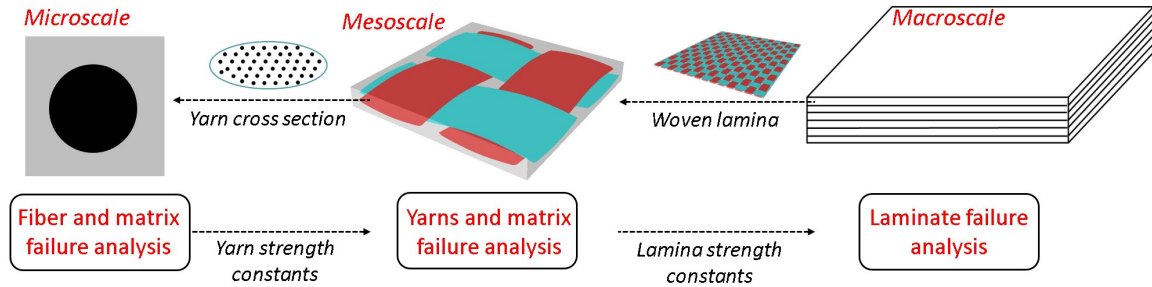
Figure 6.2. Multiscale analysis of textile composites

The above approach can be considered as a decoupled multiscale analysis, which means that the mesoscale modeling only uses the homogenized failure information from the microscale modeling. This approach has excellent efficiency as the microscale modeling only needs to be performed a handful times to determine the corresponding strength constants. On the other hand, a more accurate prediction can be obtained if a fully coupled multiscale analysis (e.g. FE^2 [9]) is used. For the fully coupled multiscale analysis, the stress or strain fields at each integration point in the yarn elements are obtained from the mesoscale modeling and are subsequently applied to the microscale model to perform the failure analysis based on the local stress field in the fiber and matrix. In other words, a microscale modeling is required for each integration point of all yarn elements at each load step. For the initial failure analysis, a single load step at the mesoscale is enough to determine one initial strength constant. However, the microscale modeling is needed for each integration point in the yarn elements. In this chapter, the stress field is averaged over each element to reduce the effect of the stress concentration.

The microscale analysis procedure is summarized in Figure 6.3. The yarn element stress tensor is obtained by the dehomogenization analysis using the MSG solid model at the mesoscale. The yarn stress is applied to the microscale model to compute the stress field at the microscale. The microscale stress fields at the integration points are averaged within each element. The element stress field is used to compute the

strength ratio based on the failure criterion of the matrix or fiber. The maximum principal stress failure criterion is applied to matrix and the failure criterion in Eq. (6.10) is used for the fiber [91].

$$
\begin{aligned}
f &= \frac{\sigma_{11}}{X} = 1, \qquad \text{if} \quad \sigma_{11} > 0 \\
f &= \frac{|\sigma_{11}|}{X'} = 1, \qquad \text{if} \quad \sigma_{11} < 0
\end{aligned}
\tag{6.10}
$$

The terms X and X' are the tensile and compressive strength of the fiber, respectively. The strength ratio of the microscale model is defined as the minimum strength ratio among all elements.
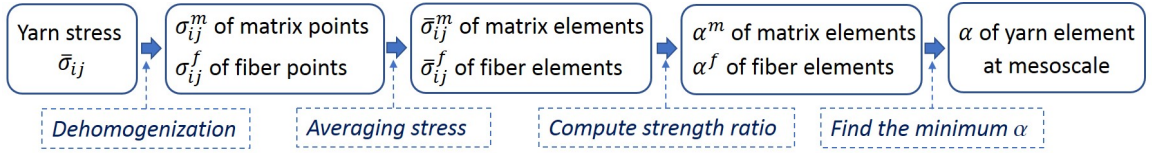
Figure 6.3. Microscale failure analysis

The goal of the failure criterion to be constructed using the DNN model is to replace this microscale FEA procedure with a functional form such that:

$$
f(\bar{\sigma}_{ij}) = \alpha
\tag{6.11}
$$

6.2.2 Training Process

In the context of neural networks, the yarn failure criterion is the mapping of the strength ratio from the stress tensor as defined in Eq. (6.11). As shown in Figure 6.3, the microscale analysis involves multiple steps: recovering the stress field at the microscale, averaging the stress field within each element, computing the strength ratio, and comparing the strength ratio of each element. It is difficult to generate a representative database of the six yarn stress components of each yarn element if the external loads are arbitrary. However, the yarn stress field linearly relates to

the strength ratio of the microscale model. Therefore, the yarn stress field can be scaled by a factor k which is defined as the maximum absolute value of the six stress components of an element. As a result, the value of the scaled stress components ranges from -1 to 1. If the strength ratio based on the scaled yarn stress components is α_0, the final strength ratio under the actual yarn stress field is $k\alpha_0$. A database, which contains 300,000 samples, is generated using the microscale failure analysis based on the MSG solid model. Each sample accepts six yarn stress components as input and provides a strength ratio of the microscale model as output. The input data is generated using the Latin hypercube sampling (LHS) [102] to make a uniform random distribution of stress components between -1 and 1. The DNN model is trained by 290,000 samples. In order to avoid over-fitting, the model is validated using 20% of these training data during the training process. The trained model is tested with the rest 10,000 samples.

Finally, a model with four hidden layers is used to construct the yarn failure criterion. The number of neurons used in each hidden layer is 300, 200, 160, 100. Figure 6.4 shows the loss of training data and validation data with respect to epochs. Based on the training loss with respect to the epochs, the accuracy of the training model can be evaluated. As the validation data set is not used in training the model, an increasing validation loss will be observed if the training model is overfitted. The loss is computed using Eq. (6.3). An epoch is defined as when an entire training data set is passed forward and backward through the neural network once. Figure 6.5 shows the comparison between the predicted strength ratio and the true strength ratio. Note that the smaller strength ratio represents the higher stress level which is more critical than the larger strength ratio. To highlight the critical strength ratios, only the stress smaller than 300 MPa are plotted. The stress at failure of plain weave material modeled in this chapter is within this range. Figure 6.5 shows that the predicted values have excellent agreements with the true values.
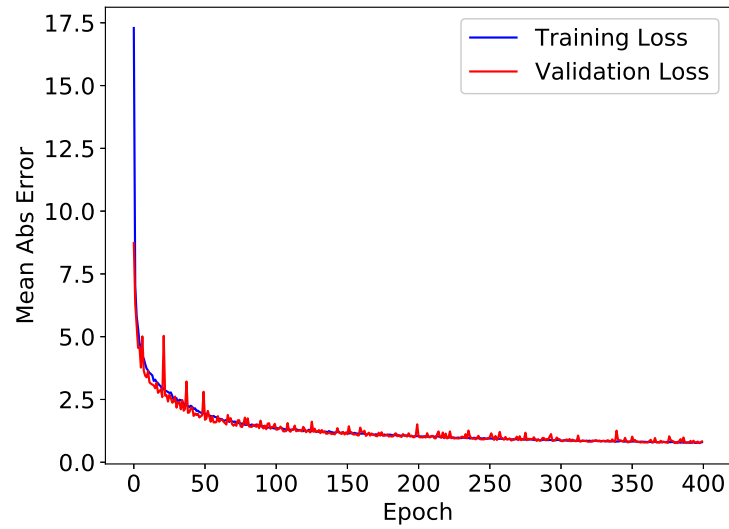
Figure 6.4. Training process
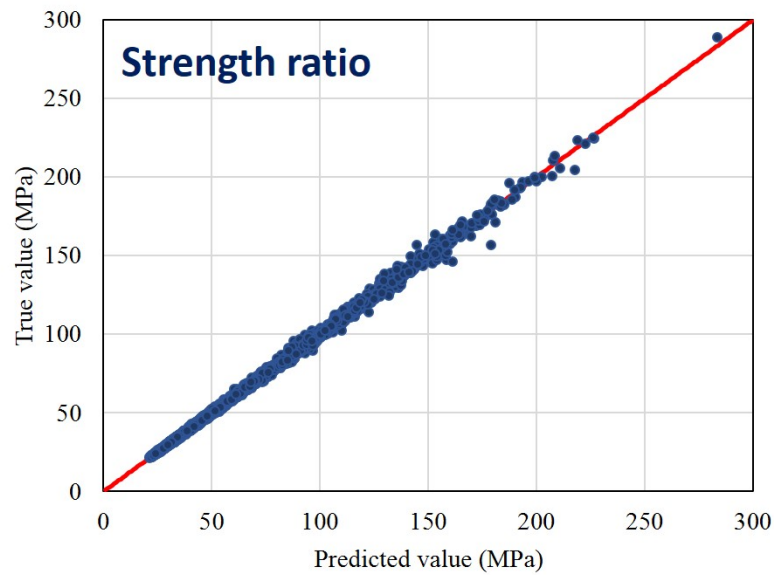

Figure 6.5. Parity plot of predicted and true values

6.3 Numerical Example

A fiber reinforced plain woven composite material example is used to study the accuracy of the proposed yarn failure criterion at predicting the initial strength con-

stants. Due to the symmetry of the plain weave in the x and y directions, the composite material only has 6 different strength constants. To be more specific, $X = Y$, $X' = Y'$ and $R = T$ and there is no sign dependence in shear strengths. Therefore, only 6 loading cases are needed at the mesoscale. The width, spacing and thickness of yarns in this example are 1.65 mm, 1.8 mm, and 0.25 mm respectively. The model, shown in Figure 6.6, contains 72,000 20-noded brick elements.
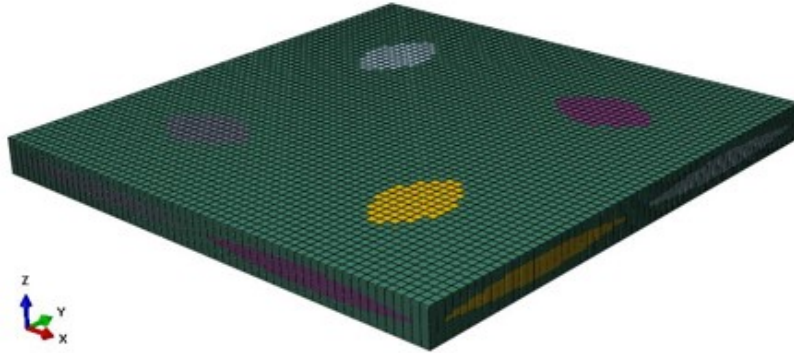
Figure 6.6. Mesoscale plain weave composites model

6.3.1 Mesoscale Analysis with Yarn Failure Criterion

The matrix of the mesoscale model uses the maximum principal stress criterion. In addition to the failure criterion constructed using DNN, the maximum stress (Max-stress), Tsai-Wu and Hashin failure criteria are also used to perform mesoscale yarn failure initiation analysis.

The Max-stress failure criterion is defined as:

$$f = \frac{\sigma_{11}}{X} = 1 \qquad f = \frac{\sigma_{22}}{Y} = 1 \qquad f = \frac{\sigma_{33}}{Z} = 1 \qquad (6.12)$$

when the stresses are tensile, and

$$f = \frac{|\sigma_{11}|}{X'} = 1 \qquad f = \frac{|\sigma_{22}|}{Y'} = 1 \qquad f = \frac{|\sigma_{33}|}{Z'} = 1 \qquad (6.13)$$

when the stresses are compressive, and

$$f = \frac{|\sigma_{23}|}{R} = 1 \qquad f = \frac{|\sigma_{13}|}{T} = 1 \qquad f = \frac{|\sigma_{12}|}{S} = 1 \qquad (6.14)$$

when the material is subject to shear stresses.

The Tsai-Wu failure criterion can be expressed as:

$$f = F_1\sigma_{11} + F_2\sigma_{22} + F_3\sigma_{33} + F_{11}\sigma_{11}^2 + F_22\sigma_{22}^2 + F_{33}\sigma_{33}^2 +$$
$$2F_{12}\sigma_{11}\sigma_{22} + 2F_{13}\sigma_{11}\sigma_{33} + 2F_{23}\sigma_{22}\sigma_{33} + \tag{6.15}$$
$$F_{44}\sigma_{23}^2 + F_{55}\sigma_{13}^2 + F_{66}\sigma_{12}^2 = 1$$

The 12 coefficients in this failure criterion can be written in terms of the failure constants calibrated from subscale modelings or experiments [103].

The Hashin failure criterion can be expressed in terms of the following four equations with the corresponding failure mode. For tensile fiber failure mode:

$$f = \frac{\sigma_{11}^2}{X^2} + \frac{1}{S^2}(\sigma_{12}^2 + \sigma_{13}^2) = 1 \tag{6.16}$$

For compressive fiber failure mode:

$$f = \frac{|\sigma_{11}|}{X'} = 1 \tag{6.17}$$

For tensile matrix failure mode:

$$f = \frac{(\sigma_{22} + \sigma_{33})^2}{Y^2} + \frac{1}{R^2}(\sigma_{23}^2 - \sigma_{22}\sigma_{33}) + \frac{1}{S^2}(\sigma_{12}^2 + \sigma_{13}^2) = 1 \tag{6.18}$$

For compressive matrix failure mode:

$$f = \left[(\frac{Y'}{2R})^2 - 1\right]\frac{\sigma_{22} + \sigma_{33}}{Y'} + \left(\frac{\sigma_{22} + \sigma_{33}}{2R}\right)^2 + \frac{\sigma_{23}^2 - \sigma_{22}\sigma_{33}}{R^2} + \frac{\sigma_{12}^2 + \sigma_{13}^2}{S^2} = 1 \tag{6.19}$$

While the above functions are used to predict the failure index, the corresponding strength ratio also can be obtained. The strength constants used in the above failure criteria are usually derived from microscale models [51, 104]. A microscale square packed model is used to compute the effective stiffness and strength constants for yarns based on the MSG solid model. The MSG solid model has been demonstrated to provide an accurate prediction of the effective properties and local stress field using the square packed microstructure [86]. As mentioned previously, the maximum principal stress criterion is used for matrix failure and Eq. (6.10) is used for fiber failure. The fiber and matrix properties are given in Table 6.1. The effective engineering and strength constants for yarns computed based on the MSG solid model are given in Tables 6.2 and 6.3.

Table 6.1. Elastic and strength constants of fiber and matrix. [92]

Material	E_1 (MPa)	E_2 (MPa)	G_{12} (MPa)	G_{23} (MPa)	ν_{12}	X (MPa)	X' (MPa)
Fiber	230000	15000	15000	7000	0.20	25000	2000
Matrix	4200	4200	1567	1567	0.34	69	250

Table 6.2. Elastic constants of the yarn

Material	E_1 (MPa)	$E_2 = E_3$ (MPa)	$G_{12}=G_{13}$ (MPa)	G_{23} (MPa)	$\nu_{12}=\nu_{13}$	ν_{23}
Yarn	139700	9537	4700	3060	0.252	0.259

Table 6.3. Effective strength constants of yarns (MPa)

X	X'	$Y=Z$	$Y' = Z'$	R	$S = T$
1518.86	1215.09	49.21	178.29	56.96	41.80

6.4   Results and Discussion

6.4.1   Meso-micro Scale Model vs Mesoscale Model

The results based on the DNN mesoscale and meso-micro scale models, as well as their relative differences, are provided in Table 6.4. Note that the minimum yarn strength ratio is smaller than the minimum matrix strength ratio at the mesoscale. As a result, all the strength constants listed in Table 6.4 are associated with the yarn failure. This implies that the failure initiation tends to occur in the yarns which is in accordance with previous conclusions by other researchers [93]. These results give evidence that the DNN model has a better accuracy than other mesoscale models. The mesoscale models with traditional failure criteria show significant loss of accuracy for some of the strength constants compared with the meso-micro coupled model. For example, the Hashin failure criterion led to a 38.65% difference in Z'. The Tsai-Wu failure criterion led to a 45.61% difference in Z', and the maximum stress criterion led to a 13.86% difference in X' and Y'.

Table 6.4. Initial strength constants (MPa)

Model	$X=Y$	$X'=Y'$	Z	Z'	$R=S$	T
Meso-micro scale	149.81	294.25	39.91	144.60	22.94	19.10
DNN	146.54	281.48	38.73	140.78	22.86	18.92
Hashin	143.81	267.83	32.63	200.48	24.03	19.34
Tsai-Wu	147.50	234.71	36.22	210.55	23.41	19.23
Max-stress	150.60	253.46	38.06	137.89	24.10	19.36
Diff (DNN)	2.18%	4.34%	2.95%	2.64%	0.35%	0.92%
Diff (Hashin)	4.01%	8.98%	18.25%	38.65%	4.76%	1.24%
Diff (Tsai-Wu)	1.54%	20.23%	9.24%	45.61%	2.06%	0.67%
Diff (Max-stress)	0.53%	13.86%	4.64%	4.64%	5.05%	1.35%

To study the site of failure initiation, the contour plots of the failure index (FI) of yarn elements under the loading condition Z' are given in Figure 6.7. As shown in Table 6.4, the Hashin and Tsai-Wu failure criterion gives the largest error under Z' loading condition. The meso-micro scale model as well as the mesoscale model with DNN, Hashin, and Tsai-Wu failure criterion are analyzed. It is easy to observe that the critical elements or damage initiation sites in Figures 6.7(a) and 6.8(b) are similar while the critical elements predicted by Tsai-Wu and Hashin failure criterion are different from ones computed by the meso-micro scale model. Due to the symmetric configuration of the plain weave composite, the failure indexes between each yarn are very close as shown in Figure 6.7. Therefore, it is very difficult to accurately identify the initial failure element. However, the critical elements from different models can be analyzed to show the differences using different failure criteria. For example, the FI at the element 69402 and element 38807 in the meso-micro scale model are 1.000 and 0.997 respectively. As these two failure indexes are very close, the element 38807 can also be considered as a critical site for failure initiation, and this element is also considered as the critical site using DNN failure criterion. On the other hand, the

FI at element 39020 in meso-micro scale model is 0.958 that may not be considered as a critical element due to the 4.2% percentage difference, which means that the critical elements or sites predicted by Tsai-Wu and Hashin failure criterion may not be the damage initiation sites in the meso-micro scale model. In addition, the failure indexes at element 69402 using DNN, Tsai-Wu and Hashin failure criterion are 0.993, 0.844 and 0.861 respectively. Compared these failure indexes with the corresponding critical FI in each model, the percentage differences are 0.7%, 15.6% and 13.9%, which means that using DNN failure criterion can also detect the critical failure initial sites while using Tsai-Wu and Hashin failure criterion cannot predict the critical sites in the meso-micro scale model.

(a) Meso-micro scale model

(b) DNN failure criterion

(c) Tsai-Wu failure criterion

(d) Hashin failure criterion
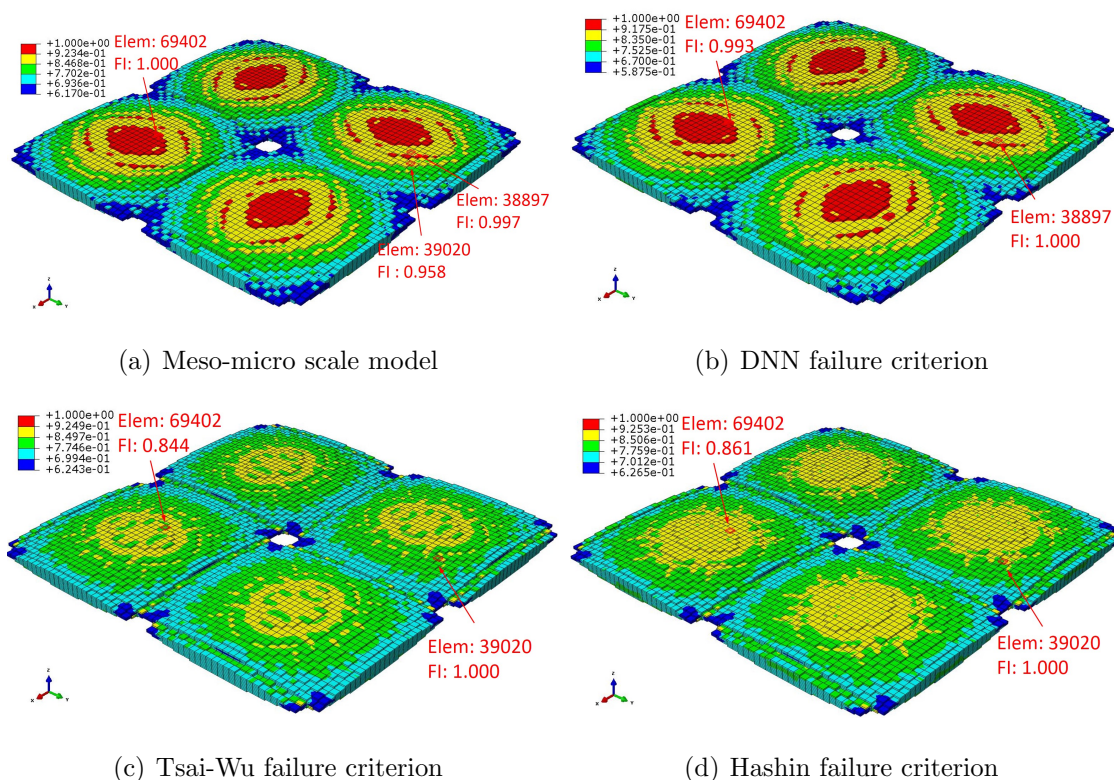
Figure 6.7. Initial failure sites based on different criteria

The traditional failure criteria are formulated by an assumed equation (e.g. Tsai-Wu) or a system of equations (e.g. Max-stress and Hashin) that include a number of

coefficients determined by sub-scale modeling. Therefore, given a set of yarn strength constants derived from microscale modeling, each failure criteria provides a different prediction. However, if a DNN-based failure criterion is directly constructed using the failure information from the microscale models without assuming a functional form, the accuracy can be improved as demonstrated by the results in Table 6.4.

6.4.2 Failure Envelope

The failure envelope analysis is performed to show the failure strength under combined loading conditions. A failure envelope can be used to graphically depict the critical stress/strain state field. In general, a failure envelope is a six-dimensional surface. In order to graphically represent and intuitively visualize them, only 2D failure envelopes are computed and plotted hereinafter. The envelope is computed numerically by gradually increasing the ratio of two load components and performing failure initiation analysis at each load step.

Another advantage of MSG models compared with the RVE models based on FEM is the efficiency in computing the failure envelope. First, most RVE-based analysis only computes the failure index to determine the point on the failure envelope. If the failure criterion is not linear (e.g., Tsai-Wu), multiple analyses are required to determine one failure point on the envelope. Since MSG uses the strength ratio, the analysis only needs to be performed once for the non-linear failure criterion. Second, RVE models must solve the system of equations for the entire model every time for different loads. Once the fluctuating functions are solved from the MSG models, the local stress field can be obtained by matrix multiplication directly. For a fix SG or RVE, MSG models only need to solve the system equations once.

The MSG solid model is used to perform the failure envelope analysis. The above numerical method has been implemented into the MSG companion code SwiftComp$^{\text{TM}}$ [105] to compute the failure envelopes. Since woven composites are often used as plies in laminated structures, the in-plane stress components usually

receive more attention in the design. The failure envelopes with respect to the $\overline{\sigma}_{11}$-$\overline{\sigma}_{22}$ and $\overline{\sigma}_{11}$-$\overline{\sigma}_{12}$ stress components are plotted in Figure 6.8. Note that the over-line on the stress components means that the failure envelope is constructed by the stress components applied at the mesoscale model, which are corresponding to the stress field of a material point in a woven lamina in a macroscale laminate structure.

The failure envelopes associated with the Max-stress and DNN yarn criterion are constructed to further study the accuracy of the proposed criterion. Based on the failure envelopes, two check points, a and b, are selected as shown in Figure 6.8. These points are associated with loading conditions under which the material should not fail according to the Max-stress failure criterion but fails using the DNN-based failure criterion. The corresponding applied stress loads to the mesoscale model are $\bar{\sigma}_{ij}^a = \begin{bmatrix} 130 & -150 & 0 & 0 & 0 & 0 \end{bmatrix}$ and $\bar{\sigma}_{ij}^b = \begin{bmatrix} 120 & 0 & 0 & 0 & 0 & 15 \end{bmatrix}$. Stresses are expressed in MPa. To determine if failure initiates under these loading conditions, the meso-micro scale model is used to perform the failure analysis. The resulting strength ratios are $\alpha^a = 0.914$ and $\alpha^b = 0.725$. As α^a and α^b are smaller than one, the material is expected to fail under these conditions. Since point a and b falls outside the failure envelope based on DNN failure criterion, the DNN failure criterion predicts failure as well. However, if the Max-stress criterion was applied to these loading conditions, failure would not be detected, thereby leading to unconservative predictions. Figure 6.9 shows the strength ratio computed at the microscale using the meso-micro scale model. The elements with the strength ratio larger than 1.1 has been hidden. Figure 6.9 shows that failure initiation occurs at multiple elements under the loading conditions a and b.

6.4.3   Computational Efficiency Analysis

All the computations in this chapter are performed in a windows system work-station using a single CPU. The processor of the computer is Inter(R) Xeon(R) @ 2.60 GHz and the RAM is 256 GB. The meso-micro scale modeling took 8.1 hours
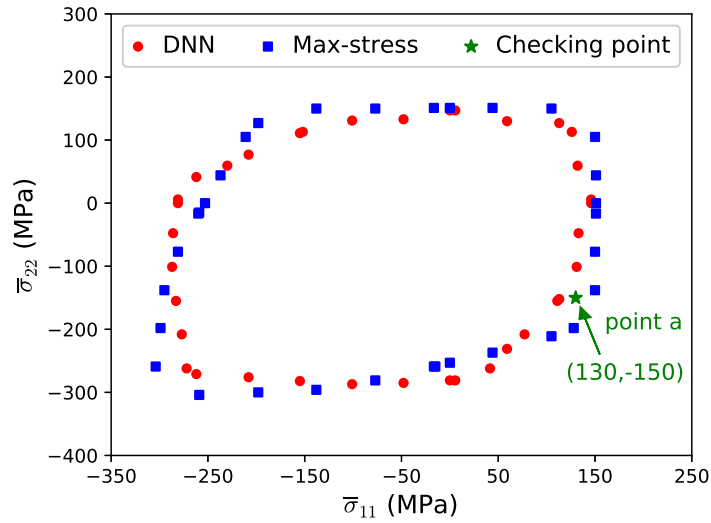
(a) $\overline{\sigma}_{11}$-$\overline{\sigma}_{22}$
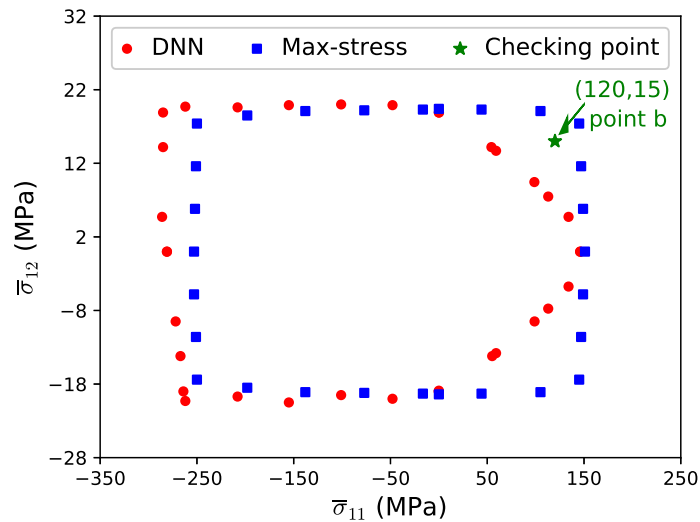
(b) $\overline{\sigma}_{11}$-$\overline{\sigma}_{12}$

Figure 6.8. Failure envelopes based on the DNN and Max-stress failure criterion

to determine the strength constants under 6 loading cases. The DNN mesoscale modeling using the proposed yarn failure criterion took 0.32 hours to determine the strength constants under 6 loading cases. For constructing the failure criterion, the

(a) Loading $\bar{\sigma}_{ij}^a$ (b) Loading $\bar{\sigma}_{ij}^b$
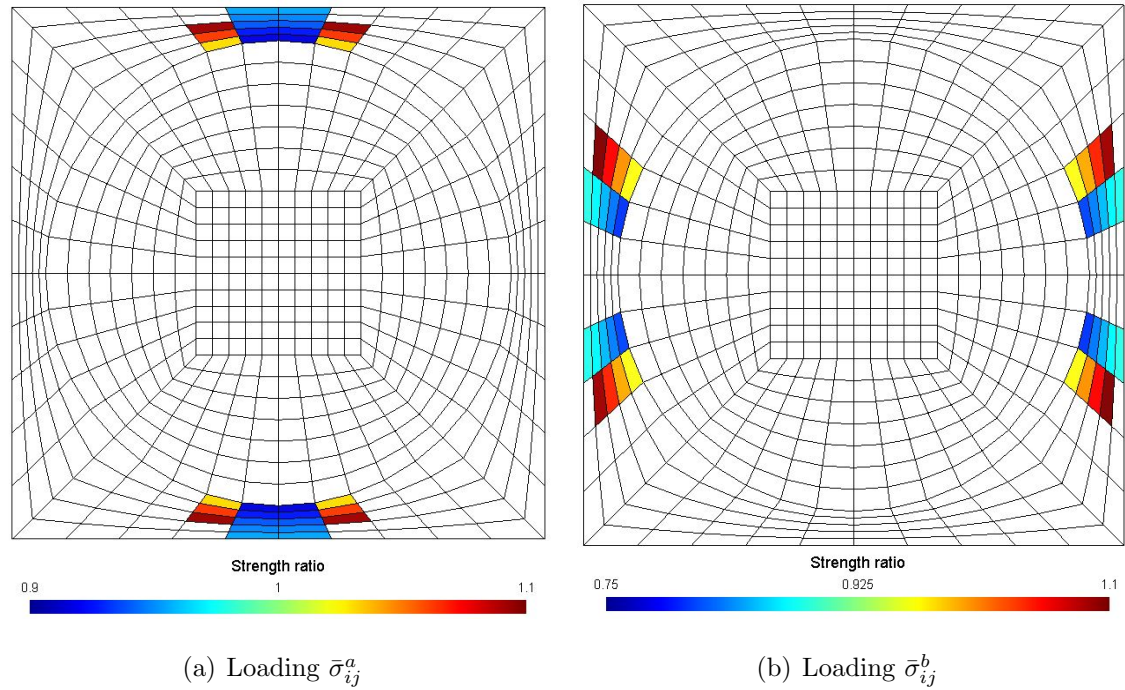
Figure 6.9. Strength ratio at microscale under loading condition a and b

DNN model took 8.3 hours including sampling and performing the MSG microscale analysis. The computing time associated with the training process performed using Tensorflow is negligible compared to the computing time for sampling and microscale modeling. However, the hyperparameters (e.g. number of hidden layers and neurons) in the DNN model need to be manually adjusted by the user. The time associated with this operation varies depending on the experience of the user. It takes minutes by an experienced user, while it can take hours by an inexperienced one. Therefore, the following comparison is based on computing time only and does not include hyperparameters adjustment. Figure 6.10 shows the computing time of the meso-micro scale and DNN model with respect to the number of loading cases. For the DNN model, the initial computing time is larger as it took 8.3 hours to obtain the yarn failure criterion. However, this is a one-time (i.e. non recurring) computational cost. After about 7 loading cases, the meso-micro scale model run time exceeds the computing time of the DNN model and it becomes more and more expensive compared with the

DNN model. As mentioned in the previous section, to construct a failure envelope, two stress components need to be gradually increased. This process typically involves a considerable number of load cases. Therefore, the proposed DNN model provides a more efficient approach for constructing failure envelopes without significant loss of accuracy. The constructed failure criterion can be used in many other computational expensive analyses such as predicting failure envelopes with different load combinations and modeling the woven composites using plate or beam model with the same microscale model.
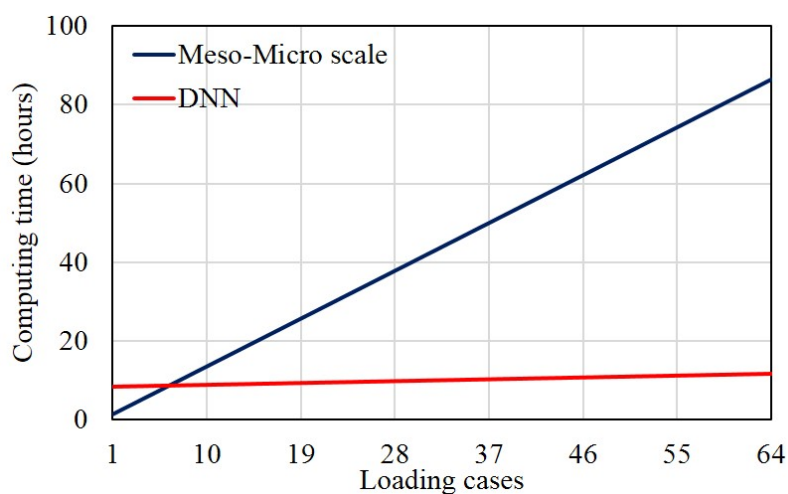
Figure 6.10. Computing time of the meso-micro scale and DNN model

6.5 Summary

A new yarn failure criterion is developed based on the MSG microscale failure analysis and a DNN model. The mesoscale failure analysis of a plain woven composite material example is performed using the proposed yarn failure criterion and other well established failure criteria. In addition, a meso-micro scale coupled model is used to provide benchmark results to verify the accuracy and efficiency of the proposed model. The results show that the proposed model agrees well with the benchmark results while the traditional failure criteria show significant loss of accuracy in some

strength constants. The failure envelope analysis is also performed to show that the proposed failure criterion provides a more accurate prediction under multiaxial loading conditions than traditional criteria. The inaccuracy from the traditional failure criteria is likely due to the inherent assumptions built in their formulation. Therefore, constructing a failure criterion based on advanced machine learning models (i.e. deep learning model) could potentially give more accurate predictions. The proposed DNN modeling approach can be applied to high fidelity multiscale failure analysis models as well as experimental data, regardless of the material microstructure, mesostructure and failure mechanism.

7. SUMMARY

In this dissertation, a novel multiscale modeling approach to predicting the behaviors of textile composite materials and structures is developed based on mechanics of structure genome (MSG) and artificial neural network (ANN) models. The MSG theory has been extended to perform multiscale modeling of textile composites in elastic, viscoelastic, thermoelastic, and failure analysis. The proposed method has been validated using 3D RVE analysis, DNS based on 3D FEA, or experimental data. The results show that the proposed approach achieves the same accuracy as the ones based on 3D FEA while the computational efficiency has been greatly improved. Moreover, ANN models are used to construct a new yarn failure criterion to accelerate the multiscale failure analysis which also avoids the inaccuracies associated with the postulated expressions in traditional failure criteria.

A two-step homogenization is first proposed to predict the effective properties of textile composites. In the first step, the effective properties of yarns are computed based on fiber and matrix properties using the MSG solid model at the microscale. The effective properties of textile composites are subsequently obtained based on the effective properties of yarns and matrix. Different weave patterns (e.g., 2D and 3D woven) and manufacturing features (e.g. inter-ply shift) are studied using the MSG solid model. The results are compared with the ones from RVE analysis using 3D FEA. It shows that the MSG solid model achieves the same accuracy as RVE analysis with a significantly reduced computational cost. In addition, the MSG plate and beam models are used to analyze thin and slender textile structures. Both structural responses and local stress fields can be captured with the same accuracy as the DNS models while the computing time is greatly reduced. To better apply this novel multiscale modeling approach to the real engineering analysis and design, the approach has been integrated into commercial FEM software MSC.Patran/Nastran

as a multiscale constitutive modeling module. The constitutive information obtained from MSG models is used along with the built-in structural elements in MSC.Nastran, which can capture the behavior of complex woven composite structures using normal structural elements.

MSG theory has been extended to predict the viscoelastic behavior of textile composites based on the quasi-elastic approach. At the microscale, the fiber is elastic and the matrix is viscoelastic. The MSG solid model is used to predict the effective viscoelastic properties of yarns which are in terms of Prony series. At the mesoscale, the MSG plate model is used to predict the time-dependent plate stiffness matrix which is used to capture the viscoelastic behavior of thin-ply textile composites. The developed approach provides a fast and accurate alternative to the commonly used RVE analysis approach. In addition, the viscoelastic properties of non-isotropic materials can be easily defined in the MSG models while complex user subroutines are required in the commercial FEM codes. The predicted behavior is compared with the experimental data from literature and a excellent agreement is found.

In addition, the MSG theory has been extended to capture the thermoelastic behavior of textile composites. The pointwise temperature load along the thickness of thin or across the cross-section of slender structures are taken into account at the SG level. For thin and slender structures, the plate and beam stress resultants are used to capture the thermal-induced behaviors. Different 2D and 3D textile composites are analyzed using the proposed approach and the results are compared with the ones from DNS. The results show that the proposed approach has the same accuracy as the DNS with a significant improved efficiency.

The MSG models are applied to initial failure analysis of textile composites. A meso-micro scale coupled approach is proposed which avoids using questionable failure criterion of yarns. Moreover, the stress gradient along the thickness of thin textile composite structures is captured by using the strength constants in terms of plate stress resultants. Since MSG models only need to perform one homogenization to

determine the fluctuating functions, MSG models show a great benefit in efficiency for computing the failure envelopes.

To accelerate the multiscale failure analysis, the advanced deep learning neural network models are used to construct a new yarn failure criterion based on a series of microscale failure analysis. The new yarn failure criterion as well as other commonly used failure criteria are applied to mesoscale failure analysis. The mesoscale failure strength constants predicted by the new yarn failure criterion agree well with the ones based on the scale-coupled approach while the results based on other traditional failure criteria show great loss of accuracy in some of the strength constants. The new yarn failure criterion is constructed in a form-free manner to avoid the inaccuracies associated with the postulated expressions. In addition, the new yarn failure criterion only needs to be trained once and can be used in other computational expensive simulations such as constructing failure envelopes and progressive failure analysis.

The present work can be safely applied to multiscale modeling of textile composite materials and structures with different micro/mesoscale features and defects. The author also would like to recommend the possible future work of this research. First, extending the current theory to predict the nonlinear behavior of textile composite materials and structures. The present work demonstrates the advantages of MSG models in the linear analysis in elastic, viscoelastic and thermoelastic analysis. The nonlinear analysis can be roughly considered as a series of linear analyses in the time domain, which means the proposed framework will maintain the same advantages in the efficiency and accuracy. There are some important nonlinear problems in textile composites such as geometry nonlinear behaviors in forming simulations or packing/deploying of thin-ply composites and material nonlinear behavior such the progressive failure due to the damage. In addition, ANN models would potentially provide a good complement to multiscale constitutive modeling. There are two important applications. First, ANN models provide an efficient approach for nonlinear multiscale modeling where the subscale modeling will be replaced by ANN-based surrogate models. Second, the ANN models provide the universal approximation theory

which can be used to capture unknown physical laws (e.g., the failure criterion of yarns) using the functions in a form-free manner.

REFERENCES

[1] A. Alzina, E. Toussaint, and A. Béakou. Multiscale modeling of the thermoelastic behavior of braided fabric composites for cryogenic structures. *International Journal of Solids and Structures*, 44(21):6842–6859, 2007.

[2] Z. Hashin. Viscoelastic fiber reinforced materials. *AIAA Journal*, 4(8):1411–1417, 1966.

[3] E. Gdoutos, A. Truong, A. Pedivellano, F. Royer, and S. Pellegrino. Ultralight deployable space structure prototype. In *AIAA SciTech 2020 Forum*, page 0692, 2020.

[4] A. Stabile and S. Laurenzi. Coiling dynamic analysis of thin-walled composite deployable boom. *Composite Structures*, 113:429–436, 2014.

[5] R.T. Bhatt, S.R. Choi, L.M. Cosgriff, D.S. Fox, and K.N. Lee. Impact resistance of uncoated SiC/SiC composites. *Materials Science and Engineering: A*, 476(1-2):20–28, 2008.

[6] F. Tao, X. Lyu, X. Liu, and W. Yu. Multiscale analysis of multilayer printed circuit board using mechanics of structure genome. *Mechanics of Advanced Materials and Structures*, pages 1–10, 2019.

[7] M.J. Hinton, A.S. Kaddour, and P.D. Soden. The world-wide failure exercise: Its origin, concept and content. In *Failure Criteria in Fibre-Reinforced-Polymer Composites*, pages 2–28. Elsevier, 2004.

[8] F. Feyel and J. Chaboche. FE2 multiscale approach for modelling the elastoviscoplastic behaviour of long fibre SiC/Ti composite materials. *Computer Methods in Applied Mechanics and Engineering*, 183(3-4):309–330, 2000.

[9] M.G.D. Geers, V.G. Kouznetsova, and W.A.M. Brekelmans. Multi-scale computational homogenization: trends and challenges. *Journal of Computational and Applied Mathematics*, 234(7):2175–2182, 2010.

[10] X. Liu, K. Rouf, B. Peng, and W. Yu. Two-step homogenization of textile composites using mechanics of structure genome. *Composite Structures*, 171:252–262, 2017.

[11] K. Rouf, X. Liu, and W. Yu. Multiscale structural analysis of textile composites using mechanics of structure genome. *International Journal of Solids and Structures*, 136:89–102, 2018.

[12] X. Liu, T. Tang, W. Yu, and R.B. Pipes. Multiscale modeling of viscoelastic behaviors of textile composites. *International Journal of Engineering Science*, 130:175–186, 2018.

[13] X. Liu, W. Yu, F. Gasco, and J. Goodsell. A unified approach for thermoelastic constitutive modeling of composite structures. *Composites Part B: Engineering*, 172:649–659, 2019.

[14] X. Liu, F. Gasco, W. Yu, J. Goodsell, and K. Rouf. Multiscale analysis of woven composite structures in MSC.Nastran. *Advances in Engineering Software*, 135:102677, 2019.

[15] X. Liu, F. Gasco, J. Goodsell, and W. Yu. Initial failure strength prediction of woven composites using a new yarn failure criterion constructed by deep learning. *Composite Structures*, 230:111505, 2019.

[16] A. Hallal, R. Younes, and F. Fardoun. Review and comparative study of analytical modeling for the elastic properties of textile composites. *Composites Part B: Engineering*, 50:22–31, 2013.

[17] T. Ishikawa and T-W. Chou. Elastic behaviour of woven hybrid composites. *Journal of Composites Materials*, 16(1):2–19, 1982.

[18] T. Ishikawa and T-W. Chou. Stiffness and strength behaviour of woven fabric composites. *Journal of Materials Science*, 17(11):3211–3220, 1982.

[19] S.L. Angioni, M. Meo, and A. Foreman. A critical review of homogenization methods for 2D woven composites. *Journal of Reinforced Plastics and Composites*, 42(2):1895–906, 2011.

[20] B. Gommers, I. Verpoest, and P. Van Houtte. The Mori–Tanaka method applied to textile composite materials. *Acta Materialia*, 46(6):2223–2235, 1998.

[21] I. Verpoest and S.V. Lomov. Virtual textile composites software wisetex: Integration with micro-mechanical, permeability and structural analysis. *Composites Science and Technology*, 65(15):2563–2574, 2005.

[22] J. Whitcomb and K. Woo. Enhanced direct stiffness method for finite element analysis of textile composites. *Composite Structures*, 28(4):385–390, 1994.

[23] S.V. Lomov, D.S. Ivanov, I. Verpoest, M. Zako, T. Kurashiki, H. Nakai, J. Molimard, and A. Vautrin. Full-field strain measurements for validation of meso-FE analysis of textile composites. *Composites Part A: Applied Science and Manufacturing*, 39(8):1218–1231, 2008.

[24] M. Zako, Y. Uetsuji, and T. Kurashiki. Finite element analysis of damaged woven fabric composite materials. *Composites Science and Technology*, 63(3):507–516, 2003.

[25] G. Nicoletto and E. Riva. Failure mechanisms in twill-weave laminates: FEM predictions vs. experiments. *Composites Part A: Applied Science and Manufacturing*, 35(7):787–795, 2004.

[26] J. Guedes and N. Kikuchi. Preprocessing and postprocessing for materials based on the homogenization method with adaptive finite element methods. *Computer Methods in Applied Mechanics and Engineering*, 83(2):143–198, 1990.

[27] S.L. Angioni, M. Meo, and A. Foreman. A comparison of homogenization methods for 2-D woven composites. *Composites Part B: Engineering*, 42(2):181–189, 2011.

[28] M.R.E. Nasution, N. Watanabe, A. Kondo, and A. Yudhanto. A novel asymptotic expansion homogenization analysis for 3-D composite with relieved periodicity in the thickness direction. *Composites Science and Technology*, 97:63–73, 2014.

[29] B.V. Sankar and R.V. Marrey. A unit-cell model of textile composite beams for predicting stiffness properties. *Composites Science and Technology*, 49(1):61–69, 1993.

[30] T-W. Chou and T. Ishikawa. One-dimensional micromechanical analysis of woven fabric composites. *AIAA Journal*, 21(12):1714–1721, 1983.

[31] P. Chaphalkar and A. Kelkar. Classical laminate theory model for twill weave fabric composites. *Composites Part A: Applied Science and Manufacturing*, 32(9):1281–1289, 2001.

[32] R.V. Marrey and B.V. Sankar. A micromechanical model for textile composite plates. *Journal of Composite Materials*, 31(12):1187–1213, 1997.

[33] Z. Hashin. Viscoelastic behavior of heterogeneous media. *Journal of Applied Mechanics*, 32:630–636, 1965.

[34] L.C. Brinson and W.G. Knauss. Finite element analysis of multiphase viscoelastic solids. *Journal of Applied Mechanics*, 59(4):730–737, 1992.

[35] A.H. Muliana and R. Haj-Ali. Multiscale modeling for the long-term behavior of laminated composite structures. *AIAA Journal*, 43(8):1815–1822, 2005.

[36] T. Tang and S.D. Felicelli. Computational evaluation of effective stress relaxation behavior of polymer composites. *International Journal of Engineering Science*, 90:76–85, 2015.

[37] P. Upadhyaya and C.S. Upadhyay. A three-dimensional micromechanical model to predict the viscoelastic behavior of woven composites. *Composite Structures*, 93(11):2733–2739, 2011.

[38] P. Shrotriya and N.R. Sottos. Viscoelastic response of woven composite substrates. *Composites Science and Technology*, 65(3):621–634, 2005.

[39] K. Kwok and S. Pellegrino. Micromechanics models for viscoelastic plain-weave composite tape springs. *AIAA Journal*, 55(1):309–321, 2016.

[40] A. El Mourid, R. Ganesan, and M. Lévesque. Comparison between analytical and numerical predictions for the linearly viscoelastic behavior of textile composites. *Mechanics of Materials*, 58:69–83, 2013.

[41] E.J. Barbero. *Finite Element Analysis of Composite Materials using Abaqus^{TM}*. CRC press, 2013.

[42] P. Tan, L. Tong, and G.P. Steven. Models for predicting thermomechanical properties of three-dimensional orthogonal woven composites. *Journal of Reinforced Plastics and Composites*, 18(2):151–185, 1999.

[43] J. Cho, Y. Kang, K. Jeong, Y. Noh, and O. Lim. Homogenization and thermoelastic analysis of heterogenous materials with regular and random microstructures. *Composites Part B: Engineering*, 43(5):2313–2323, 2012.

[44] M.R.E. Nasution, N. Watanabe, A. Kondo, and A. Yudhanto. Thermomechanical properties and stress analysis of 3-D textile composites by asymptotic expansion homogenization method. *Composites Part B: Engineering*, 60:378–391, 2014.

[45] O. Rique, J. Goodsell, W. Yu, and R.B. Pipes. Three-dimensional thermoelastic properties of general composite laminates. *Journal of Composite Materials*, 52(13):1799–1808, 2018.

[46] F.A. Fazzolari and E. Carrera. Thermal stability of FGM sandwich plates under various through-the-thickness temperature distributions. *Journal of Thermal Stresses*, 37(12):1449–1481, 2014.

[47] Y. Zhou, T. Nyberg, G. Xiong, and D. Liu. Temperature analysis in the fused deposition modeling process. In *3rd International Conference on Information Science and Control Engineering (ICISCE)*, pages 678–682. IEEE, 2016.

[48] S.V. Lomov, D.S. Ivanov, I. Verpoest, M. Zako, T. Kurashiki, H. Nakai, and S. Hirosawa. Meso-FE modelling of textile composites: Road map, data flow and algorithms. *Composites Science and Technology*, 67(9):1870–1891, 2007.

[49] W.R. McLendon and J.D. Whitcomb. Characteristic failure initiation sites in plain weave textile composites. *Journal of Composite Materials*, 47(25):3143–3161, 2013.

[50] Y. Zhou, Z. Lu, and Z. Yang. Progressive damage analysis and strength prediction of 2D plain weave composites. *Composites Part B: Engineering*, 47:220–229, 2013.

[51] G. Ernst, M. Vogler, C. Hühne, and R. Rolfes. Multiscale progressive failure analysis of textile composites. *Composites Science and Technology*, 70(1):61–72, 2010.

[52] H. Jiang, Y. Ren, Z. Liu, S. Zhang, and G. Yu. Multi-scale analysis for mechanical properties of fiber bundle and damage characteristics of 2D triaxially braided composite panel under shear loading. *Thin-Walled Structures*, 132:276–286, 2018.

[53] L. Wang, J. Wu, C. Chen, C. Zheng, B. Li, S. C. Joshi, and K. Zhou. Progressive failure analysis of 2D woven composites at the meso-micro scale. *Composite Structures*, 178:395–405, 2017.

[54] X.S. Sun, V.B.C. Tan, and T.E. Tay. Micromechanics-based progressive failure analysis of fibre-reinforced composites with non-iterative element-failure method. *Computers & Structures*, 89(11-12):1103–1116, 2011.

[55] R.L. Karkkainen and B.V. Sankar. A direct micromechanics method for analysis of failure initiation of plain weave textile composites. *Composites Science and Technology*, 66(1):137–150, 2006.

[56] R.L. Karkkainen, B.V. Sankar, and J.T. Tzeng. Strength prediction of multilayer plain weave textile composites using the direct micromechanics method. *Composites Part B: Engineering*, 38(7-8):924–932, 2007.

[57] DS Simulia. Abaqus 2017 documentation, 2017.

[58] M. Lefik, D.P. Boso, and B.A. Schrefler. Artificial neural networks in numerical modelling of composites. *Computer Methods in Applied Mechanics and Engineering*, 198(21-26):1785–1804, 2009.

[59] J.F. Unger and C. Könke. Neural networks as material models within a multi-scale approach. *Computers & Structures*, 87(19-20):1177–1186, 2009.

[60] B.A. Le, J. Yvonnet, and Q. He. Computational homogenization of nonlinear elastic materials using neural networks. *International Journal for Numerical Methods in Engineering*, 104(12):1061–1084, 2015.

[61] Y. LeCun, Y. Bengio, and G. Hinton. Deep learning. *Nature*, 521:436–444, 2015.

[62] F. Chollet. *Deep Learning with Python*. Manning Publications Co., 2017.

[63] B.C. Csáji. Approximation with Artificial Neural Networks. Master's thesis, Etvs Lornd University, June 2001.

[64] W. Yu. A unified theory for constitutive modeling of composites. *Journal of Mechanics of Materials and Structures*, 11(4):379–411, 2016.

[65] W. Yu, D.H. Hodges, and J.C. Ho. Variational asymptotic beam sectional analysis–an updated version. *International Journal of Engineering Science*, 59:40–64, 2012.

[66] V. Berdichevsky. *Variational Principles of Continuum Mechanics: I. Fundamentals*. Berlin: Springer Science & Business Media, 2009.

[67] W. Yu. Simplified formulation of mechanics of structure genome. *AIAA Journal*, 57(10):4201–4209, 2019.

[68] W. Yu and T. Tang. A variational asymptotic micromechanics model for predicting thermoelastic properties of heterogeneous materials. *International Journal of Solids and Structures*, 44(22):7510–7525, 2007.

[69] H. Lin, L.P. Brown, and A.C. Long. Modelling and simulating textile structures using texgen. In *Advanced Materials Research*, volume 331, pages 44–47. Trans Tech Publ, 2011.

[70] M. Sherburn. *Geometric and Mechanical Modelling of Textiles*. PhD thesis, University of Nottingham, Jul. 2007.

[71] N. Gommer, L.P. Brown, and K.C.A. Wedgwood. Analytical method using gamma functions for determining areas of power elliptical shapes for use in geometrical textile models. *Composites Part A: Applied Science and Manufacturing*, 81:222–224, 2016.

[72] K. Kirane, M. Salviato, and Z. Bažant. Microplane triad model for simple and accurate prediction of orthotropic elastic constants of woven fabric composites. *Journal of Composite Materials*, 50(9):1247–1260, 2016.

[73] D.S. Ivanov, S.G. Ivanov, S.V. Lomov, and I. Verpoest. Unit cell modelling of textile laminates with arbitrary inter-ply shifts. *Composites Science and Technology*, 72(1):14–20, 2011.

[74] M.Y. Matveev, A.C. Long, and I.A. Jones. Modelling of textile composites with fibre strength variability. *Composites Science and Technology*, 105:44–50, 2014.

[75] J.J. Espadas-Escalante, N.P. van Dijk, and P. Isaksson. A study on the influence of boundary conditions in computational homogenization of periodic structures with application to woven composites. *Composite Structures*, 160:529–537, 2017.

[76] MSC SimCompanion. *MSC Nastran 2016 Reference Manual*, 2016.

[77] H. Chen, W. Yu, and M. Capellaro. A critical assessment of computer tools for calculating composite wind turbine blade properties. *Wind Energy*, 13(6):497–516, 2010.

[78] E.J. Barbero. *Introduction to Composite Materials Design*. CRC press, 2010.

[79] X. Liu and W. Yu. A novel approach to analyze beam-like composite structures using mechanics of structure genome. *Advances in Engineering Software*, 100:238–251, 2016.

[80] B. Peng and W. Yu. A micromechanics theory for homogenization and de-homogenization of aperiodic heterogeneous materials. *Composite Structures*, 199:53–62, 2018.

[81] O. Rique, X. Liu, W. Yu, and R.B. Pipes. Constitutive modeling for time-and temperature-dependent behavior of composites. *Composites Part B: Engineering*, 184:107726, 2020.

[82] A. Naik, N. Abolfathi, G. Karami, and M. Ziejewski. Micromechanical viscoelastic characterization of fibrous composites. *Journal of Composite Materials*, 42(12):1179–1204, 2008.

[83] J.J. Moré. The levenberg-marquardt algorithm: implementation and theory. In *Numerical Analysis*, pages 105–116. Springer, 1978.

[84] T. Tang and W. Yu. A variational asymptotic micromechanics model for predicting conductivities of composite materials. *Journal of Mechanics of Materials and Structures*, 2(9):1813–1830, 2007.

[85] N.K. Naik and E. Sridevi. An analytical method for thermoelastic analysis of 3D orthogonal interlock woven composites. *Journal of Reinforced Plastics and Composites*, 21(13):1149–1191, 2002.

[86] H. Sertse, J. Goodsell, A.J. Ritchey, R.B. Pipes, and W. Yu. Challenge problems for the benchmarking of micromechanics analysis: Level I initial results. *Journal of Composite Materials*, 52(1):61–80, 2018.

[87] K. Dong, K. Liu, Q. Zhang, B. Gu, and B. Sun. Experimental and numerical analyses on the thermal conductive behaviors of carbon fiber/epoxy plain woven composites. *International Journal of Heat and Mass Transfer*, 102:501–517, 2016.

[88] M.J. Hinton, A.S. Kaddour, and P.D. Soden. *Failure Criteria in Fibre Reinforced Polymer Composites: The World-wide Failure Exercise*. Elsevier, 2004.

[89] R. Talreja. Assessment of the fundamentals of failure theories for composite materials. *Composites Science and Technology*, 105:190–201, 2014.

[90] S.W. Tsai and E.M. Wu. A general theory of strength for anisotropic materials. *Journal of Composite Materials*, 5(1):58–80, 1971.

[91] N.V. De Carvalho, S.T. Pinho, and P. Robinson. Numerical modelling of woven composites: Biaxial loading. *Composites Part A: Applied Science and Manufacturing*, 43(8):1326–1337, 2012.

[92] P.D. Soden, M.J. Hinton, and A.S. Kaddour. Lamina properties, lay-up configurations and loading conditions for a range of fibre-reinforced composite laminates. *Composites Science and Technology*, 58(7):1011–1022, 1998.

[93] W.R. Mclendon and J.D. Whitcomb. Failure initiation prediction in textile composites under complex thermo-mechanical loading based on meso-scale analysis. *53rd AIAA/ASME/ASCE/AHS/ASC Structures, Structural Dynamics and Materials Conference*, pages 1–18, 2012.

[94] SIMULIA. *ABAQUS Documentation*, 2017.

[95] K. Wang and W. Sun. A multiscale multi-permeability poroplasticity model linked by recursive homogenizations and deep learning. *Computer Methods in Applied Mechanics and Engineering*, 334:337–380, 2018.

[96] Z. Liu, C.T. Wu, and M. Koishi. A deep material network for multiscale topology learning and accelerated nonlinear modeling of heterogeneous materials. *Computer Methods in Applied Mechanics and Engineering*, 345:1138–1168, 2019.

[97] G. Balokas, S. Czichon, and R. Rolfes. Neural network assisted multiscale analysis for the elastic properties prediction of 3D braided composites under uncertainty. *Composite Structures*, 183:550–562, 2018.

[98] X. Glorot, A. Bordes, and Y. Bengio. Deep sparse rectifier neural networks. In *Proceedings of the Fourteenth International Conference on Artificial Intelligence and Statistics*, pages 315–323, 2011.

[99] J. Duchi, E. Hazan, and Y. Singer. Adaptive subgradient methods for online learning and stochastic optimization. *Journal of Machine Learning Research*, 12:2121–2159, 2011.

[100] M.A. Nielsen. *Neural Networks and Deep Learning*, volume 25. Determination press USA, 2015.

[101] M. Abadi, P. Barham, J. Chen, Z. Chen, A. Davis, J. Dean, M. Devin, S. Ghemawat, G. Irving, M. Isard, et al. Tensorflow: A system for large-scale machine learning. In *12th {USENIX} Symposium on Operating Systems Design and Implementation ({OSDI} 16)*, pages 265–283, 2016.

[102] M. Hadigol and A. Doostan. Least squares polynomial chaos expansion: A review of sampling strategies. *Computer Methods in Applied Mechanics and Engineering*, 332(15):382–407, 2018.

[103] R.M. Christensen. *The Theory of Materials Failure*. Oxford University Press, 2013.

[104] S. Dai and P.R. Cunningham. Multi-scale damage modelling of 3D woven composites under uni-axial tension. *Composite Structures*, 142:298–312, 2016.

[105] W. Yu and X. Liu. Swiftcomp, 2015. https://cdmhub.org/resources/scstandard.

[106] Multiscale Structural Mechanics. Multiscale structural mechanics youtube channel. https://www.youtube.com/channel/UCqiIUid7Xj4JXlQskD7g7Iw.

[107] X. Liu and W. Yu. Texgen4sc, 2020. https://cdmhub.org/resources/texgen4sc.

[108] C. Geuzaine and J. Remacle. Gmsh: A 3-D finite element mesh generator with built-in pre-and post-processing facilities. *International Journal for Numerical Methods in Engineering*, 79(11):1309–1331, 2009.

A. OPERATOR MATRIX

Γ_h is an operator matrix, and it depends on the dimensionality of the SG. For the 3D SG, we have

$$\Gamma_h = \begin{bmatrix} \frac{\partial}{\partial y_1} & 0 & 0 \\ 0 & \frac{\partial}{\partial y_2} & 0 \\ 0 & 0 & \frac{\partial}{\partial y_3} \\ 0 & \frac{\partial}{\partial y_3} & \frac{\partial}{\partial y_2} \\ \frac{\partial}{\partial y_3} & 0 & \frac{\partial}{\partial y_1} \\ \frac{\partial}{\partial y_2} & \frac{\partial}{\partial y_1} & 0 \end{bmatrix} \tag{A.1}$$

For the 2D or 1D SG, we just need to vanish the corresponding terms which contain the micro-coordinates that are not used in describing the SG. For example, if the SG is 2D, we have

$$\Gamma_h = \begin{bmatrix} 0 & 0 & 0 \\ 0 & \frac{\partial}{\partial y_2} & 0 \\ 0 & 0 & \frac{\partial}{\partial y_3} \\ 0 & \frac{\partial}{\partial y_3} & \frac{\partial}{\partial y_2} \\ \frac{\partial}{\partial y_3} & 0 & 0 \\ \frac{\partial}{\partial y_2} & 0 & 0 \end{bmatrix} \tag{A.2}$$

For the SG is 1D, we have

$$\Gamma_h = \begin{bmatrix} 0 & 0 & 0 \\ 0 & 0 & 0 \\ 0 & 0 & \frac{\partial}{\partial y_3} \\ 0 & \frac{\partial}{\partial y_3} & 0 \\ \frac{\partial}{\partial y_3} & 0 & 0 \\ 0 & 0 & 0 \end{bmatrix} \tag{A.3}$$

Γ_ϵ is an operator matrix depending on the macroscopic structural model. If the macroscopic structural model is the 3D Cauchy continuum model, Γ_ϵ is the 6×6 identity matrix. If the macroscopic structural model is a beam model, we have

$$\Gamma_\epsilon = \begin{bmatrix} 1 & 0 & \varepsilon y_3 & -\varepsilon y_2 \\ 0 & 0 & 0 & 0 \\ 0 & 0 & 0 & 0 \\ 0 & 0 & 0 & 0 \\ 0 & \varepsilon y_2 & 0 & 0 \\ 0 & -\varepsilon y_3 & 1 & 0 \end{bmatrix} \tag{A.4}$$

If the macroscopic structural model is a plate/shell model, we have

$$\Gamma_\epsilon = \begin{bmatrix} 1 & 0 & 0 & \varepsilon y_3 & 0 & 0 \\ 0 & 1 & 0 & 0 & \varepsilon y_3 & 0 \\ 0 & 0 & 0 & 0 & 0 & 0 \\ 0 & 0 & 0 & 0 & 0 & 0 \\ 0 & 0 & 0 & 0 & 0 & 0 \\ 0 & 0 & 1 & 0 & 0 & \varepsilon y_3 \end{bmatrix} \tag{A.5}$$

Since ε does not affect the results, we choose $\varepsilon = 1$ in the numerical calculations.

B. SOFTWARE DEVELOPMENT

TexGen4SC

TexGen is a geometric textile modelling software package which can be used to create the geometry and mesh for textile composites. It is an open source code licensed under the General Public License developed at the University of Nottingham [69]. The software here is modified so that it can call SwiftComp to compute the effective properties. Taking advantage of the versatile model generation capability by TexGen and constitutive modelling by SwiftComp, TexGen4SC provides a fast and easy way to compute properties of textile composites. If you want a quick start, please watch out TexGen4SC Tutorial Video Series [106]. User manual and the source codes can be found in the supporting documents [107]. TexGen4SC provides microscale and mesoscale homogenization to compute the effective structural properties of textile composites and the main window is given in Figure B.1.
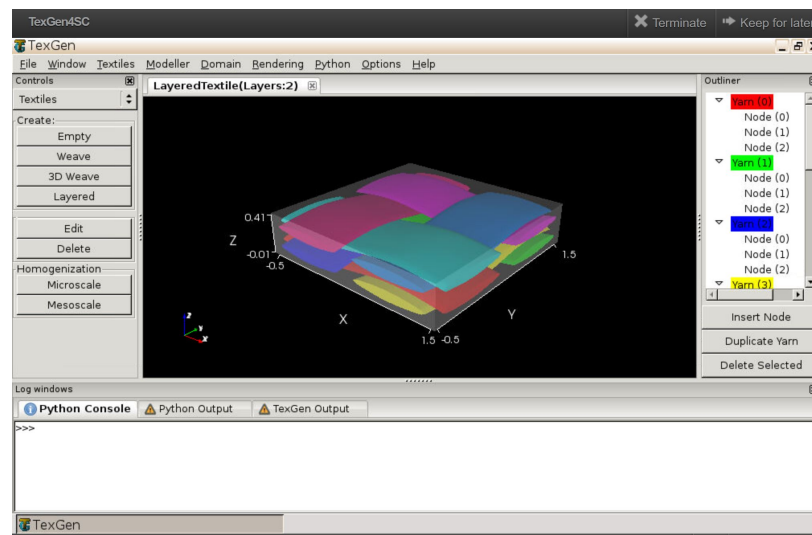
Figure B.1. TexGen4SC on the cloud through cdmHUB.org

For the microscale homogenization as shown in Figure B.2, MSG solid model is used to compute the effective properties of yarns. Two micromechanical models Square pack and Hexagonal pack are provided. The finite element mesh is internally generated by gmsh [108]. At the microscale, users can perform elastic, thermoelastic, viscoelastic, and thermoviscoelastic analysis based on different needs. The computed effective properties will be automatically assigned to the yarns for the mesoscale analysis.
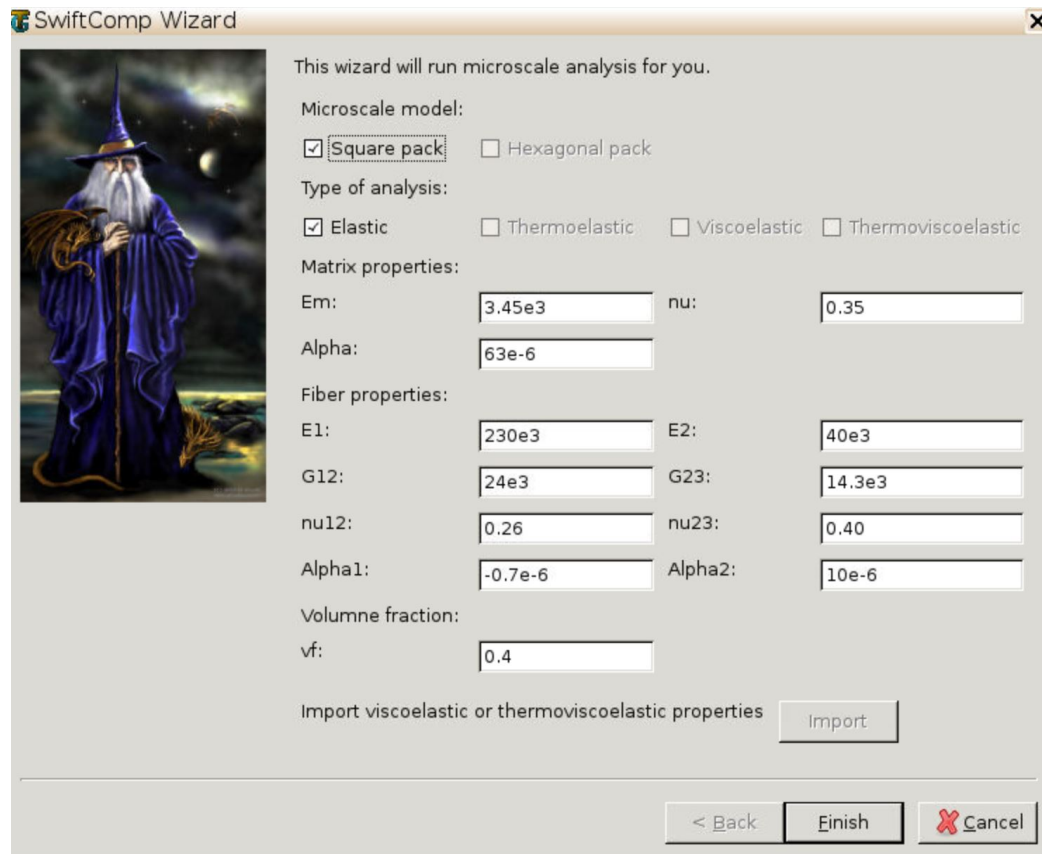
Figure B.2. Microscale homogenization in TexGen4SC

For the mesoscale homogenization as shown in Figure B.3, the mesh size which is defined using voxel should be input first. Similar to the microscale analysis, the mesoscale analysis provides elastic, thermoelastic, viscoelastic, and thermoviscoelastic analysis. Moreover, users can choose different MSG models such as solid, plate or

beam models based on different needs. In addition, the aperiodic functions can be selected which is able to take into consideration of the finite thickness effects for textile composites.
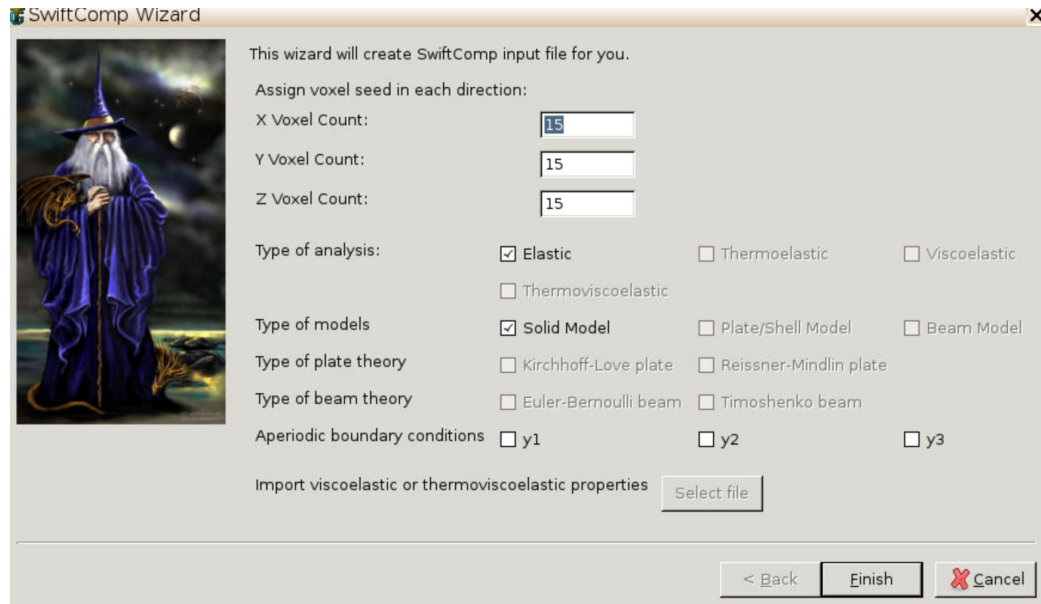

Figure B.3. Mesoscale homogenization in TexGen4SC

MSC.Patran/Nastran-SwiftComp GUI

A novel multiscale modeling module has been developed in MSC.Patran/Nastran through a graphic user interface (GUI). The developed constitutive modeling module is to integrate SwiftComp^{TM} into the MSC.Patran through MSC.Patran/Nastran-SwiftComp^{TM} GUI. An overview of MSC.Patran/Nastran-SwiftComp^{TM} GUI is given in Figure B.4.

In the MSC.Patran/Nastran-SwiftComp^{TM} GUI, the constitutive modeling functions provide homogenization and dehomogenization analysis for different MSG models as shown in Figures B.5 and B.6.

In addition, the GUI provides the recent developed MSG initial failure analysis functions, which include computing the initial failure strength constants, failure in-
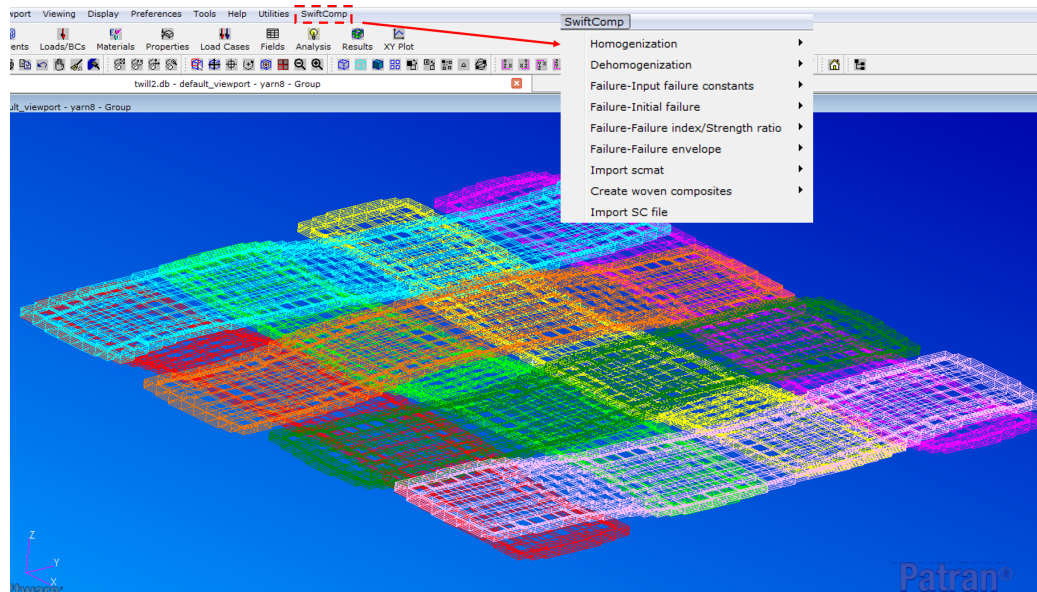
Figure B.4. MSC.Patran/Nastran-SwiftComp^{TM} GUI
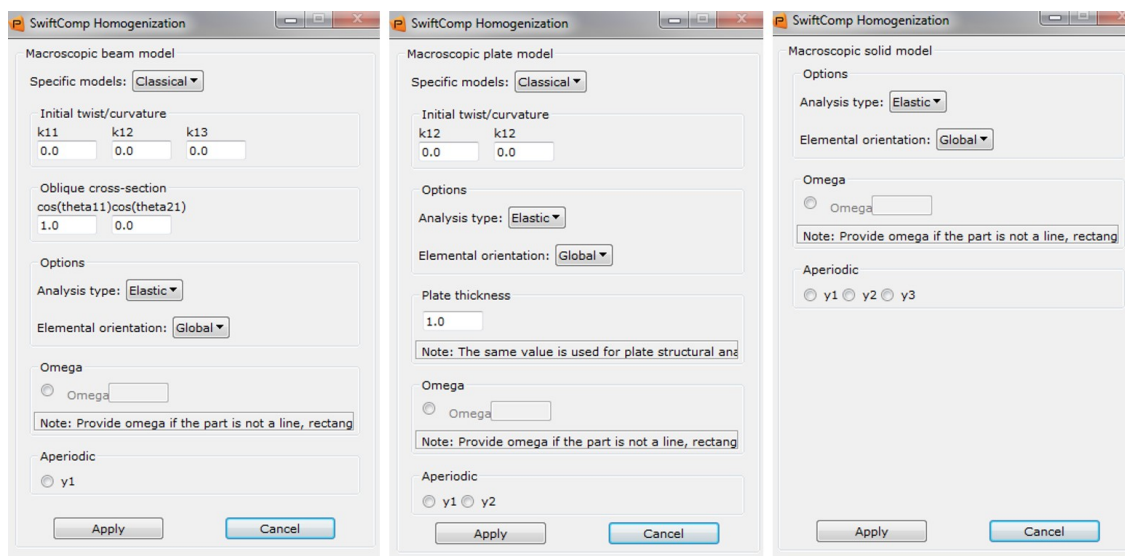

Figure B.5. Homogenization analysis of MSG-based multiscale modeling
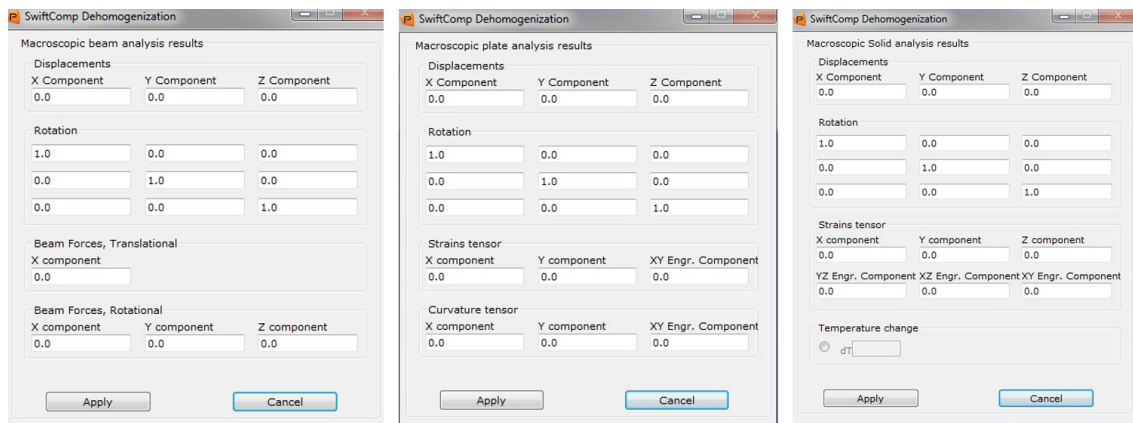
Figure B.6. Dehomogenization analysis of MSG-based multiscale modeling

dex/strength ratio, and failure envelope. Figure B.7 shows the overview of the initial failure functions in the GUI.
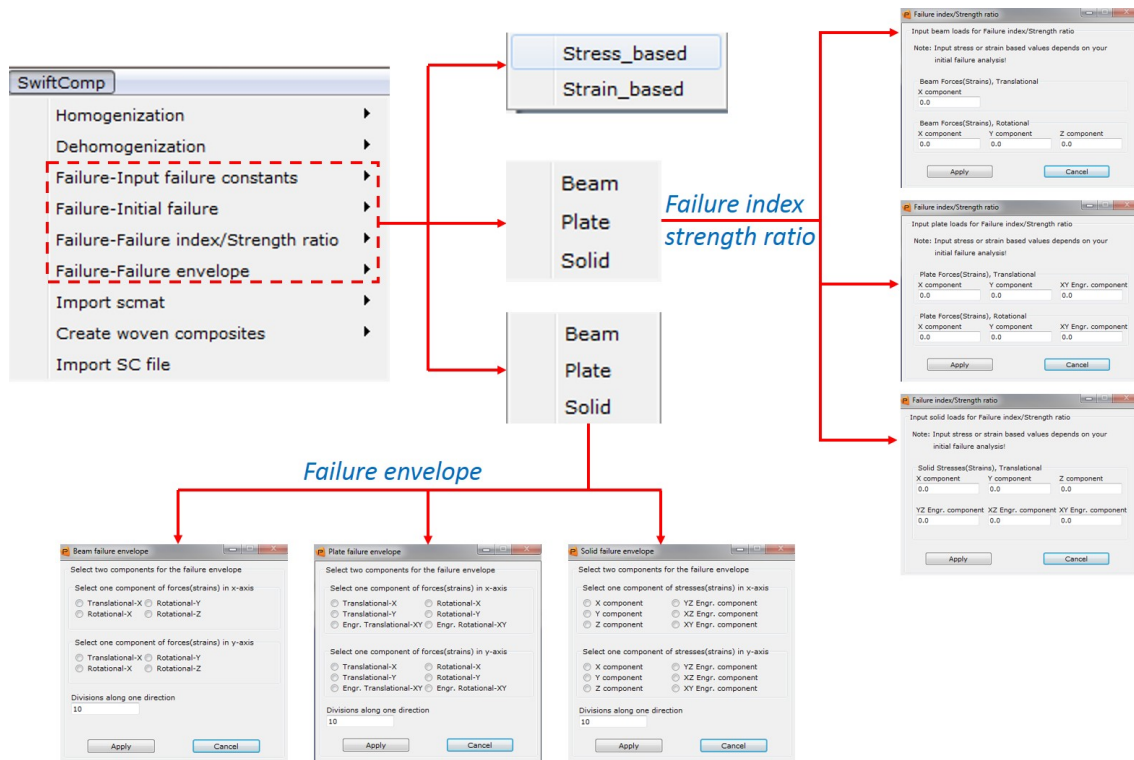

Figure B.7. Initial failure analysis of MSG-based multiscale modeling

The GUI also has special designed functions to import the effective properties (i.e. 3D material properties, plate stiffness and beam stiffness) into Patran database so that users can easily use the effective properties to perform structural analysis with the Nastran built-in finite elements. In addition, the GUI incorporated another open source codes called texgen, which provides a rapid textile composite microstructure generation for constitutive modeling.

VITA

Xin Liu was born on Sept. 9, 1988, in Heihe, Heilongjiang, China. He received his Bachelor's and Master's degrees in Civil Engineering in July 2011 and June 2014 from Nanjing Tech University in Nanjing, China. In Spring 2015, he started his graduate program in Prof. Wenbin Yu's group in School of Aeronautics and Astronautics at Purdue University. In May 2016, he received another Master's degree in Aeronautics and Astronautics Engineering from Purdue University and continued his study in Prof. Wenbin Yu's group. Most of the work done in this study at Purdue University is presented here for the requirement of Doctor of Philosophy in Aeronautics and Astronautics Engineering. His expertise is multiscale modeling of textile composites, machine learning (neural networks), finite element analysis, and scientific software development.

Award

- 2018, American Society for Composites (ASC) Ph.D. Research Scholarship

- 2018, Finalist, Student Paper Competition, AIAA SciTech Conference

- 2017, Purdue University Koerner Scholarship

Publication

1. Liu, X., Tao, F. and Yu, W. A neural network enhanced system for learning nonlinear constitutive relation and failure criterion of fiber reinforced composites, *Composite Structures*, under review.

2. Liu, X., Tao, F., Du, H.,Yu, W., and Xu, K., Learning nonlinear constitutive laws using neural network models based on indirectly measurable data, *Journal of Applied Mechanics*, revision submitted.

3. Tao, F., Liu, X., Du, H. and Yu, W., 2020. Physics-informed artificial neural network approach for axial compression buckling analysis of thin-walled cylinder, *AIAA Journal*, available online, https://doi.org/10.2514/1.J058765.

4. Rique, O., Liu, X., Yu, W. and Pipes, R.B., 2020. Constitutive modeling for time-and temperature-dependent behavior of composites. *Composites Part B: Engineering, 184,* p.107726.

5. Liu, X., Gasco, F., Goodsell, J. and Yu, W., 2019. Initial failure strength prediction of woven composites using a new yarn failure criterion constructed by deep learning. *Composite Structures, 230,* p.111505.

6. Liu, X., Gasco, F., Yu, W., Goodsell, J. and Rouf, K., 2019. Analyze complex woven composite structures using MSC.Nastran, *Advances in Engineering Software, 135,* pp. 102677.

7. Liu, X., Yu, W., Gasco, F. and Goodsell, J., 2019. A unified approach for thermoelastic constitutive modeling of composite structures, *Composites Part B: Engineering, 172,* pp. 649-659.

8. Tao F., Lyu, X., Liu, X. and Yu, W., 2019. Multiscale analysis of multilayer printed circuit board using mechanics of structure genome. *Mechanics of Advanced Materials and Structures,* pp. 1-10.

9. Liu, X., Tang, T., Yu, W. and Pipes, B., 2018. Multiscale modeling of viscoelastic behaviors of textile composites, *International Journal of Engineering Science, 130,* pp. 175-186.

10. Rouf, K., Liu, X. and Yu, W., 2018. Multiscale structural analysis of textile composites using mechanics of structure genome, *International Journal of Solids and Structures, 136,* pp. 89-102.

11. Liu, X., Rouf, K., Peng, B. and Yu, W., 2017. Two-step homogenization of textile composites using mechanics of structure genome, *Composite Structures, 171,* pp. 252-262.

12. Liu, X. and Yu, W., 2016. A novel approach to analyze beam-like composite structures using mechanics of structure genome, *Advances in Engineering Software, 100,* pp. 238-251.